The functional role of the endothelial lipase LIPG in breast cancer

Dissertation

zur Erlangung des akademischen Grades des Doktors der Naturwissenschaften (Dr. rer. nat.) an der Fakultät für Chemie und Chemische Biologie der Technischen Universität Dortmund

vorgelegt von

Sonja Vosbeck

Dortmund, 2015

1. Gutachter: Prof. Dr. J.G. Hengstler
2. Gutachter: Prof. Dr. F. Wehner

Table of contents

1. Introduction

1.1 Cancer and mammary tumorigenesis

Breast cancer is the most common type of cancer found in women, with about 70.000 new cases diagnosed per year. In addition, it is the leading cause of cancer death among women in Germany with 17.4% patients succumbing to the disease (Cancer in Germany 2009/2010). However, breast cancer mortality is declining because of novel and more effective treatment regimens, and improvements in cancer screening and prevention programs (Jemal et al. 2009).

In routine clinical laboratory testing, pathological markers are used to classify tumors and to stratify patients for outcome predictions and treatment selection. In addition to patient age, node status, tumor size and histological grade, expression of estrogen receptor (ER), progesterone receptor (PR) and human epidermal growth factor receptor 2 (HER2) are all used for the classification of tumors (Holliday and Speirs 2011, The Cancer Genome Atlas Network 2012, Tab. 1.1). Molecular taxonomy of breast cancers based on variations in gene expression derived from cDNA microarrays classifies six intrinsic subtypes of breast cancer, namely luminal A, luminal B, HER2-enriched, claudin-low, basal-like and normal breast-like (Perou et al. 2000, Sorlie et al. 2001, Prat and Perou 2011).

Tab. 1.1: Molecular classification of breast carcinomas

classification	immunoprofile	proliferation
luminal A	ER^+, $PR^{+/-}$, $HER2^-$	low proliferation
luminal B	ER^+, $PR^{+/-}$, $HER2^+$	high proliferation
basal-like	ER^-, PR^-, $HER2^-$, $CK5/6^+$ &/or $EGFR^+$	high proliferation
claudin-low	ER^-, PR^-, $HER2^-$	low proliferation
HER2	ER^-, PR^-, $HER2^+$	high proliferation
normal breast-like	ER^-, PR^-, $HER2^-$, $CK5/6^-$, $EGFR^-$	low proliferation

The majority of all breast cancers (up to 80%) are hormone-receptor-positive (Hart et al. 2015), thus underlining the importance of molecular tumor classification to define therapy options, such as treatments with Tamoxifen as an antagonist for estrogen-positive receptor, or Trastuzumab (Herceptin®) to block the HER2 receptor in HER2-positive tumors (Bezwoda et al. 1982, Vogel et al. 2002).

Tumorigenesis is a multistep process based on several genetic alterations which causes progressive transformation of healthy normal cells to malignant cancer cells. Hanahan and Weinberg (2000) postulated that malignant cell growth is characterized by several alterations in cell physiology, such as evading apoptosis, self-sufficiency in growth signals, insensitivity to anti-growth signals, tissue invasion and metastasis, limitless replicative potential and sustained angiogenesis. More recently (Hanahan and Weinberg 2011), the authors extended the list to include two further hallmarks: reprogramming of energy metabolism and evading immune cell surveillance. Genes that are involved in the multistep process of tumorigenesis are widely divided into proto-oncogenes and tumor suppressor genes. Gene products of proto-oncogenes promote normal cell proliferation, but a mutation at a single allele can result in cell transformation. Tumor suppressor genes (recessive oncogenes) on the other hand, counteract excessive proliferation. This results presented in this thesis originated from observations made while investigating one member of the epidermal growth factor receptor (EGFR) family belonging to the group of proto-oncogenes - the EGFR -, where it is well characterized that overexpression or mutations within the gene result in dysregulation of cell growth leading to tumorigenesis.

1.2 Lipid metabolism in cancer cells

Several diseases, including cancer, are accompanied by changes in the lipid composition of cellular membranes and alterations in lipid metabolism. It is well known that cancer cells have increased requirement for energy and adjust their metabolism to meet their demands, a process termed “metabolic reprogramming” (Santos and Schulze 2012). The Warburg effect, defined as elevated glycolytic activity and impaired oxidative phosphorylation even in the presence of sufficient oxygen, is the best known and characterized feature of this metabolic reprogramming (Hanahan and Weinberg 2011). Tumor metabolism may therefore support recycling

and remodeling of damaged cellular components, such as organelles or membranes, as well as their high proliferating capacity (Muńoz-Pinedo et al. 2012).

Besides being the essential structural components of all biological membranes, lipids are involved in the regulation of proliferation, inflammation, apoptosis, differentiation, autophagy, motility, and can function as second messengers and hormones. Consequently, to ensure proper homeostasis, their biosynthesis must be strictly controlled (Baumann et al. 2013). Figure 1.1 illustrates several features of lipids that could contribute to the development of cancer (Santos and Schulze 2012). For instance, based on their high proliferation rate, cancer cells require increased lipid amounts for membrane synthesis in general. In addition, cancer cells tend to have increased amounts of lipids with saturated (no double bonds) acyl chains in their membrane, as both saturated and monounsaturated acyl chains are less susceptible to peroxidation, compared to carbon atoms between double bonds in acyl chains that are morelikely damaged by oxidative attack and chemotherapeutics (Hulbert 2006, Rysman et al. 2010). Accumulated lipids stored in lipid droplets facilitate survival in phases of starvation. Perilipins contribute to this survival by enabling the mobilization of lipid droplets to provide energy by β-oxidation in mitochondria (Wang et al. 2011). A further adaptation is that nicotinamide adenine dinucleotide phosphate (NADPH) can be used as an electron donor when oxygen is not available in hypoxia- tolerant cancer cells (Hochachka et al. 2002). Finally, cholesterol and fatty acids represent precursors for hormones which stimulate proliferation and invasion-related pathways, both of which are critical for tumorigenesis and cancer progression.

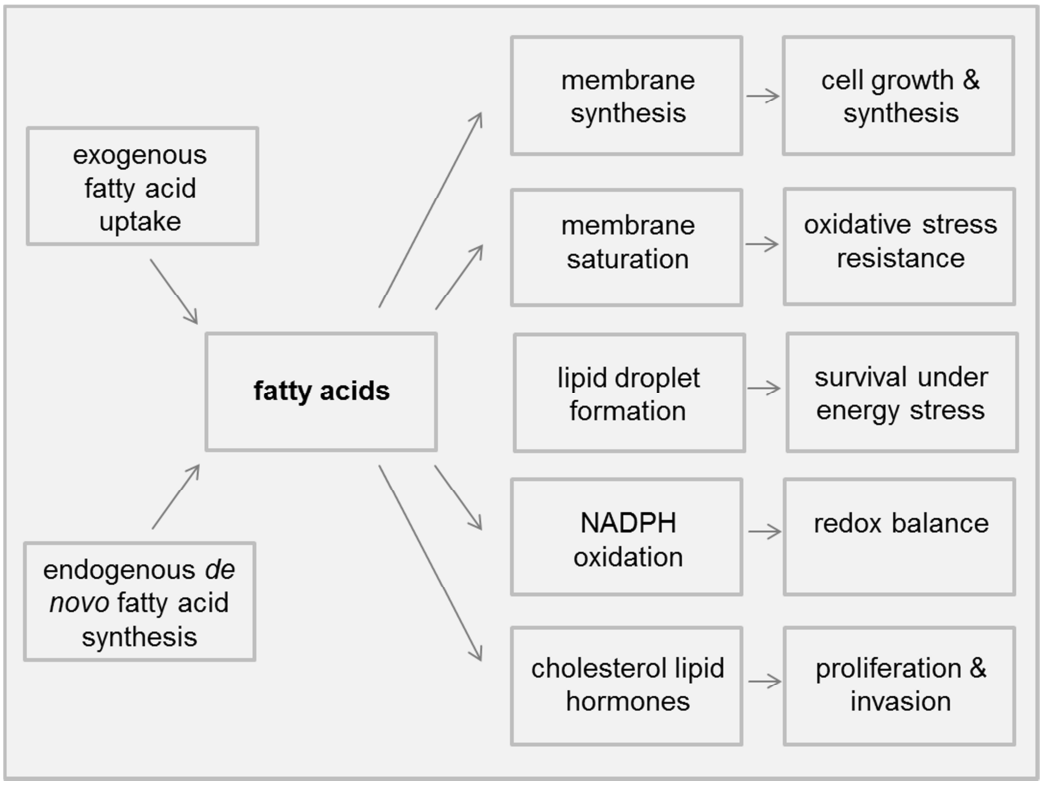

Fig. 1.1: **Lipids support several aspects of cancer development**. Fatty acids taken up from exogenous sources or generated via endogenous *de novo* fatty acid synthesis support multiple cellular processes: They represent building blocks for membrane synthesis in case of proliferation and membrane saturation; and they become stored in lipid droplets to ensure lipid survival under stress conditions. Nicotinamide adenine dinucleotide phosphate (NADPH) is used from hypoxia-tolerant cancer cells when oxygen is not available. Cholesterol lipid hormones influence proliferation- and invasion-related pathways (source: Santos and Schulze 2012; the figure is modified)

Fatty acids can be taken up exogenously from the environment, transported for example, by lipoproteins or mobilized from adipose tissue, and can be as well endogenously produced by *de novo* synthesis.

1.2.1 Lipids can influence immune cell behavior

Otto Warburg described in 1924 that tumor cells exhibit increased glycolysis despite the presence of oxygen (Hanahan and Weinberg 2011). This metabolic shift represents only one aspect of tumor cell metabolism. Tumor cells accumulate specific metabolic determinants (for example cytokines, chemokines and growth factors) in their environment to create a favorable milieu supporting tumor growth, progression and metastasis (Gottfried et al. 2012). These secreted metabolites protect cancer cells from tumor infiltrating immune cells, or help increase their

immunity. The immune system distinguishes the innate from the adaptive immune system. The former initiates an immediate but non-specific response, like inflammation, and comprises leukocytes, such as macrophages, neutrophils and dendritic cells, in addition to natural killer cells. The adaptive immune system, on the other hand offers a pathogen or antigen-specific response mediated by lymphocytes, including B- and T-cells.

As mentioned, cancer cells produce and secrete numerous tumor-specific metabolites, such as amino acids, lipids and chemical compounds into their environment to escape immune cells and increase immunosuppression. For example, an altered fatty acid supply in the tumor environment can change the immune response by inducing perturbations in the composition of membrane phospholipids of immune cells, which can ultimately influence signal transduction (Calder et al. 2011). Herber et al. (2010) reported that dendritic cells phagocytize lipids and cholesterol in their tumor-bearing hosts. The resulting lipid-laden dendritic cells have a reduced capacity to process and present antigens, such as MHC class I and II, leading to reduced antigen presentation and diminished T-cell stimulation. Lysophosphatidic acid blocks the cytotoxic activity of natural killer cells by inhibiting their release of the cytolytic protein, perforin which enables tumor cell escape from the immune cell attack (Lagadari et al. 2009). Furthermore, *in vitro* incubation of Jurkat T-cells with increased free fatty acids or albumin-bound fatty acids inhibited T-cell signaling (Stulnig et al. 2000). On the other hand, lysophosphatidylcholine has been shown to stimulate the maturation of dendritic cells (Jin et al. 2005). In summary, lipids can positively as well as negatively affect immune cell behavior.

1.2.2 Lipid classification and cellular lipid uptake

Lipids are involved in several essential physiological pathways as mentioned before. They are defined as hydrophobic or amphipathic small molecules and divided into eight categories in ‘the Comprehensive Classification System for Lipids’ by the International Lipid Classification and Nomenclature Committee (ILCNC). These eight categories comprise fatty acyls, glycerolipids, glycerophospholipids, sphingolipids, sterol lipids, prenol lipids, saccharolipids and polyketides (Fahy et al. 2009). Each category contains distinct classes and subclasses of molecules. Fatty acids (FA) are

major building blocks of complex lipids and are distinguished by the number of carbon atoms and double bonds. A saturated fatty acid carries no double bond compared to unsaturated ones, which may contain different numbers of double bonds. Glycerolipids include mono-, di-, and tri- substituted glycerol, with fatty acid triesters of glycerol, such as triacylglycerides (TAG). Most prominent are triacylglycerides (TAG), which function as energy storage in lipid droplets. Phospholipids or glycerophospholipids are key components of the lipid bilayer of cellular membranes and are also involved in metabolism and cell signaling pathways (Fahy et al. 2005).

As described above, fatty acids are the basic building blocks for more complex lipids. Cells are able to produce fatty acids either via endogenous synthesis or by extracellular uptake. Two types of free fatty acid uptake exist across the membrane passive diffusion or protein-facilitated transfer. The aqueous solubility of fatty acids is in the range of 1-10nM; therefore, fatty acids in blood serum or in the extracellular environment are bound to the protein albumin in a ratio of 1:6 (albumin:fatty acid) (Vorum et al. 1992). The physical transport of fatty acids includes seven kinetic steps: 1) dissociation of fatty acid from albumin into the aqueous phase; 2) diffusion through the outer aqueous phase; 3) insertion into the outer leaflet of the cell bilayer membrane by receptors like CD36; 4) flip-flop from the external to the internal membrane face; 5) dissociation from the inner leaflet; 6) diffusion through the inner aqueous phase and 7) binding to fatty acid binding proteins (Glatz et al. 2010, Hajri and Abumrad 2002, Potter et al. 1989, Mashek and Coleman 2006). Several lipids are enclosed by lipoproteins to emulsify the lipid molecules and enable their transport through the blood.

1.2.3 Lipoproteins and the lipase superfamily

Lipoproteins are complexes of lipids and proteins which transport lipids (mostly TAG, cholesteryl esters and fat-soluble vitamins) through body fluids to and from organs. They are mainly spherical complexes classified into five major classes based on their relative density (determined by the amount of lipid and protein per particle) as shown in Tab. 1.2: chylomicrons, very low density lipoproteins (VLDL), intermediate density lipoprotein (IDL), low density lipoproteins (LDL) and high density lipoproteins (HDL, Fig. 1.2). Each lipoprotein class differs in density, size and migration during

electrophoresis, and protein composition. Apo-lipoproteins are required for the structure and assembly of lipoproteins, and can mediate and determine the binding of the lipoproteins to cell-surface receptors (Eren et al. 2012).

Tab. 1.2: Major lipoprotein classes sorted by density

lipoprotein	diameter [nm]	major apo-lipoproteins
chylomicrons	75-1200	apoB-48
VLDL	30-80	apoB-100
IDL	25-35	apoB-100
LDL	18-25	apoB-100
HDL	5-12	apoA-1

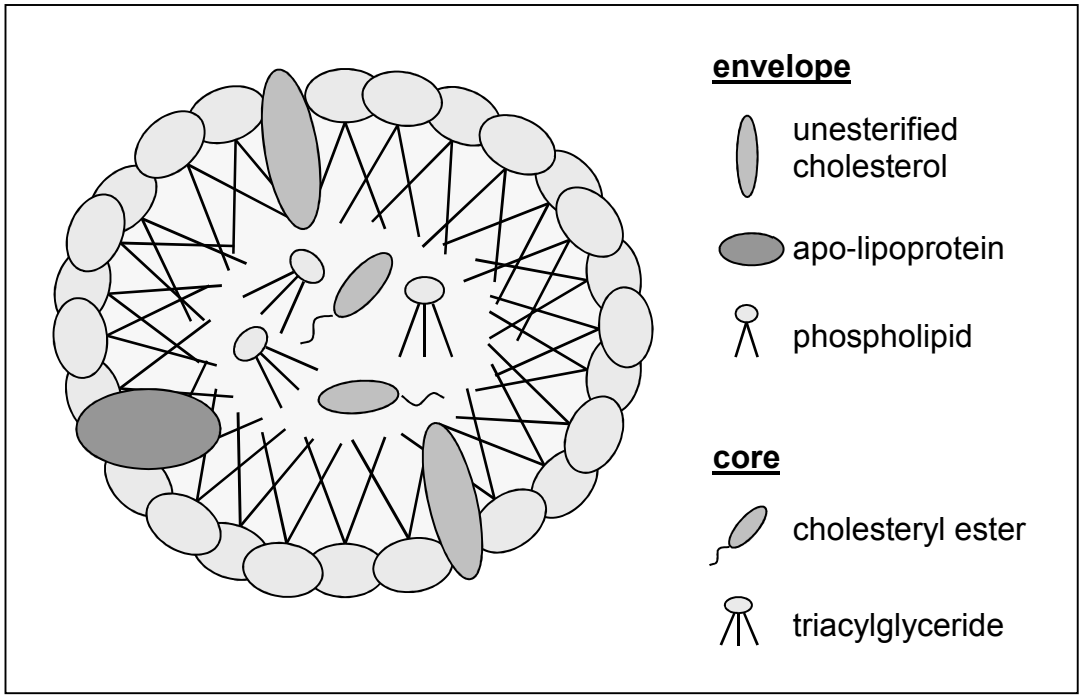

Fig. 1.2: Schematic illustration of a high-density lipoprotein molecule. The HDL envelope consists of a phospholipid monolayer, unesterified cholesterol and apo-lipoprotein. The core contains cholesteryl ester and fatty acids, including triacylglycerides

Many lipases are involved in the binding and processing of extracellular lipoproteins (holoparticle uptake or cleavage). Lipases are enzymes which catalyze the hydrolysis of lipids. They can be classified into different protein families, with the majority belonging to the subclass of esterases (Staege et al. 2010). Lipases support cellular metabolism via digestion, transport and processing of lipids. Tab 1.3 contains a selection of some lipases and their functional role.

Tab. 1.3: Overview of some lipases and their functions

gene	name	description	references
LIPC (HL)	hepatic lipase	hydrolysis of phospholipids, MAG, DAG, TAG, and acyl-CoA thioesters	Wang et al. 2013
LIPD (LPL)	lipoprotein lipase	hydrolysis of TAG of circulating chylomicrons and VLDL	Kersten 2014
LIPE (HSL)	hormone sensitive lipase	regulatory role in initiating the degradation of TAG	Watt and Spriet 2004
LIPG (EL)	endothelial lipase	phospholipase A1 activity	Riederer et al. 2012
LIPH	lipase H	hydrolysis of TAG	Cui et al. 2014
MAGL	monoacylglycerol lipase	hydrolysis of MAG	Nomura et al. 2010

Our initial findings of LIPG induction by NeuT expression in MCF7/NeuT cells (Cadenas et al. 2012) were the first report linking LIPG expression to breast cancer. However, the mechanism underlying LIPG's function in oncogene-induced senescence in breast cancer remained unexplored.

1.3 Structure of the endothelial lipase

In the year of 1999, two working groups reported simultaneously the discovery of the endothelial lipase (LIPG; EL; EDL) (Jaye et al. 1999, Hirata et al. 1999). Lipase G expression was observed in cultured endothelial cells and on the wall of blood vessels, providing a mechanism for local regulation of lipolytic activity and processes related to atherosclerosis and other vascular diseases (Hirata et al. 1999). LIPG, located on chromosome 18q21.1, encodes a protein of 500 amino acids and belongs to the triglyceride lipase gene family with 46% identity to lipase member H (LIPH), 45% to lipoprotein lipase (LPL), 40% to hepatic lipase (HL, HTGL or LIPC) and 31% to pancreatic lipase (PNLIP) (Choi et al. 2002, Cui et al. 2014, Wu et al. 2010). Ishida et al. (2004) described three LIPG mRNA isoforms, EDL1a, EDL2a and EDL2b, expressed by endothelial cells. EDL1a represents the previously characterized full-length isoform; whereas, EDL2a and EDL2b appear to result from alternative splicing.

Both splicing isoforms lack the first 80 amino acids residues (containing a signal peptide) at the N-terminal, with EDL2b lacking an additional 74 amino acid region, which encodes a portion of the lid domain (part of the catalytic triad) (Fig. 1.3). As a result, both isoforms display no catalytic activity and are localized in the cytosol compared to the enzymatic active EDL1a isoform, which has catalytic activity and can be secreted into the cell supernatant.

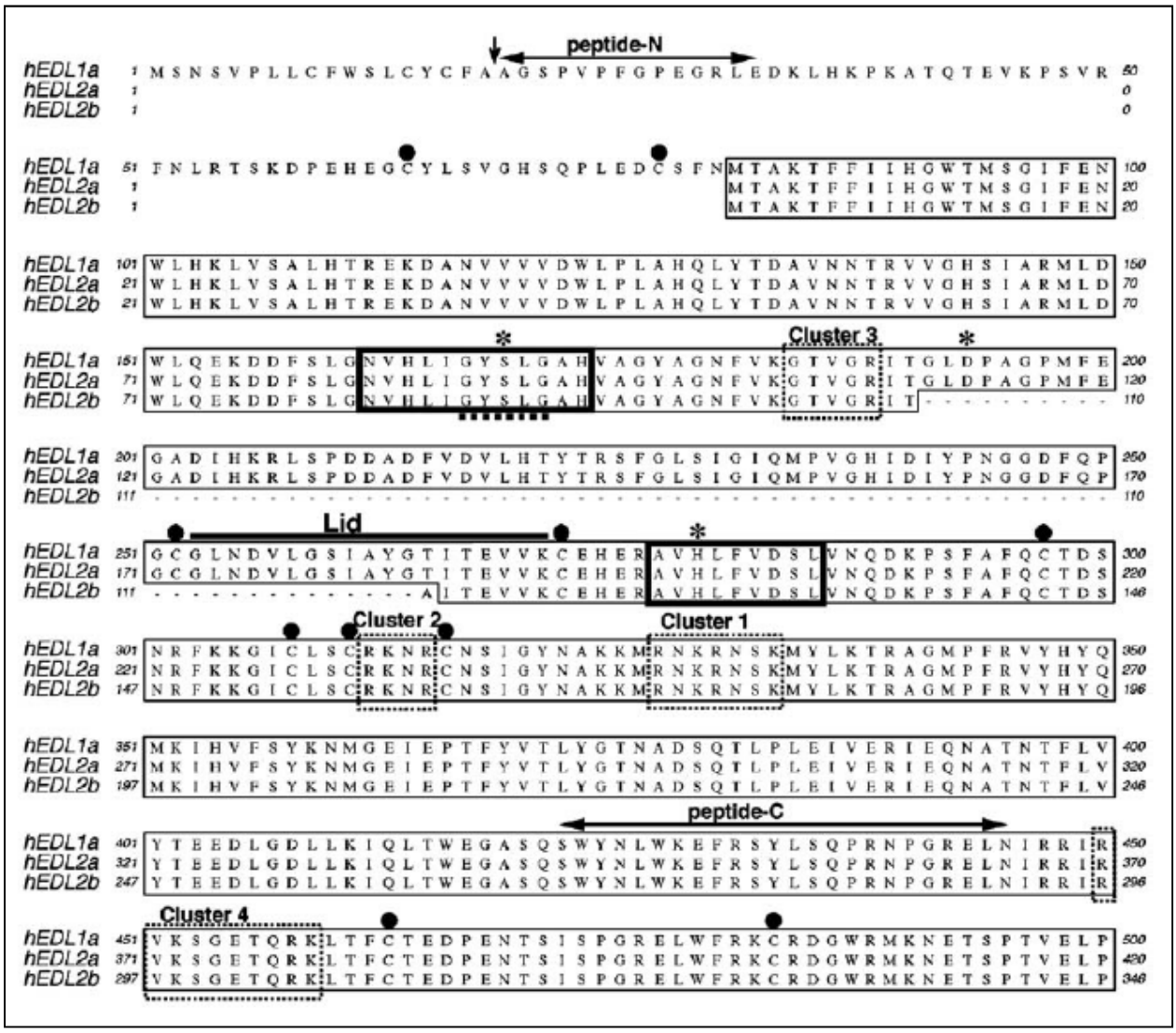

Fig. 1.3: **Human amino acid sequences of human EDL2a and EDL2b compared with EDL1a (full-length)**. Boxes mark identical amino acids. Dashed lines indicate the GXSXG lipase motif. Vertical arrow shows EDL1a signal peptide cleavage site. Asterisks illustrate the catalytic triads, and dots the conserved cysteines. Dashed boxes mark heparin binding positions. Solid bars indicate hydrophobic sequences. Horizontal bars show the lid region with 19 residues whereas horizontal bars with arrows indicate the peptide sequences which were chosen to generate antibodies in this publication (Ishida et al. 2004_Genbank Accesssion No. NM_006033)

In Figure 1.3, asterisks illustrate the three catalytic residues, including the cysteine residues that form intramolecular disulfide bonds, the lid that covers the catalytic pocket, as well as lipid and heparin binding regions (addition of heparin increases EDL/LIPG release into environment). These features are conserved in all members of the triglyceride lipase gene family (Miller et al. 2004).

1.3.1 Enzymatic and non-enzymatic function of LIPG protein

Adenoviral-based overexpression of full length LIPG cDNA in mice resulted in a decrease in plasma HDL-cholesterol and apo-A1-lipoprotein, and to a lesser extent VLDL- and LDL-cholesterol levels (Jaye et al. 1999), showing that indeed HDL is the preferred substrate of LIPG. LIPG-overexpressing COS-7 kidney cells incubated with phosphatidylcholine labeled at the sn-1 position accumulated increased levels of labeled free fatty acids (Hirata et al. 1999), indicating cellular uptake of hydrolyzed sn-1 fatty acids. Also, McCoy et al. (2002) confirmed this observation by incubating conditioned media from LIPG-overexpressing COS-7 cells with radioactive labeled-phosphatidylcholine containing glycerol-tri-oleate in order to detect increased free fatty acid amounts in the aqueous phase. These results support the phospholipase A1 and triacylglycerol lipase activity of LIPG, as well as the preference of LIPG for HDL as its main substrate. However, other studies involving LIPG overexpression in HepG2 cells incubated with HDL in presence or absence of tetrahydrolipstatin, an inhibitor of the enzymatic activity, demonstrated that LIPG mediates HDL binding and holoparticle uptake together with selective HDL-cholesterol ester uptake independent of its enzymatic activity (Strauss et al. 2002).

The analysis of cellular lipids released by LIPG-overexpressing cells incubated with HDL-phosphatidylcholine ^{14}C-HDL-PC revealed increased levels of intracellular ^{14}C-lipids which were mainly incorporated into phospholipids and TAGs. Furthermore, LIPG is able to cleave HDL-PC into free fatty acids (FFA) and lysophosphatidylcholine (LPC). These liberated saturated and unsaturated FFA serve as substrates for the biosynthesis of intracellular synthesized lipids (Strauss et al. 2003, Gauster et al. 2005).

Mass spectrometric-based analysis of LIPG-overexpressing human aortic endothelial HAEC cells in the presence of HDL resulted in the generation of LPC and lysophosphatidylethanolamine (LPE) species in cell culture supernatant, together with increased intracellular phosphatidylcholine, TAG, LPC and FFA content (Riederer et al. 2012). Razzaghi et al. (2013) postulated that LIPG does not lead to complete HDL catabolism but instead remodels HDL into smaller pieces with higher preferences to release certain fatty acids like palmitic acid (C16:0), stearic acid (C18:0), oleic acid (C18:1), linoleic acid (C18:2), arachidonic acid (C20:4) and docosahexaenoic acid (C22:6).

Altogether, the results of these studies elucidate that LIPG has both enzymatic as well as a non-enzymatic activity (Fig. 1.4), and influences both the intracellular and the extracellular lipid composition (Fig. 1.5).

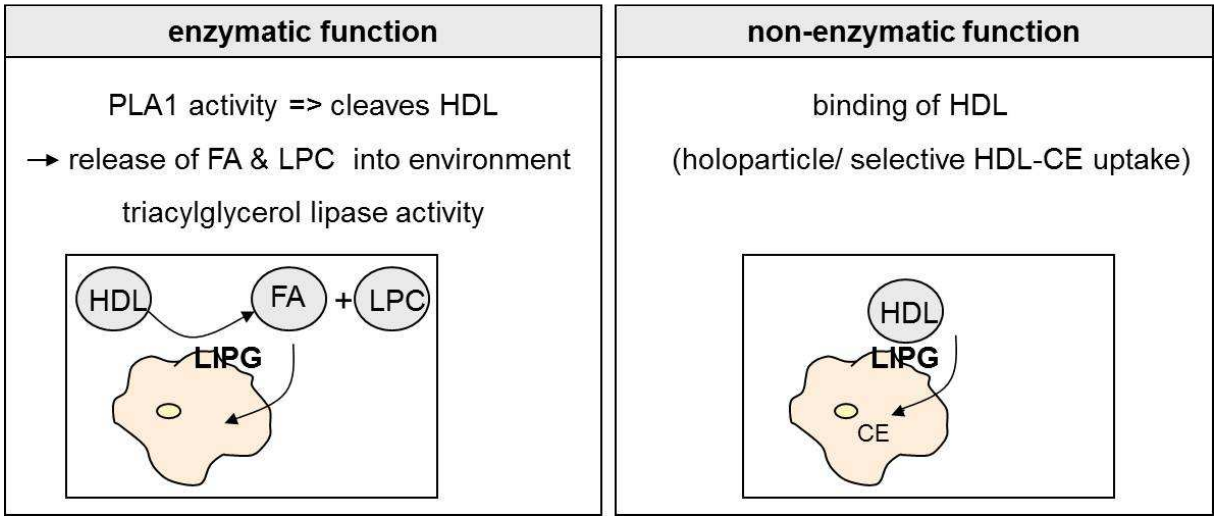

Fig. 1.4: **Illustration of LIPG-enzymatic and non-enzymatic activities**. Left: By virtue of its phospholipase activity and also triacylglycerol lipase activity LIPG is able to bind and cleave HDL into free fatty acids (FFA) and lysophosphatidylcholine (LPC). Right: Blocking the enzymatic activity of LIPG does not inhibit the HDL-binding, holoparticle uptake and selective HDL-cholesterol ester uptake

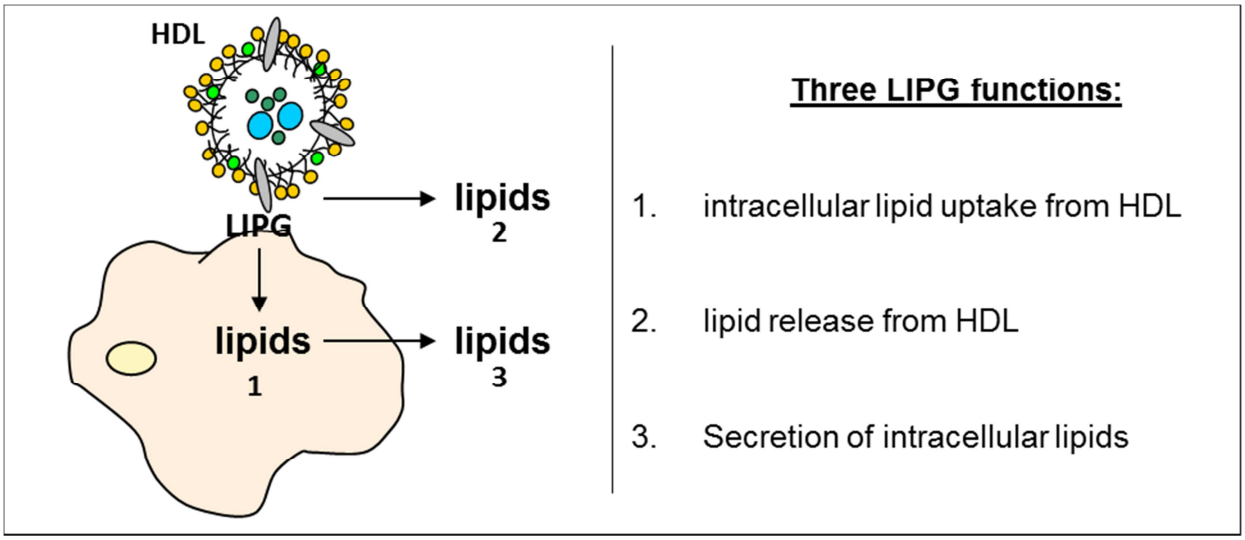

Fig. 1.5: **LIPG alters by HDL bridging intracellular and extracellular lipid composition**. LIPG-related cell surface binds HDL and enables the cellular uptake of lipids (1) and cleavage of HDL resulting in lipid release into cell media (2). Internalized lipid can be secreted by cells (3)

Analysis of LIPG-overexpressing cells incubated with heparin or the inhibition of proteoglycans sulfation revealed decreased HDL-bridging on the cell surface by LIPG. Heparan sulfate proteoglycans- (HSPG) deficient Chinese hamster ovary CHO-677 cells also showed decreased lipoprotein binding compared to control cells. LIPG-expressing kidney COS cells were incubated with HDL at 4°C to minimize the enzymatic activity of LIPG, which resulted in a significantly higher HDL- binding compared to control cells. The same was measured with a catalytically inactive LIPG mutant, and the results showed that binding of lipoproteins by LIPG is independent of its enzymatic activity, but requires active HSPGs (syndecans, glypicans and perlecans) on the cell surface (Fuki et al. 2003).

1.3.2 N-linked glycosylated maturation and cleavage processes of LIPG

Western blotting analyses have been crucial to elucidate the maturation steps of the translated LIPG product, and cleavage processes of the secreted LIPG protein. LIPG contains five potential N-linked glycosylation sites. The full-length 68kDa LIPG form was reduced to 55kDa using glycosidase F, the predicted size of unglycosylated LIPG. Cellular lysates, cell membranes and conditioned media from LIPG-overexpressing cells with or without tunicamycin (glycosylation inhibitor) were

isolated and analyzed for protein sizes and lipase activity. All three compartments showed the presence of a 68kDa and 40kDa protein fragment in untreated LIPG-overexpressing cells. However, tunicamycin-treated cells only displayed a 55kDa LIPG protein band in the intracellular and in the membrane-bound fraction. Retention of an inactive 55kDa protein in tunicamycin-treated cells revealed a lack of secretion and abolished triglyceride lipase and phospholipase activities. The importance of four out of five putative N-linked glycosylation sites for LIPG secretion and activation was demonstrated by site-directed mutagenesis experiments (Miller et al. 2004, Skropeta et al. 2007).

Gauster et al. published in 2005 that in addition to the 68kDa mature LIPG proteins found in cell lysates and media, two additional LIPG fragments with 40kDa and 28kDa could be identified in the supernatant. These are the products of extracellular proteolytic cleavage of the mature catalytic active 68kDa LIPG protein by pro- protein convertases (Fig. 1.6). Although the N-terminal 40kDa fragment of LIPG harbors the catalytic site, a phospholipase activity assay could demonstrate that this LIPG fragment it is unable to bridge and hydrolyze HDL. Therefore, the proteolytic cleavage of LIPG results in its inactivation.

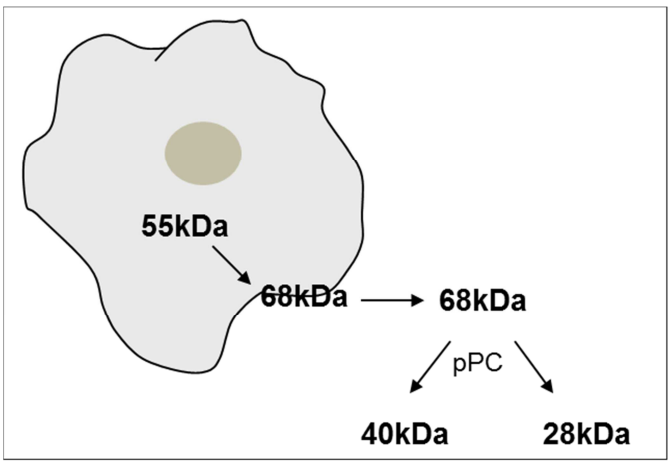

Fig. 1.6: **Illustration of LIPG protein maturation and cleavage**. LIPG is synthesized as an inactive 55kDa protein. It is then glycosylated intracellularly to a mature catalytic active 68kDa LIPG protein and transported to the cell membrane. The secreted enzymatically active 68kDa LIPG protein is cleaved by pro-protein convertases (pPC) into inactive LIPG fragments with 40kDa and 28kDa

1.3.3 LIPG expression in human cell lines and tissues

Angiogenesis, the formation of new blood vessels, occurs in numerous physiological and pathophysiological processes, like wound healing, placental development, as well as tumor growth. Rapidly dividing and growing cancer cells or tumors need an enormous supply of oxygen and nutrients, and the generation of new blood vessels is required to ensure sufficient supply. Tumor-induced angiogenesis offers potential for treatment. Therefore, understanding the molecular angiogenesis pathways which regulate endothelial cell differentiation and growth is of fundamental interest. Endothelial cells cover the interior surface of blood vessels and are in direct contact with circulating blood. LIPG (endothelial lipase) was initially identified in an analysis of genes involved in vascular formation (Hirata et al. 1999). LIPG RNA expression measurements in different human cell lines performed by the Human Protein Atlas show high RNA expression in endometrial AN3-CA cancer cells, colon CACO2 cancer cells, ovarian Efo21 cancer cells, keratinocytes HACAT cells, and endothelial time cells (Fig. 1.7) (http://www.proteinatlas.org).

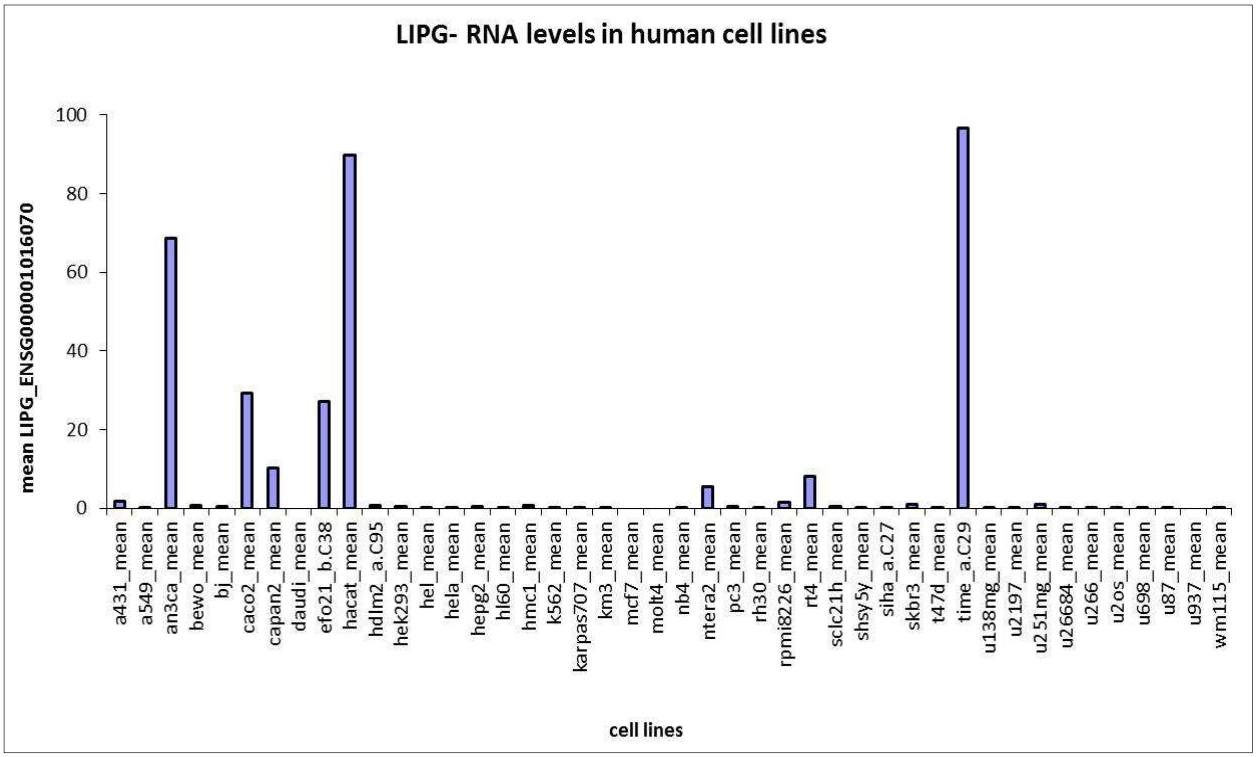

Fig. 1.7: **LIPG RNA levels in different human cell lines**. LIPG show a high RNA expression in endometrial AN3-CA cancer cells, colon CACO2 cancer cells, ovarian Efo21 cancer cells, keratinocytes HACAT cells and endothelial time cells (source: Human Protein Atlas_ ENSG00000101670)

Figure 1.8, based on Human Protein Atlas data, illustrates the LIPG mRNA expression level in different human tissues which shows an enormous amount in placenta and thyroid gland.

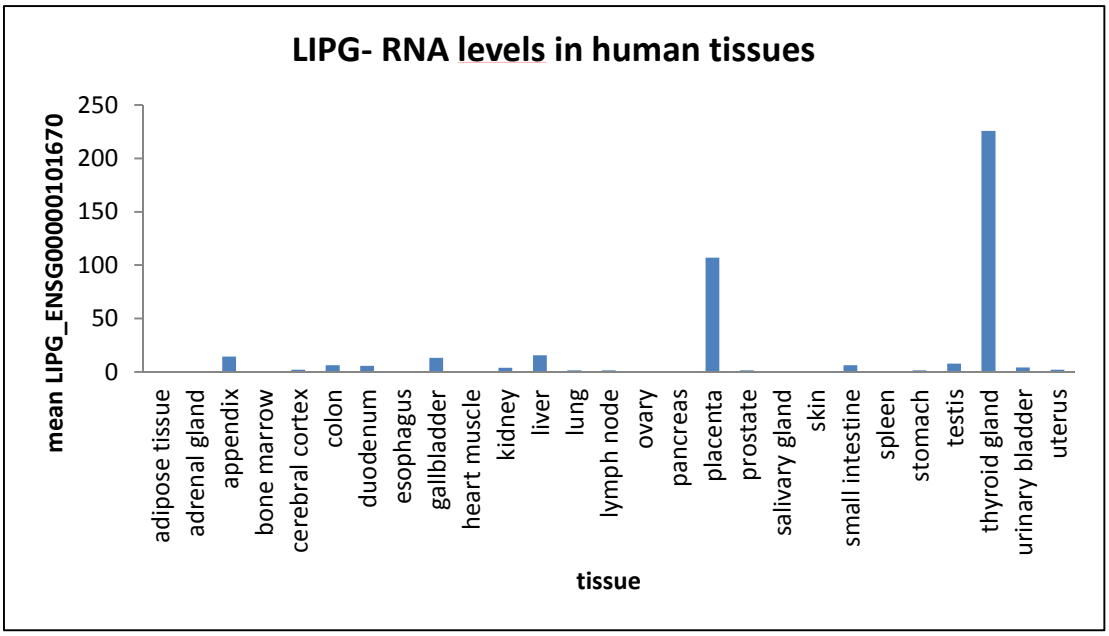

Fig. 1.8: **LIPG RNA expression in human tissues**. LIPG shows enormous expression in the thyroid gland and placenta. A moderate expression is detectable in the appendix, gallbladder and liver (source: Human Protein Atlas_ ENSG00000101670)

1.3.4 Functional role and stimulation factors of LIPG

Analysis of the functional role of LIPG on endothelial cell surfaces revealed enhanced binding of monocytes (THP-1 or U-937 cells) to COS7 cells overexpressing LIPG, which normally do not express endogenous LIPG. Heparin treatment, which detaches cell-surface associated LIPG, disrupted this binding. Furthermore, incubation of LIPG-overexpressing COS7 or THP-1 cells together or separately with heparinase I (degradation of HSPGs) abolished monocyte binding. These results suggest that LIPG-mediated monocyte binding depends on functional HSPGs both on the monocyte surface and on the surface of LIPG-expressing cells (Kojma et al. 2004). Accumulation of monocytes/macrophages on the inner layers of the artery walls is a common feature of inflammation and the earliest event in atherosclerosis (chronic inflammatory disease). Atherosclerosis is referred to an accumulation of fatty materials, like cholesterol, on the vessel walls, and since overexpression of LIPG is accompanied by decreased HDL-cholesterol levels, it has

been suggested that, increased LIPG expression is associated with the development of atherosclerosis (Dalan et al. 2013).

Injection of lipopolysaccharide (LPS; a mediator of inflammation) into C57BL/6 mice has been shown to increase LIPG expression at both the RNA and protein level (Kojma et al. 2004). Incubation of three different endothelial cell types with inflammatory cytokines - including IL-1β (produced mainly by monocytes) and TNF-α (mainly produced by macrophages) - resulted in increased LIPG protein expression, secretion, and phospholipase as well as triglyceride lipase activity in the media. Conversely, lipoprotein lipase (LPL) and hepatic lipase (HL) were downregulated by inflammatory cytokines. Accordingly, LIPG-upregulation during inflammatory processes could offer an alternative way of generating fatty acid support derived from HDL (Jin et al. 2003). The study of Nakajima et al. (2013) reporting LIPG induction and concomitant decrease in LPL expression upon heart failure (HF; the heart muscle being unable to pump sufficiently to maintain the blood flow through the body) supports this hypothesis. Interestingly, patients with early phase exhibited enhanced inflammatory cytokine levels in heart tissue and circulation. In conclusion, LIPG may represent an alternative way by which cells are supported with fatty acids under inflammatory conditions.

Besides the induction of LIPG expression in cells by inflammatory cytokines, Azumi et al. (2003) published that macrophages themselves also express LIPG. Suppression of LIPG expression in THP-1 macrophages resulted in decreased concentration of pro-inflammatory cytokines IL-1β, TNF-α, IL-6, IL-8 and MCP-1 (monocyte chemoattractant protein-1) and reduced levels of total cellular cholesterol, triacylglycerides, and lysophosphatidylcholine (lyso-PC) (Qiu et al. 2007). Furthermore, Yasuda et al. (2007) postulated that LPS mediates the induction of LIPG expression in macrophages via the functional toll-like receptor 4 (TLR4) cascade and intracellular H_2O_2-production (reactive oxygen species, oxidative stress). In summary, LIPG-transcription in endothelial cells that line blood vessels in numerous organs, as well as in macrophages is induced by inflammatory signals. Conversely, LIPG can also control cytokine expression and alter the cellular lipid composition.

In vivo studies revealed a statistically significant, direct correlation of obesity-associated inflammation in humans and upregulated LIPG plasma concentrations accompanied by low HDL-cholesterol levels (Badellino et al. 2008). The intravenous LPS injection in twenty human healthy volunteers has contributed to a statistically significant increase in LIPG plasma concentration and a concomitant statistically significant reduction of total plasma phospholipid plus HDL-phospholipid concentration. In addition LIPG plasma concentrations in pre- and post-heparin plasma showed a statistically significant correlation with obesity (body mass index) and atherosclerosis (Badellino et al. 2005, Paradis et al. 2006).

1.3.5 LIPG protein contribution in carcinogenesis

There is only little known and published about the contribution of LIPG in human cancer progression. Our laboratory (Cadenas et al. 2012) reported the expression of LIPG after HER2/ErbB2 overexpression in MCF7 breast cancer cells. Mudvari et al. (2013) established an isogenic stable cell line representing HER2-positive breast cancers by introducing HER2 into the breast cancer cell lines MDA-MB-231 and MDA-MB-468 (both triple-negative breast cancer cell lines). Cancer cells showed down-regulated LIPG expression pattern compared to HER2-positive clones. Nevertheless, nothing is known and published about the functional role of LIPG in breast cancer.

Dong et al. (2013) reported that LIPG is a highly accurate and statistically significant urinary biomarker for gastric cancer. LIPG levels in tissue and serum of gastric cancer patients compared to healthy donors were not as discriminative as in urine samples. Gastric cancer patients exhibited an approximately 9.9-fold average decrease in LIPG protein levels compared to healthy urine controls. The glomerular filtration system of the kidney filters small positively charged molecules, such as LIPG that has a number of positively charged clusters, more easily. Interestingly, this finding was not linked to tumor grade or stage. LIPG urinary protein level was also investigated in lung, colon and rectum cancer, but was not found to be as significant as for gastric cancer.

LIPG protein expression was highly expressed in human testicular germ cell tumors (Nielsen et al. 2010), which may facilitate nutrient supply in the testis, and may be involved in steroidogenesis, providing cholesterol for testosterone production in Leydig cells.

Finally, Füri et al. (2015) reported that tumor tissue-derived DNA-treated HT-29 cells exhibited upregulated LIPG RNA expression compared to control cells.

The above publications are the only studies currently available that discuss a possible role for LIPG in cancer. They all reported increased LIPG expression in human breast cancer cell lines, human gastric cancer patients, human testicular germ cell tumors and human colon cancer cells; however, the contribution of LIPG in carcinogenesis or tumor development remains to be elucidated.

Several oncogenes have been found to be related to tumorigenesis including the tyrosine kinase family. As mentioned our initial findings revealed LIPG induction upon HER2/ErbB2 expression in MCF7/NeuT cells (Cadenas et al. 2012).

1.4 The ErbB family

Our initial findings revealed LIPG induction upon HER2/ErbB2 expression in MCF7/NeuT cells (Cadenas et al. 2012). The epidermal growth factor receptor (EGFR) family comprises four members, all of which are receptor tyrosine kinases that play an important role in development and tumorigenesis: EGFR (HER1 or ErbB1), HER2 (ErbB2 or Neu), HER3 (ErbB3) and HER4 (ErbB4) (Casalini et al. 2004). All ErbBs are transmembrane receptors that dimerize in response to the binding of their specific ligand(s), but differ regarding their kinase activity, ligand specificity, and downstream signaling activation. Ligand-binding results in the formation of ErbB- receptor homo- and heterodimers. Activation of intrinsic kinase domain induces autophosphorylation as well as phosphorylation of other signaling molecules on specific tyrosine residues (Simon 2000). A range of downstream effector proteins bind these phosphorylated residues resulting in the activation of intracellular signaling pathways (Yarden 2001, Yarden and Sliwkowski 2001) (Fig. 1.9). Of the four family members, the overexpression of HER2/ErbB2 is well

described as associated with malignancy and poor outcome in breast cancer (Rubin and Yarden 2001).

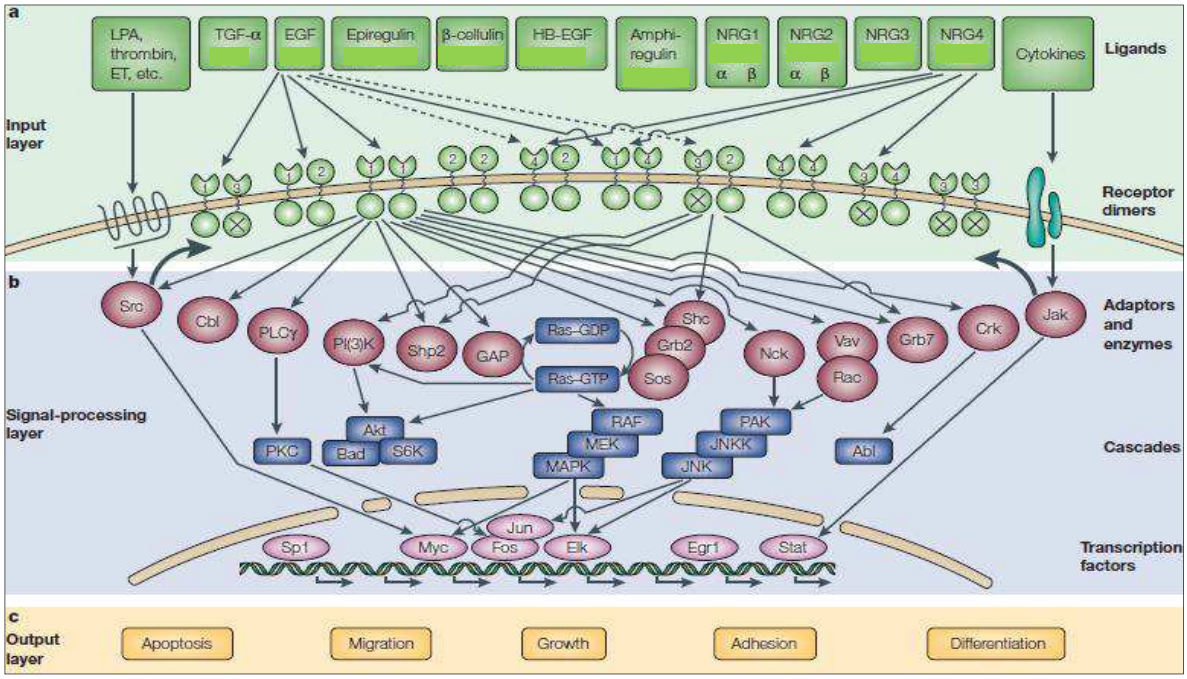

Fig. 1.9: Illustration of the ErbB signaling network. The signaling network comprises an input, a signal-processing and an output layer. The input layer illustrates the ten dimeric receptor combinations with corresponding ligands. Until now no ErbB2-specific ligand has been identified and ErbB3 homodimers are catalytically inactive. The signaling-processing layer shows the corresponding adaptors and enzymes of only two receptor dimers (ErbB1 homodimer & ErbB3/ ErbB2 heterodimer) that lead to initiation of different cascades and induction of several transcription factors. The output layer illustrates possible cellular events like apoptosis, migration, cell growth, adhesion and differentiation (source: Yarden and Sliwkowski 2001; the figure is modified)

1.4.1 The receptor tyrosine kinase HER2/ErbB2

Human ErbB2 gene is localized on chromosome 17q21 and encodes a transmembrane protein with a homology of 50% to the EGF-receptor. To date, no ErbB2-specific ligand has been identified, but ErbB2 can act as a co-receptor and is a preferred heterodimerization partner for the other ErbB family members (Neve et al. 2000). Rubin and Yardin (2001) described that on the cell surface of normal cells only few ErbB2 molecules existing compared to the other ErbB family receptors, meaning that only a few heterodimers with ErbB2 are formed and consequently weak growth signals are developed. Upon ErbB2 overexpression, the number of ErbB2 heterodimers increases, resulting in a strong downstream signal. It was shown by

Slamon et al. (1987) that 30% of all breast tumors overexpress ErbB2 and this correlates with worse prognosis for the patients (Ross and Fletcher 1999). Aberrant ErbB2 activation can be a precursor for tumorigenesis and the development of breast cancer due to its influence on cell proliferation, angiogenesis, invasive growth therapy resistance, and metastatic behavior (Menard et al. 2004, Yu et al. 2000, Eccles 2001, Holbro et al. 2003). ErbB2 overexpression has also been reported in other types of cancer, including ovarian carcinoma (Zhang et al. 1989), non-small lung cancer (Schneider et al. 1989) and other human malignancies (Menard et al. 2001).
An oncogenic variant of ErbB2, named NeuT, was isolated from rats (Shih et al. 1981). This activated NeuT carries a point mutation (amino acid exchange from valine to glutamine at position 664) in the transmembrane domain of the receptor resulting in a constitutively active variant (Bargmann et al. 1986) as a result of ligand-independent dimerization. In order to investigate ErbB2/NeuT-mediated oncogenic transformation, Trost et al. (2005) generated a MCF7 breast cancer cell system with doxycycline-inducible expression of the oncogene, NeuT. Unexpectedly, overexpression of NeuT by the addition of tetracycline in MCF7/NeuT cells triggered premature senescence (Trost et al. 2005, Cadenas et al. 2012).

1.5 Oncogene-induced premature senescence

Cellular senescence represents a state of irreversible cell cycle arrest. It is divided into replicative- or oncogene-induced senescence (OIS) and represents, along with apoptosis, a tumor-protective failsafe mechanism (Ohtani et al. 2009). OIS is considered a defense barrier against tumors, but under certain circumstances senescent cells may support tumor progression caused by their secretory phenotype that is enriched in proteases, cytokines and growth factors (Rodier and Campisi 2011). Despite their growth arrest in the G1-phase of the cell cycle (decreased S-phase), senescent cells remaining metabolically active, often acquiring resistance against apoptosis signals and display an altered gene expression pattern (Campisi and d'Abba di Fagagna 2007). Typical senescence markers include the expression of the cell-cycle inhibitor, cyclin-dependent kinase inhibitor p21 (CDKI, WAF1/ CIP1), and the decreased incorporation of 5-bromodeoxyuridine as a marker for DNA replication.

Oncogene-induced senescence has been associated with a decline in lipid synthesis, significant increase in fatty acid oxidation, and elevated inflammatory cytokine production (Quijano et al. 2012). Senescent cells show elevated overall lipid content with evidence of impaired mitochondrial function resulting in a high rate of oxidant formation (Cadenas et al. 2010). Mitochondrial dysfunction leads to increased amounts of reactive oxygen species (ROS), accumulation of depolarized mitochondria around the nucleus accompanied by oxidative DNA damage, decreased ATP production and 5' AMP-activated protein kinase (AMPK) activation (Moiseeva et al. 2009).

Doxycycline-inducible expression of NeuT (oncogenic variant of HER2) in MCF7 cells leads to the expression of the aforementioned senescence-related markers and characteristics in approximately 90% of cells (Trost 2005, Dissertation). Therefore, MCF7/NeuT cells provide a suitable cell model for studying ErbB2-mediated oncogene transformation and subsequent premature senescence.

1.6 Abstract

The association of endothelial lipase LIPG and atherosclerosis is widely accepted but there is only little known and published about the contribution of LIPG in human carcinogenesis. LIPG shows strong phospholipase A1 and little triacylglycerol lipase activity with high-density lipoprotein (HDL) as main substrate. Located on the cell surface binds and cleaves LIPG surrounding HDL followed by cellular fatty acid uptake. Several diseases, including cancer, are accompanied by changes in lipid composition of cellular membranes and alterations in lipid metabolism. The aim of this study was to investigate the contribution of LIPG expression in human breast cancer cells under cellular stress conditions as well as LIPG expression distribution in breast cancer patients and its role in human cancer progression. Affymetrix gene array data analysis in breast cancer patients exhibit LIPG expression in some tumors associated with poor outcome like short metastatic-free survival. *In vitro* shows oncogene NeuT-induced senescence in MCF7 breast cancer cells a LIPG-upregulation in a HER2 independent manner. Our experiments showed that LIPG-overexpression may support tumor cells with exogenous fatty acids in phases of energy deprivation. LIPG expression is a mechanism to preserve mitochondrial integrity in terms of impaired fatty acid synthesis and may protect against reactive oxygen species-induced damage under oxidative stress.

1.7 Zielsetzung der Arbeit

Die Assoziation der endothelialen Lipase LIPG mit Arteriosklerose ist weitgehend akzeptiert, allerdings ist bis heute nur wenig bekannt und publiziert über die LIPG-Beteiligung in der humanen Krebsprogression. LIPG weist eine starke Phospholipase A1, aber nur schwache Triacylglycerid Lipase Aktivität auf mit Lipoproteinen hoher Dichte (HDL) als Hauptsubstrat. Zelloberflächen-assoziiertes LIPG bindet und spaltet umliegendes HDL und ermöglicht die zelluläre Aufnahme von Fettsäuren. Etliche Erkrankungen, Krebs eingeschlossen, sind begleitet durch Umwandelung der Lipid-Zusammensetzung der Zellmembran, sowie Veränderung des Lipidmetabolismus. Ziel dieser Arbeit war es die Beteiligung der LIPG Expression in humanen

Brustkrebszellen unter zellulärem Stress, sowie dessen Verteilung und Funktion in Brustkrebstumoren zu ermitteln. *Affymetrix gene array* Datenanalysen von Brustkrebspatientinnen zeigen LIPG Expression in nur wenigen Tumoren, welche wiederum assoziiert sind mit schlechter Prognose (kürzeres metastasenfreies Überleben). *In vitro* zeigt die onkogene NeuT-induzierte Seneszenz in MCF7 Brustkrebszellen eine HER2-unabhängig erhöhte LIPG Expression. Unsere Experimente zeigten, dass Tumorzellen in Phasen des Energiemangels durch eine LIPG Überexpression mit exogenen Fettsäuren versorgt werden. Darüber hinaus ermöglicht die LIPG Expression einen Mechanismus zur Aufrechterhaltung der mitochondrialen Integrität in Zeiten blockierter Fettsäuresynthese und schützt dadurch gegen reaktive Sauerstoffspecies-induzierte Schäden unter oxidativem Stress.

2. Materials and Methods

2.1 Materials

2.1.1 Cell lines

MCF7: MCF7 (Michigan Cancer Foundation-1; Barbara Ann Karmanos Cancer Institute; ATCC: HTB-22) is an adherent growing breast cancer cell line. It was isolated 1970 from mammary gland of a 69-year old Caucasian woman suffering from invasive breast adenocarcinoma. MCF7 show an epithelial like cell growth with capability of forming domes (Soule et al. 1973).

MCF7/NeuT: MCF7/NeuT cell line was established by Tatjana Trost (Trost et al. 2005) in order to study the consequences of NeuT overexpression (oncogenic variant of receptor tyrosine kinase ErbB2). In this cell lines the NeuT expression is controlled by Tet-On-system meaning a tetracyclin-induced (doxycyclin) expression of the gene of interest. For this purpose MCF7 cells were stably transfected with pcDNA3Neo/rtTA2 plasmid which enables the expression of the reverse tetracyclin-dependent transactivator (rtTA). The second transfected plasmid was pINSpBI-EGFP/NeuT-containing eGFP (enhanced green fluorescent protein) reporter as well as NeuT gene under the control of a tetracyclin responsive element (TRE) as a bidirectional promoter (Fig. 2.1). Through addition of doxycycline to cell media binds rtTA on TRE and initiates the target gene expression. The bidirectional promoter enables simultaneously the expression of the gene of interest and expression of eGFP which facilitates an optic control of expression efficiency. The NeuT gene is coming from the proto-oncogene of rats and carries a point mutation (amino acid change from valine to glutamine at position 664; Bargmann et al. 1986) in

transmembrane domain of NeuT-receptor and results in a constitutive active version.

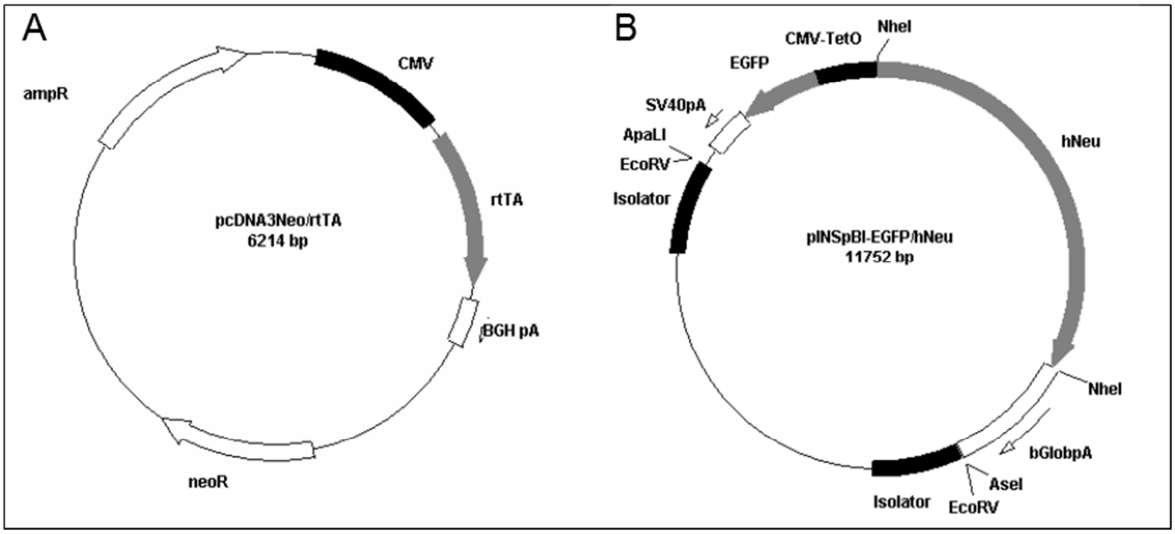

Fig. 2.1: MCF7/NeuT transfection constructs. (A) expression plasmid pcDNA3Neo/rtTA; (B) expression plasmid pINSpBI-EGFP/hNeu

K-562: K-562 cells are a human myelogenous leukemia cell lines derived from a 53 year old female chronic myeloid leukemia (CML) patient in blast crisis (last stage of CML with fast progression and short overall survival) (Drexler 2000, Academic Press). This leukemia cell lines grows as suspension and exhibit less clumping than other suspension cell lines. They lack the MHC molecule complex required to inhibit natural killer (NK) cells activity so they are favored target cells for ^{51}Chromium- release assay application.

NK cells: Natural killer cells (NK cells) are a part of the innate immune system and belong to lymphocytes. They recognize tumor cells or virus-infected cells by missing-self-hypothesis (absence of MHC-I molecules on cell surface) results in binding and disrupting integrity of target cell membrane. In this thesis NK cells were isolated from whole blood samples of voluntary healthy donors.

2.1.2 Antibodies

2.1.2.1 Primary antibodies

antibody	host	company	Catalog No.
α-tubulin	rabbit	cell signaling	2144
Akt-antibody	rabbit	cell signaling	9272
p-Akt (Ser473)	rabbit	cell signaling	9271
ADFP (Plin2)	rabbit	abcam	ab52356
β-actin	mouse	sigma Aldrich	A5316
Cleaved PARP	rabbit	cell signaling	9541
ERK5	rabbit	cell signaling	3372
FLAG	mouse	sigma Aldrich	F1804
Lcn2	rabbit	abcam	ab125075
LIPG (WB)	mouse	sigma Aldrich	WH0009388M2
LIPG (IF)	rabbit	abcam	ab24447
MEK1/2	rabbit	cell signaling	9122
Neu	rabbit	Santa Cruz	sc-284
p38 MAPK	rabbit	cell signaling	9212
p-p38 MAPK	rabbit	cell signaling	9215
p44/42 MAPK	rabbit	cell signaling	9102
p-p44/42 MAPK	rabbit	cell signaling	4377
p-ERK	rabbit	cell signaling	3371
p-MEK1/2	rabbit	cell signaling	9127
p-SAPK/ JNK	rabbit	cell signaling	4668
p21 Waf1/cip	rabbit	cell signaling	2947

2.1.2.2 Secondary antibodies

antibody	company	Catalog No.
anti-mouse IgG, HRP linked	cell signaling	7076
anti-rabbit IgG, HRP linked	cell signaling	7074

anti-mouse AlexaFluor647	Invitrogen	929537
anti-rabbit AlexaFluor647	Invitrogen	A-31573

Tab. 2.1: Antibody (AB) parameters for western blot

primary/ secondary AB	**incubation**	**dilution**
α-tubulin / mouse	o.n. 4°C / 1h RT	1:1000 / 1:5000 in BSA
β-actin / mouse	o.n. 4°C / 1h RT	1:5000 / 1:5000 in BSA
ERK5 / rabbit	o.n. 4°C / 1h RT	1:1000 / 1:1000 in BSA
LIPG / mouse	o.n. 4°C / 1h RT	1:2500 / 1:5000 in BSA
MEK1/2 / rabbit	o.n. 4°C / 1h RT	1:1000 / 1:1000 in BSA
Neu / rabbit	o.n. 4°C / 1h RT	1:500 / 1:1000 in BSA
phospho Akt / rabbit	o.n. 4°C / 1h RT	1:1000 / 1:5000 in BSA
p38 MAPK / rabbit	o.n. 4°C / 1h RT	1:1000 / 1:1000 in BSA
phospho MAPK / rabbit	o.n. 4°C / 1h RT	1:1000 / 1:1000 in BSA
p44/42 MAPK / rabbit	o.n. 4°C / 1h RT	1:1000 / 1:1000 in BSA
phospho p44/42 MAPK / rabbit	o.n. 4°C / 1h RT	1:1000 / 1:1000 in BSA
phospho JNK / rabbit	o.n. 4°C / 1h RT	1:1000 / 1:1000 in BSA
p-ERK5 / rabbit	o.n. 4°C / 1h RT	1:1000 / 1:1000 in BSA
p21 Waf1/cip / rabbit	o.n. 4°C / 1h RT	1:1000 / 1:1000 in BSA
phospho MEK1/2 / rabbit	o.n. 4°C / 1h RT	1:1000 / 1:1000 in BSA
total Akt / rabbit	o.n. 4°C / 1h RT	1:1000 / 1:1000 in BSA

Tab. 2.2: Antibody (AB) parameters for immunofluorescence (IF)

primary/ secondary AB	**incubation**	**dilution**
ADFP (Plin2) / rabbit	o.n. 4°C /2h RT	1:500/ 1:300 in BSA
Bodipy	30min RT	50µg/mL in 1x PBS
DAPI	5min RT	1:20000 in dH_2O

FLAG-Tag/ mouse	o.n. 4°C / 2h RT	1:2000 / 1:500 in BSA
LIPG / rabbit	o.n. 4°C / 2h RT	1:500 / 1:100 in BSA
Rhodamin-Phalloidin	2h RT	1:500 in BSA

2.1.3 Primer and probes

primer	company	Catalog No.
ACSL3	life technologies	Hs00244853_m1
β-actin	Qiagen	QT01680476
CDH1	life technologies	Hs01023894_m1
CDKN1	life technologies	Hs00355782_m1
CHPT1	life technologies	Hs00220348_m1
GAPDH	life technologies	Hs02758991_g1
LDLR	life technologies	Hs00181992_m1
LIPG	life technologies	Hs00195812_m1
MGLL	life technologies	Hs00200752_m1
Nedd9	life technologies	Hs00610590_m1
NeuT	Qiagen	QT00193466
NPC1	life technologies	Hs00181192_m1
PLD1	life technologies	Hs00160118_m1
Plin2	life technologies	Hs00605340_m1
Snai1	life technologies	Hs00195591_m1
TBP	Qiagen	QT00000721
Twist1	life technologies	Hs01675818_s1
TXN	life technologies	Hs01555214_g1
TXNIP	life technologies	Hs01006900_g1
TXNRD1	life technologies	Hs00917067_m1
UBC	life technologies	Hs00824723_m1
Vim	life technologies	Hs00958111_m1

2.1.4 Small interfering RNA (siRNA)

siRNA	company	Catalog No.
β-actin	Ambion (life technologies)	12935-141
GAPDH	Thermo Scientific Dharmacon	D-001830-01-05
LIPG	Invitrogen	HSS190264
LIPG	Invitrogen	HSS113931
LIPG	Invitrogen	HSS113929
Non-sense siRNA	Invitrogen	VHS40202
LIPG	Ambion (life technologies)	s17961
LIPG	Ambion (life technologies)	s17962
LIPG	Ambion (life technologies)	s17963
LIPG	Thermo Scientific Dharmacon	J-009601-05
LIPG	Thermo Scientific Dharmacon	J-009601-06
LIPG	Thermo Scientific Dharmacon	J-009601-07
LIPG	Thermo Scientific Dharmacon	J-009601-08
Non-sense siRNA	Thermo Scientific Dharmacon	D-001810-01-05

2.1.5 Cell culture media

cell lines	media	company
MCF7	500mL Dulbecco's modified eagle media (DMEM) 4.5g/L glucose	PAN biotech
	5mL sodium pyruvate	sigma Aldrich
	50mL heat-inactivated FCS	PAN biotech
	500µL 100x mem NEAA	Gibco
	500µL insulin	sigma Aldrich
MCF7/NeuT	500mL Dulbecco's modified eagle media (DMEM) 4.5g/L glucose	PAN biotech
	50mL tetracyclin-free FCS	PAN biotech

K-562	500mL Iscove's modified Dulbecco's media (IMDM)	Gibco
	50mL heat-inactivated FCS	PAN biotech
NK cells	500mL Iscove's modified Dulbecco's media (IMDM)	Gibco
	50mL heat-inactivated FCS	PAN biotech

experiments	**media/ reagent**	**company**
siRNA transfection & LIPG overexpression	Opti-Mem	Invitrogen
	lipofectamin 2000	Invitrogen
	nanofectin	PAA
	prime kit	PAA
	interferin	Polyplus
	JetPrime	Polyplus
PBMC isolation	LSM 1077 Lymphocytes (Ficoll)	PAA
starvation experiments	500mL Dulbecco's modified eagle media (DMEM) 0g/L glucose	PAN biotech

2.1.6 Inhibitors

inhibitor	**company**	**inhibitor**	**company**
Cerulenin	sigma Aldrich	Oligomycin	sigma aldrich
PD98059	sigma Aldrich	LY294002	sigma Aldrich
SP600125	sigma Aldrich	SB203538	sigma Aldrich
TOFA	sigma Aldrich	Protease inh.	sigma Aldrich
Phosphatase inh.	sigma Aldrich		

2.1.7 Chemical reagents and kits

reagent / kit (company)	reagent /kit (company)
2-mercaptoethanol (sigma Aldrich)	acrylamide (Carl Roth)
albumin fraction V (BSA; Carl Roth)	ammonium chloride (Carl Roth)
ammonium persulfate (APS; sigma A.)	BCA protein assay kit (Thermo S.)
BSA (fatty acid free; sigma Aldrich)	bromophenol blue (Carl Roth)
cDNA kit (applied Biosystems)	CellTiter-Blue cell viability assay
DEPC treated water (Invitrogen)	(Promega)
DMSO (Carl Roth)	DTT (Carl Roth)
EDTA (Carl Roth)	entellan (Merck)
ethanol (Th. Geyer)	FluorPreserve reagent (calbiochem)
formaldehyde (Carl Roth)	glycerol (Carl Roth)
high capacity cDNA RT kit (applied Bios.)	human high density lipopr. (BioTrend)
human low density lipopr. (BioTrend)	glycin (Carl Roth)
hydrochloride acid (Carl Roth)	innuPREP RNA kit (analytic jena)
isopropanol (Carl Roth)	methanol (Carl Roth)
magic marker (Invitrogen)	nonidet P-40 substitute (Roche)
oleic acid (sigma Aldrich)	oil red O (sigma Aldrich)
paraformaldehyde 4% (PFA; C. Roth)	PMSF (Carl Roth)
Rotihistol (Carl Roth)	SDS-pellets (Carl Roth)
sera plus (PAN biotech)	Sodium chloride (Carl Roth)
sodium hydroxide (Carl Roth)	TaqMan master mix (applied Bios.)
TAG quantification kit (abcam)	TEMED (Carl Roth)
TMRE (molecular probes)	Tris (Carl Roth)
Triton X-100 (Carl Roth)	Tween 20 (sigma Aldrich)
western lightning Plus-enhanced chemiluminescence substrate (Perkin-Elmer)	
X-treme gene HP DNA transfection reagent (Roche)	

2.1.8 Commercial buffers and solutions

buffer / solution	company
2x laemmli sample buffer	BioRad
anode buffer concentrate A	C. Roth
cathode buffer concentrate	Carl Roth
Precision plus protein dual color standard	BioRad
Stripping buffer	Thermo Scientific
Trypsin 0.05% / EDTA	PAN biotech

2.1.8.1 Prepared buffers and solutions

buffer / solution	components
APS solution	10% (w/v) APS in H_2O
anode buffer	100mL buffer concentrate + 200mL methanol + 700mL dH_2O
blocking solution	5% (w/v) BSA in TBS-T
cathode buffer	100mL buffer concentrate + 200mL methanol + 700mL dH_2O
loading buffer (5x)	2.25mL 1M Tris-HCL pH 6.8 + 5mL glycerol + 0.5g SDS + 5mg bromophenol blue + 2.5mL 1M DTT
cDNA synthesis reaction mix	4.2µL H_2O + 2µL 10x RT-buffer + 2µL random primer + 0.8µL 25x d'NTP + 1µL reverse transcriptase
PBS (10x) pH 7.4	2g KCL + 2g KH_2PO_4 + 9.2g Na_2HPO_4 + 80g NaCl adjust to a volume of 1L with H_2O
precipitation buffer (proteins)	4M ammonium sulfate in H_2O
RIPA lysis buffer recipe	1% NP-40 (tergitol) + 150mM NaCl + 20mM Tris pH 7.4 + 1mM EDTA pH 8 +

	10mM NaF + 1mM $MgCl_2$ + 1mM Na_3VO_4 pH 10 +
	10% glycerin; adjust with dH_2O up to 500Ml
	add directly per mL RIPA: 1mM DTT +
	1mM protease inhibitor cocktail + 1mM PMSF
running buffer (10x)	30.3g Tris + 144g glycerol + 10g SDS
	adjust to a volume of 1L with H_2O
	pH should be 8.3
separation buffer	3M Tris in H_2O pH 8.8 with HCL
separation (10%) two gels	16mL H_2O + 13.2mL 30% acrylamide +
	10mL separation buffer 0.47M Tris pH 6.8 +
	400µL 10% SDS + 400µL 10% APS + 16µL Temed
stacking buffer	0.47M Tris in H_2O pH 6.8 with HCL
stacking (4%) two gels	14.5mL H_2O + 3mL 30% acrylamide +
	2.5mL stacking buffer 3M Tris pH 8.8 +
	200µL 10% SDS + 300µL 10% APS + 15µL Temed
TaqMan reaction mix	1.25µL TaqMan probe + 12.5µL PCR master mix +
	6.25µL H_2O + 5µL DNA (2ng/µL)
TBS (10x) pH 7.4	12g Tris + 53h NaCl +
	adjust to a volume of 1L with H_2O
TBS-T	250mL TBS (10x) + 2.5mL Tween 20
	adjust to a volume of 2.25L with H_2O
triacylglyceride reaction mix	47.6µL assay buffer + 0.4µL probe +
	2µL enzyme mix

2.1.9 Technical equipment

equipment	**company**
blot imager Vilber Fusion Fx7	Vilber Lourmat
blot chamber fast blot B44	Biometra
Casy cell Counter	Innovatis AG/ Roche

centrifuge megafuge 10R	Thermo Scientific
centrifuge MiniSpin plus	Eppendorf
confocal microscope (LSM) FV1000	Olympus
electrophoresis chamber	BioRad
incubator	Binder
magnetic stirrer IKAMAG RCT	Ikamag
NanoDrop ND-1000	Thermo Scientific
optical microscope eclipse TS 100	Nikon
pH meter	Schott
plate reader Tecan SpectraFluor Plus	Tecan
plate reader Tecan infinite 200Pro	Tecan
power supplies	Biometra
qRT-PCR system ABI 7500	applied Biosystems
precision balance EW150-3M	Kern
sterile hood	Hereaus
thermo cycler Tgradient	Biometra
transfer chamber	Biometra
UV/ Vis spectrometer V-530	Jasco
Water bath	Labortechnik

2.1.10 Consumables

consumables (company)	consumables (company)
6-well plates (Sarstedt)	24-well plates (Sarstedt)
96-well pl. Black clear bottom (Greiner)	175cm^2 cell culture flasks (Sarstedt)
cell scraper (Sarstedt)	cover slips (Menzel)
disposal cuvettes (Brand)	microscope slides (Thermo Scientific)
pipettes sterile (Sarstedt)	PVDF membrane (Perkin Elmer)
reaction tubes (Eppendorf & Falcon)	Whatman paper 3mm (Schleicher)

2.2 Methods

2.2.1 Cell culture

All cell lines were routinely cultured under sterile conditions in the corresponding culture media (material part) and incubated at constant humidity at 37°C with 5% CO_2 and aqueous vapor saturated atmosphere. Cells were sub-cultured twice a week. For this purpose, cells were washed with 1x PBS and detached by trypsin/EDTA. Suspended in fresh full media, cells were re-plated with a 1:3 dilution. The CASY®-Technology (Innovatis AG) was used to determine cell number.

2.2.2 DNA vectors

Two expression vectors were utilized to analyze the transient overexpression of LIPG. The human LIPG Gene cDNA Clone/ORF Clonep/pCMV/hygro-FLAG vector encodes for the human LIPG cDNA whereas the pCMV/hygro-negative control vector (FLAG-tagged) vector was used as an empty vector control (Hölzl Diagnostika Handels GmbH) (Fig. 2.2).

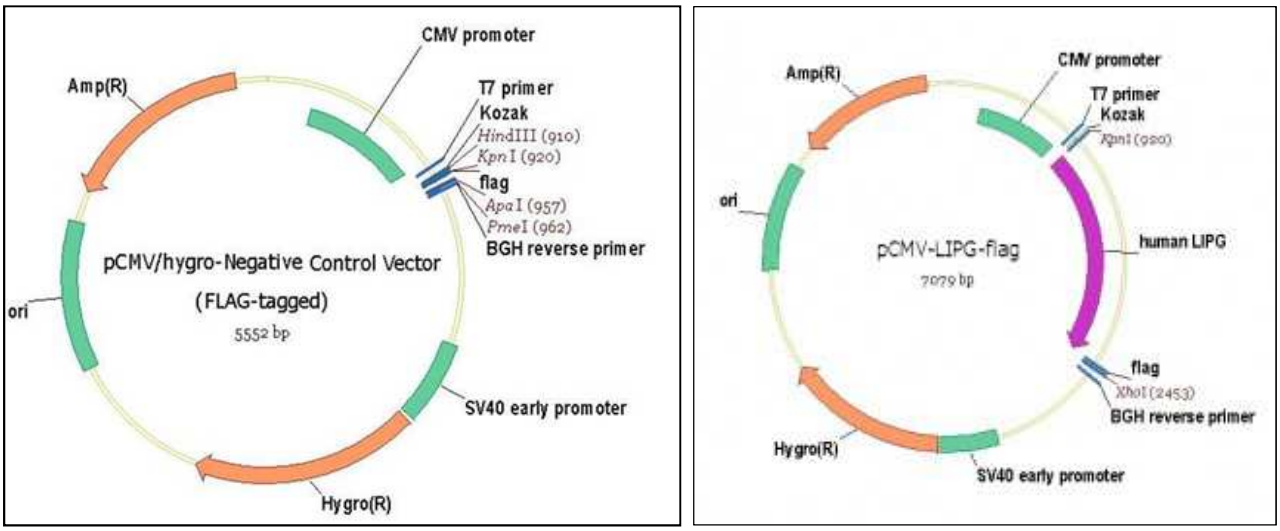

Fig. 2.2: **Illustration of pCMV/hygro-negative control vector (left) and pCMV-LIPG-FLAG vector (right)** (source: http://www.sinobiological.com)

Both vectors carry a cytomegalovirus promoter (CMV), an antibiotic resistance (ampicillin) allowing selection and a FLAG-tag (polypeptide protein tag; Munro and Pelham in 1984) to detect transfected cells and cellular localization by using a specific anti-flag antibody. In contrast to the control vector the pCMV-LIPG-FLAG vector is extended by human LIPG cDNA.

Delivered 10µg vector cDNA had to be amplified and isolated. Therefore followings steps were attached: 1) transformation of bacteria with vectors, 2) culturing and multiply vector-containing bacteria and 3) terminated by vector cDNA isolation by QIAfilter Plasmid Maxi Kit (Qiagen).

2.2.2.1 Transformation of bacteria

Transformation of cells is defined as a permanent, heritable alteration resulting from the uptake and incorporation of a foreign DNA into the host-cell genome (Lodish et al. molecular cell biology, 7th edition). In this thesis DH4α-cells (competent *Escherichia coli, E. coli*) were used for transfection. 50µL *E. coli* cell suspension was defrosted and incubated with 1µL plasmid vector solution for 20min on ice. Following heat shock at 45°C for 45sec resulted in membrane holes that free vector DNA can pass through. After an incubation of two minutes on ice, cells were mixed with 900µL super optimal bouillon (SOC media) for optimal support of stressed cells for one hour at 37°C. 200µL of cell suspension was streaked on lysogene bouillon plates (LB agar media plates) containing ampicillin. Plates were incubated over night at 37°C. For bacteria culturing, a colony was picked from the plate and transferred to 250mL LB media with 25mg/mL ampicillin. Suspension was incubated over two days at 37°C under shaking conditions. The amplified vector DNA was isolated and purified according manufactures instructions of the QIAfilter Plasmid Maxi Kit (Qiagen). Bacteria cells were lysed under alkaline conditions and cleared by QIAfilter cartridges. After mixing the filtrate with endotoxin removal buffer, whole solution was loaded onto anion-exchange tips that selectively bind plasmid DNA under appropriate low-salt and pH conditions. Low-molecular-weight impurities as well as RNA, proteins and metabolites were washed away. Ultrapure plasmid DNA was eluted in high-salt buffer. Using 2-propanol precipitation, DNA that was collected by centrifugation, could be concentrated and desalted.

2.2.2.2 Transient transfection of MCF7 cells

MCF7 cells were transient transfected with the pCMV/hygro-negative control or pCMV-LIPG-FLAG vector. For transfection, MCF7 cells were plated onto 6-well plates ($2x10^5$ cells/ well) and incubated for 24 hours. Afterwards, cells were incubated with transfection mix (2mL serum containing antibiotic-free full media, 200µL OPTI-MEM, 1.5µg vector DNA, 6µL X-tremeGENE HP DNA transfection reagent per well) for 48 hours.

2.2.3 Feeding LIPG-overexpressing MCF7 cells with substrates

After transfection, LIPG-overexpressing MCF7 cells were fed with either 800µg high-density lipoprotein (HDL, BioTrend) or 800µg 1,2-dioleoyl-sn-glycero-3-phosphocholine (DOPC or PC-OA; Avanti polar Lipids) and incubated for 48 hours. HDL is ready to use whereas DOPC had to be solved. 100mg DOPC powder diluted with 10mL DEPC water was incubated for three hours at 45°C in a shaking water bath to get large multi-laminar vesicles. To disrupt these vesicles into small uni-laminar vesicles lipid solution was sonicated for 30 minutes.

2.2.4 Incubation of MCF7 cells with different inhibitors

To analyze LIPG expression change as a possible rescue system in case of starvation or cellular stress conditions, MCF7 cells were treated with inhibitors of *de novo* fatty acid synthesis. Therefore, inhibitors like 5-(Tetradecyloxy)-2-furoic acid (TOFA; sigma Aldrich) and Cerulenin or Oligomycin to block ATP production were used (Fig. 2.3).

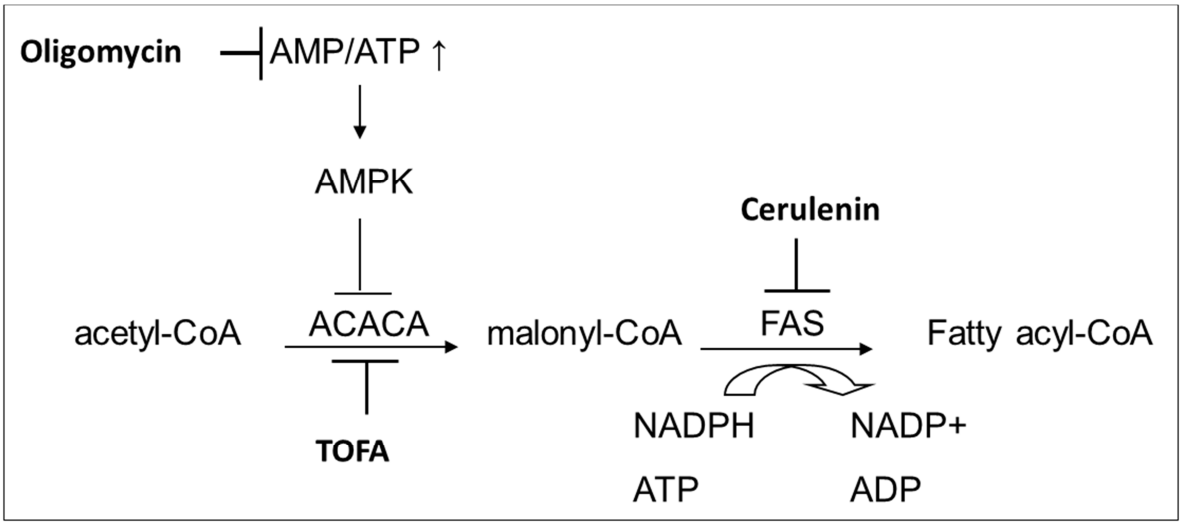

Fig. 2.3: **Blockage of *de novo* fatty acid synthesis**. 5-(Tetradecyloxy)-2-furoic acid (TOFA) blocks the enzyme acetyl-CoA carboxylase (ACACA) activity, avoids the production of malonyl-CoA and consequently blocks the cellular fatty acid production. Inhibition of the fatty acid synthase by Cerulenin results in ATP as well as malonyl-CoA accumulation. Oligomycin blocks the membrane-bound mitochondrial ATP synthase and proton channels that evokes blockage of oxidative phosphorylation and electron transport chain

MCF7 cells were incubated with: 1) 6µM TOFA for 24h or 48h, 2) with 9.98µM and 31.5µM Cerulenin for 12h, 24h and 48h or 3) with 31.5ng, 99.7ng, 315ng, 995ng and 3.15µg Oligomycin for 20min and three hours. All reagents were diluted in DMSO with serum starved media. After incubation, RNA was extracted and LIPG expression was determined by qRT-PCR.

The impact of LIPG on different pathways is quite unknown. Therefore, diverse inhibitors were tested in the MCF7/NeuT cell system to study different pathways (Ras/ Raf/ MEK/ ERK; PI3K/ Akt; p38/ MAPK and SAPK/ JNK) that affect LIPG expression. MCF7/NeuT cells were incubated with doxycycline in presence or absence of specific inhibitors LY294002 (20µM, blocks Akt/ PI3K pathway), SB203538 (25µM, blocks p38-pathway), PD98059 (25µM, blocks MEK1/2- pathway) and SP600125 (25µM; SAPK/ JNK pathway). Afterwards, cells were incubated over seven days.

2.2.5 Determination of mitochondrial membrane potential

Mitochondrial membrane potential-mediated accumulation of tetramethylrhodamine ethyl ester perchlorate (TMRE) within inner membrane regions is an indication of healthy functioning mitochondria. In case of depolarization (changes in membrane potential towards more positive potential) or inactive mitochondria, membrane potential is decreased and fails to sequester TMRE (loss of dye at least less fluorescence). LIPG-overexpressing MCF7 cells were fed with 800µg PC-OA for 48h followed by treatment with 6µM TOFA for 48h. For TMRE-staining, cells were washed once with 1x PBS and incubated with 10µM TMRE/DMSO (10mg TMRE solved in 500µL DMSO) in media containing serum for 20min at 37°C. After staining cells were trypsinated with 200µL Trypsin/EDTA and collected with 800µL media plus serum. 200µL of staining cell suspension was transferred onto black 96-well plates with clear bottom (Greiner). The TMRE fluorescence was detected by excitation 545nm and emission 575nm within a plate reader (Tecan SpectraFluor Plus). In addition, background fluorescence was measured.

2.2.6 Knock down experiments

Small interfering RNAs (siRNA) were used cells to knock down the gene of interest and to study the function of LIPG. SiRNAs are a class of double-strand RNA (20-25bp) which can interfere with the expression of a specific gene with complementary nucleotide sequence (Fire et al. 1998). In this thesis, ten different siRNAs were tested (Invitrogen, Dharmacon and Ambion) using either the transfection reagents Lipofectamin 2000 (Invitrogen), Nanofectin (PAA), Prime Kit (PAA), Interferin (Polyplus), JetPrime (Polyplus) or electroporation (Lonza). All reagents and chemicals were used according to the manufactures instructions.

2.2.7 Gene expression analysis

Analysis of gene expression in eukaryotic cells based on mRNA abundance was performed by qRT-PCR. For this purpose, RNA was isolated and transcribed into cDNA.

2.2.7.1 Isolation of RNA

Total RNA was isolated using innuPREP RNA Kit (Analytik Jena) according to manufactures instructions.

Cultured MCF7 cells were washed with 1x PBS after removing media. Afterwards, cells were detached by adding 400µL RL lysis buffer to each well. Cell suspension was collected by cell scrapers and transferred to tubes. Cells were gently mixed by pipetting up and down to insure the complete disruption. The mixture was placed into a spin filter D column that is placed in a 2mL receiver tube. Column was centrifuged at 10.000x rpm for two minutes to separate genomic DNA and proteins from RNA. The filtrate was mixed with 400µL 70% ethanol, transferred into spin filter R that is placed in a receiver tube and centrifuged at 10.000xg for two minutes. In this step total RNA will bind to the silicon filter. The filter was washed with 500µL HS buffer and subsequently with 750µL LS buffer by centrifugation at 10.000xg for one minute. To remove any residual ethanol, the column was centrifuged at 10.000xg for three minutes. Afterwards the filter was placed into a fresh tube, incubated with 20µL RNase-free water and centrifuged for one minute at 8.000xg to elute the total RNA. RNA samples were stored at -80°C.

2.2.7.2 RNA quantification

The NanoDrop-1000 spectrophotometer (Thermo Scientific) enables the quantification of isolated RNA. The principal behind is to measure the light which passes a liquid sample. A pulsed xenon flash light lamp (source of light) facilitates the computer-based analysis. The spectrophotometer is constructed by two optic fiber cables (one in the sampling arm and one on the sample receiver place) that are connected by closing the sampling arm. The machine is initialized with 1.5µL RNAse-free water (blank) followed by measurement of isolated RNA samples resulting in three values for each sample. The absorbance at 260nm reveals the RNA concentration [µg/µL]. Second the purity of RNA based on absorption at 260/280nm (values of ~2.0 are accepted as ,,pure'' for RNA). Third value gives the result of an additional measurement of nucleic acid purity based on absorbance 260/230nm (values in the range of 1.8-2.2 are accepted as ,,pure'' for RNA).

2.2.7.3 cDNA synthesis

Transcription of RNA to cDNA permits to work with stable DNA instead of susceptible RNA that degrades quickly. Based on reverse transcription reaction, the high capacity cDNA reverse transcription kit (Applied Biosystems) was used. The enzyme reverse transcriptase (RT) synthesizes cDNA strand by adding complementary nucleotide bases on mRNA template. Starting point provides a short DNA sequence of oligo-dT primer that binds on the poly-A sequence of all 3'-end mRNAs. The secondary strand will be synthesized after degradation and displacement of mRNA by RT.

The reverse transcription was performed using a thermo cycler (Biometra). Synthesized cDNA with a concentration of 1µg were diluted with 480µL DEPC water to a final concentration of 2ng/µL and stored -20°C.

Tab. 2.3: Thermo cycler program

step	temperature	time
incubation	25°C	10min
reverse transcription	37°C	120min
inactivation	85°C	5min
	4°C	∞

2.2.7.4 Quantitative real time polymerase chain reaction (qRT-PCR)

Quantitative real time polymerase chain reaction (qRT-PCR) allows the qualitative and quantitative detection of target gene expression. Figure 2.4 illustrates the principle of qRT-PCR which includes the polymerization of cDNA strands, strand displacement and cleavage of the reporter. Particularly, the TayMan probe is of importance for this technique. This oligonucleotide probe carries a quencher (low energy molecule) on the 3'-end and a reporter (high energy dye, 6-FAM fluorescence labeled) on the 5'-end. Due to the proximity the quencher reduces the intensity of the reporter fluorescence by fluorescence resonance energy transfer (FRET). The

extension phase, in which the forward primer binds on the 5'-end of DNA, induces the degradation and displacement of the TayMan probe. The growing distance between quencher and reporter leads to a released reporter fluorescence. Increasing fluorescence intensities were detected automatically and results in a Ct-value (cycle threshold). This Ct-value describes the point when reporter fluorescence intensity exceeds background fluorescence (threshold line). Beginning of the exponential amplification of a sample is accepted to set an accurate threshold line. Analysed samples are accompanied by a reference gene called endogenous gene or housekeeping gene as an internal standard. Reference genes should also be expressed in used cell lines and should not show altered expressions over experimental variables.

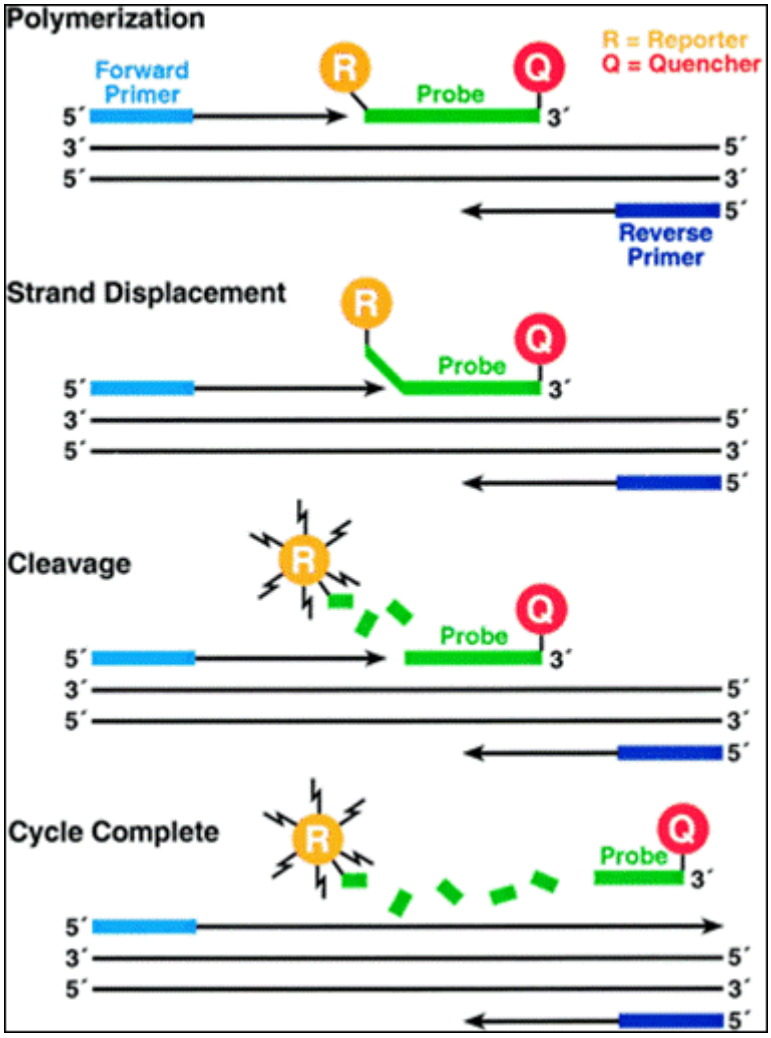

Fig. 2.4: **Principle of qRT-PCR** (source: www.lifetechnologies.com)

For this work, the qRT-PCR assay on 96-well plate formates was performed using the ABI 7500 (applied Biosystem).

Each well contained 20µL reaction mix and 5µL DNA with an end concentration of 10ng/ well. Covered plates were centrifuged 400xg for 1min and analyzed.

Tab. 2.4: Parameters of standard amplification

step	temperature	time
heating up	50°C	2min
enzyme activation	95°C	10min
denaturation	95°C	15sec
annealing & elongation	60°C	1min
repetition of denaturation and annealing & elongation		40 times

To quantify the expression of target genes the ΔΔCt-method was applied. This relative quantitative method calculates the correlation between treated against untreated samples. All expression levels of target genes were normalized to expression level of the reference gene.

The ΔΔCt-method includes following calculation steps:

- Ct = threshold cycle
  Cycle numbers to reach a constant fluorescence niveau (beginning of exponential phase)
- $\Delta Ct = Ct_{\text{target gene}} - Ct_{\text{reference gene}}$
  Normalization of all observed genes or treatments
- $\Delta\Delta Ct = \Delta Ct_{\text{treated target gene}} - \Delta Ct_{\text{target gene control sample}}$
  Relationship of $\Delta Ct_{\text{treated sample}}$ to $\Delta Ct_{\text{control}}$ (untreated sample) => modification caused by treatment
- Calculation of $2^{-\Delta\Delta Ct}$

Relative expression alteration of one sample compared treatment and control, normalized to reference relevant to standard sample calculates by arithmetic mean.

2.2.8 Protein analysis

To examine the consequences of treatments on particular proteins in a complex sample such as cell, proteins have to be isolated, quantified, separated by gel electrophoresis (SDS-page) and transferred to a membrane by western blotting (WB). Specific antibodies facilitate the detection of membrane bound proteins.

2.2.8.1 Isolation of proteins from eukaryotic cells

LIPG is synthetized intracellular with a size of 55kDa. Glycosylated LIPG (68kDa) is transported to cell membrane and will be secreted into the media. Afterwards, LIPG is cleaved into two fragments of 28kDa and 40kDa by pro-protein convertases. Therefore, whole cell protein extraction and preparation of extracellular proteins is necessary for a proper protein analysis.

2.2.8.2 Isolation of extracellular proteins

Collected cell media was incubated with 4M ammonium sulfate ($(NH_4)_2SO_4$) on an orbital shaker for 24h at 4°C. Precipitated samples were centrifuged at 2.000xg for 30min at 4°C, pellets suspended with RIPA lysis buffer and stored at -80°C.

2.2.8.3 Isolation of membrane-bound LIPG protein

Heparin are polysaccharides that interrupts heparin sulfate proteoglycans (HSPG) protein connections between LIPG protein and cell membrane. HSPGs are part of the extracellular matrix located on cell surface. As strongly glycosylated glycosaminoglycans, proteoglycans provide stability between two cells as well as the bridging of proteins to cell surface. Treatment of cells with 10U/mL heparin cleaves

membrane-bound LIPG into media. Cleaved LIPG was collected and handled as described for isolation of extracellular proteins (2.2.8.2).

2.2.8.4 Isolation of intracellular whole cell lysate proteins

Cells were grown to 70% confluence in 6-well plates using specific media. To isolate whole cell lysates each PBS-washed well was treated with 200µL RIPA lysis buffer for two minutes on ice. Cell suspension was collected in tubes by using cell scraper. For digestion, cell membrane suspensions were incubated for 20min on ice followed by centrifugation at 13.000xg for 15min at 4°C. Supernatant contained released proteins were transferred into fresh tubes. Protein lysates were stored at -80°C.

2.2.8.5 Protein quantification BCA assay

Bicinchoninic acid (BCA) assay (Thermo Scientific) enables quantification of isolated proteins (Smith et al. 1985). This bioanalytical assay is based on colorimetric detection of complexed Cu^{+} that is proportional to the proteinconcentration (Fig. 2.5).

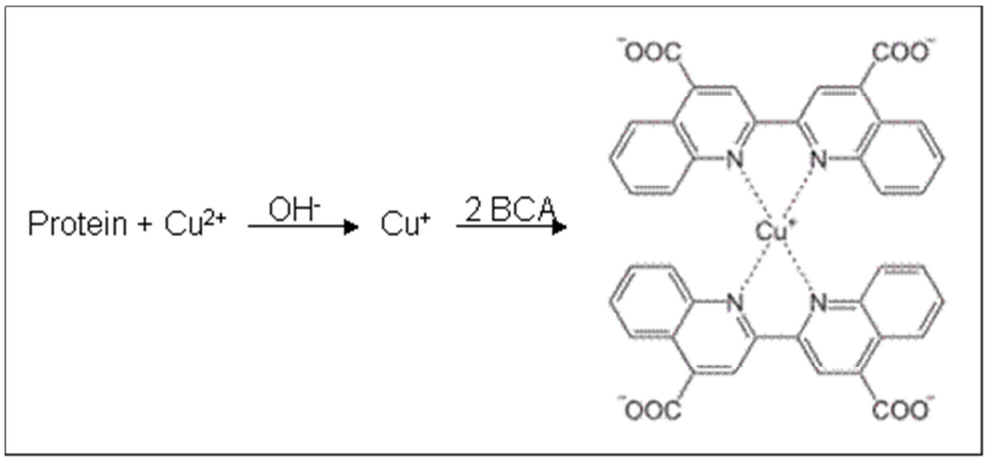

Fig. 2.5: **Principle of BCA assay** (F. Lottspeich and J.W. Engels)

First step of the BCA assay is the so called Biuret reaction describing the reduction of Cu^{2+} ions to Cu^{+} in an alkaline environment. This BCA-copper complex is water-

soluble and detectable with an absorbance at 562nm. The amount of total proteins in the samples is proportional to the amount of Cu^{+}.

Protein samples were defrosted on ice and diluted with water using 5µL sample and 795µL water. Afterwards, 196µL reagent A (bicinchoninic acid, alkaline solution) plus 4µL reagent B (4% cupric sulfate) was mixed and incubated at 60°C for 30min on a shaker. Subsequent, samples were incubated at room temperature for ten minutes. The measurement was performed in cuvettes placed in an UV/VIS spectrophotometer (V-530, Jasco). Total protein amount was determined at a wavelength of 562nm. The computer software ‚spectra manager' determines protein quantity by using a standard curve of serum albumin.

2.2.8.6 SDS polyacrylamide gel electrophoresis and western blot

Sodium dodecyl sulfate polyacrylamide gel electrophoresis (SDS-PAGE) termed a commonly used technique for separation followed by detection of proteins using western blot. Applying electric current, the gel acts as a sieve that smaller proteins can migrate faster than larger proteins. Treatment with SDS (a negatively charged detergent) dissociates multimeric proteins and denatures all polypeptide chains. Proteins were linearized and their own charge covered by SDS (constant mass/ charge ratio). Based on this initial step electrophoretic separation only depends on the molecular weight of the proteins.

2.2.8.7 Gel preparation

Gels were prepared and poured using MiniPROTEAN Tetra electrophoresis system (BioRad) following the manufacturer's instructions. For the LIPG protein with a maximal size of 68kDa a gel with 10% SDS was used. The top gel called stacking gel is slightly acidic (pH 6.8) with a low acrylamide amount to form a porous gel to collect the samples. The lower gel termed separation gel is more basic (pH 8.8) with a higher polyacrylamide content. This gel functions as a sieve to separate the proteins based on their molecular weight.

2.2.8.8 Gel electrophoresis

SDS gel electrophoresis facilitates the separation of proteins in polyacrylamide gels with an applied electric current. For protein preparation 30µg for each protein were mixed with 5x loading buffer and heated up for five minutes at 95°C (denaturation of proteins). The loading buffer contains dithiothreitol (DTT) to reduce disulphide bridges in proteins. Furthermore, the buffer contains glycerin and bromophenol blue to increase the density of samples and to visualize samples, respectively. Each well was loaded either with one sample or with standards. The precision plus protein standard dual color (BioRad) standard and the MagicMark (Invitrogen) were used. The gels were placed in chambers. Chambers were filled with 1x running buffer and initially run at 25mA until the protein samples passed into the separation gel. Afterwards, current was increased to 50mA allowing the samples to run until the dye front reached bottom of gel.

2.2.8.9 Western blotting

Western blotting is a technique to transfer proteins from gel (e.g. SDS gel) on polyvinylidene difluorid (PVDF) membranes. Proteins were immobilized on the membrane by hydrophobic interactions and hydrogen bonds without impairing their immune reactive properties. Utilizing specific antibodies, proteins of interest can be detected and visualized on the membrane.

Trans-blot semi-dry electrophoretic transfer apparatus (BioRad) transfers the separated proteins from SDS-PAGE gel to PVDF membrane. In total, 16 blotting papers (Whatman, VWR) and one PVDF membrane with the exact size of the SDS-PAGE gel were used. The PVDF membrane was activated in methanol and equilibrated in anode buffer. In addition, twelve blotting papers were placed in anode buffer. The gel and four blotting papers were equilibrated in cathode buffer. After equilibration, all components were layered from anode to cathode as followed: twelve anode blotting papers, PVDF membrane, SDS-PAGE gel and the four cathode blotting papers. The transfer was performed for 40min at 315mA per gel (5mA/cm^2). Afterwards membrane was washed for five minutes with distilled water.

2.2.8.10 Protein detection with specific antibodies

Membranes were incubated with 5% (w/v) bovine serum albumin (BSA) in TBS-T for one hour at room temperature to avoid unspecific antibody binding. Membrane was exposed to primary antibodies, diluted in blocking buffer, and incubated over night at 4°C on an orbital shaker. Unbound antibodies were removed by washing with TBS-T for 30min at room temperature. Afterwards, membrane was incubated with secondary antibodies that were conjugated to horseradish peroxidase (HRP) and diluted in blocking buffer. After incubation for 60min at room temperature, washing procedure was repeated. To detect the protein of interest, membranes were incubated with Western lightning ECL solution (Perkin Elmer). This ECL chemistry is based on a chemiluminescence reaction in which the enzyme HRP catalyses the light emission from the oxidation of luminol at a wavelength of 428nm. Detection and visualisation was performed using Fusion Fx7 imager (Vilber Lourmat).

2.2.9 Immunofluorescence

Specific proteins or antigens in tissues or fixed cells can be visualized by immunofluorescence (IF) using fluorescent dyes or fluorescently-labeled antibodies. These fluorophors absorb light at a specific wavelength and emit light of lower energy. Antigen-antibody interactions, visualized by fluorescence detection can be examined using fluorescence or confocal microscopy (Fig. 2.6).

IF methods are separated into two groups. For the direct IF, specific antibodies that are conjugated to a fluorophore (e. g. fluorescein or rhodamine) are used. For the indirect method, a primary antibody and a fluorophore-conjugated secondary antibody are necessary.

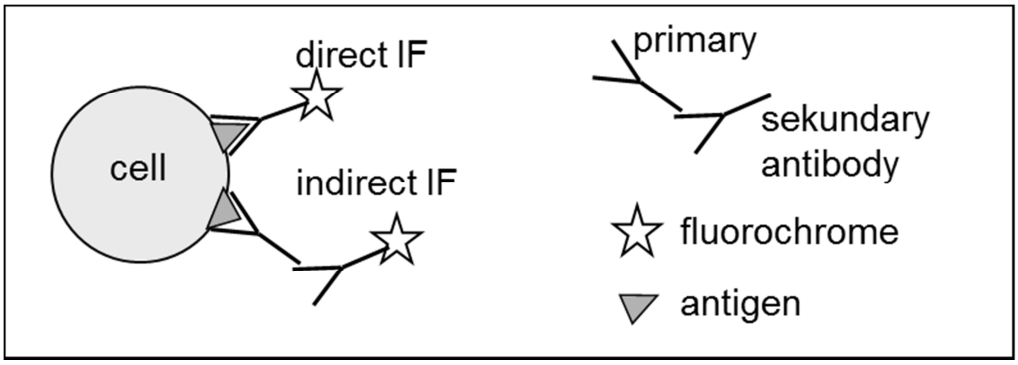

Fig. 2.6: **Schematic illustration of direct vs. indirect immunofluorescence**

2.2.9.1 Indirect immunofluorescence staining for target proteins in this thesis

MCF7 cells were cultured and treated on cover slips that were placed in 24-well plates. Cells were washed with 1x PBS and fixed with 4% paraformaldehyde (PFA) for 20min at room temperature. After three times of washing with 1x PBS, each for five minutes, cells were permeabilized for ten minutes with 0.3% Triton X-100 at room temperature and washed again. Unspecific antibody binding was avoided by incubation with 3% BSA in PBS for two hours at room temperature. Primary antibody was diluted in 0.3% BSA and incubated with MCF7 cells over night at 4°C. After washing with 1x PBS, cells were incubated with secondary antibody, diluted in 0.3% BSA in PBS, together with phalloidin-eosin (1:500 dilution) to visualize the actin-cytoskeleton filaments. Cells were washed after incubation for two hours at room temperature and subsequently incubated with DAPI (1:20.000 dilution in water; 4',6-Diamidin-2-phenylindol) for 5 min at room temperature to stain nuclei. In addition, Bodipy 493/503 (50µg/mL; life technologies) was used to visualize lipid droplets. After washing with 1xPBS, cover slips were transferred from wells onto glass slips mounted and fixed with a drop of FluorPreserve reagent (Calbiochem). The slides were dried over night at room temperature and stored at 4°C in the dark until confocal microscopic analysis (LSM, light scattered microscope; FluoView TM FV1000; Olympus).

2.2.10 Resolving and complexation of oleic acid (OA) on bovine serum albumin

MCF7 cells were incubated with OA/BSA to observe a maximum of lipid accumulation and resulting effects of increased intracellular fat content. Therefore oleic acid (OA) had to be dissolved and complexed on bovine serum albumin (BSA). Firstly 3.71g fatty acid-free BSA (FAF-BSA; sigma Aldrich) had to be solved in 22.5mL dH_2O. Oleic acid (sigma Aldrich) was solved in 2.6mL 0.01M NaOH solution under stirring for 30min at 75°C in the dark. After OA cooled down, it was mixed with three drops 1M NaOH. Complexation of 2.6mL 60mM OA on 10.4mL 2.5mM FAF-BSA was performed under stirring conditions for one hour at room temperature in the dark. OA was completely solved when ,,fat drops'' were under detection limit. Suspensions were sterile filtrated with 0.45µm filter and stored at -20°C.

2.2.10.1 Resolving oleic acid (OA) in DMSO

To avoid involuntary side effects of bovine serum albumin, cells were incubated with OA dissolved in DMSO. Therefore a stock solution of 750mM OA in DMSO was prepared and diluted with serum-starved media to a final concentration of 710µM.

2.2.11 Proliferation assay

Increased fat content is well known as an advantage under starvation conditions. To study survival advantages, MCF7 cells were treated with OA/BSA and starved over a time of period. Read out was counting the number of living cells.

50.000 MCF7 cells were seeded onto 24-well plates to let them attach for 24h. After washing once with 1x PBS, cells were incubated with 200µg, 400µg and 800µg OA/BSA for 48h in serum-free media. As control, cells were cultured in complete full media. All cells were washed once with 1x PBS and cultured in starvation media without any substrates (w/o serum, w/o glucose, w/o sodium pyruvate, w/o 100x mem NEAA and w/o insulin) except a part of control cells that were maintained in complete full media. Number of living cells were counted at different time points (0h corresponds to time point of media change after 48h incubation with OA/BSA and then after 48h, 5d, 7d and 10d).

2.2.11.1 Cell viability assay

To analyze survival advantage of LIPG-overexpressing cells, fed with PC-OA, the cell viability was measured by CellTiter-Blue® cell viability assay (Promega). Therefore, glucose- and serum-starved MCF7 cells were analyzed. MCF7 cells (50.000 cells/well) were seeded onto 24-well plates and incubated for 24h. Cells were transiently transfected with LIPG-DNA for 48h followed by PC-OA incubation in serum-starved media for 48h. Cells were washed once with 1x PBS and cultured in starvation media without any substrates (w/o serum, w/o glucose, w/o sodium pyruvate, w/o 100x mem NEAA, w/o insulin). The number of viable cells was estimated using the indicator resazurin to determine metabolic capacity of cells. Living cells reduce resazurin (blue and non-fluorescent) to resorufin (pink and highly fluorescent) by different enzymes. Resaruzin is able to penetrate cells whereas fluorescent resorufin dye is able to diffuse out of cells into supernatant. Each cell-containing well was incubated over four hours in 100µL media with serum plus 20µL resazurin solution in the dark. Fluorescence signal was determined by excitation 540nm and emission 590nm within a plate reader (Tecan infinite 200Pro) and is proportional to the number of viable cells.

2.2.12 Isolation of triglycerides from eukaryotic cells

LIPG enables fatty acid uptake based on its phospholipase A1 and triglyceride lipase activity. Addition of HDL or PC-OA to LIPG-overexpressing or OA/BSA to untreated MCF cells resulted in intracellular lipid accumulation. Cellular fatty acid uptake leads to formation of triacylglycerides (TAG) stored in lipid droplets. These accumulated TAGs can be isolated and quantified (2.2.12.1). HDL-treated cells were incubated with 10U/mL heparin for 30min to cleave membrane-bound lipoproteins which were not internalized. After washing with 1x PBS, cells were mixed with 200µL 5% NP-40 in water and heated three times up to 90°C to segregate cytoplasmic membrane. Whole insoluble material was removed by centrifugation at 4.000xg for two minutes at room temperature. The supernatant-containing mono-, di- & triacylglycerides were transferred to fresh tubes and mixed with 20µL DEPC water. Samples were stored at -20°C.

2.2.12.1 Quantification of triacylglycerides (TAG)

LIPG-overexpressing cells incorporating fatty acids that were accumulated into TAGs and stored in lipid droplets. The Triglyceride Quantification Kit (abcam) enables the quantification of TAGs based on enzymatic cleavage of TAGs into their components glycerol and free fatty acids (FFA) (Fig. 2.7). Released glycerol will be oxidized and reacts with fluorescence labeled probe.

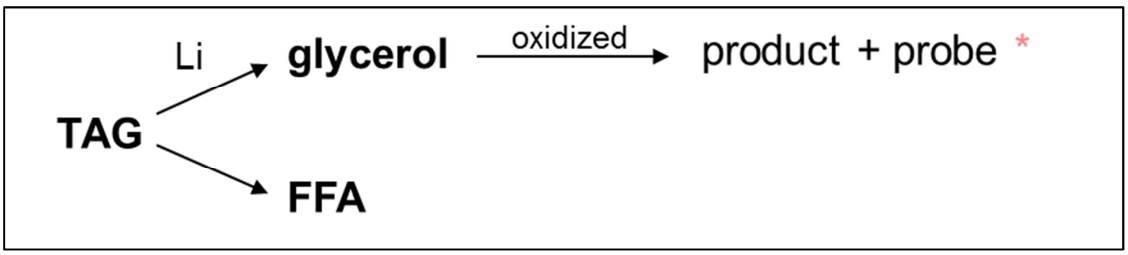

Fig. 2.7: **Principle of the Triglyceride Quantification Kit (abcam).** The enzyme lipase (Li) cleaves TAGs into the components glycerol and free fatty acid. Oxidized glycerol will react with the fluorescence labeled probe. Asteriks indicate fluorescence with excitation at 535nm and emission at 587nm

Black 96-well plates with clear bottom were used to avoid fluorescence spreading while measurement. The total protein concentration of isolated TAG samples was quantified by BCA assay (2.2.8.5) to apply a defined protein amount. 50µg sample adjusted to 50µL with assay buffer was incubated for 20min at room temperature with or without 2µL lipase enzyme. Each well was filled up with 50µL TAG reaction mix and incubated for one hour at room temperature in the dark.

Intracellular TAG amount was detected by fluorescence measurement with excitation at 535nm and emission at 587nm within a plate reader (Tecan SpectraFluor Plus). To correct the influence of background fluorescence, assay buffer plus reaction mix with or without lipase enzyme were simultaneously measured.

Quantification of TAG amount included following calculation steps:

- sample + lipase = total glycerol; sample alone = glycerol background
- RFU_{sample} - $RFU_{background}$ = RFU only from samples
- $RFU_{sample + lipase}$ – $RFU_{sample\ alone}$ => glycerol from TAG (TAG amount)

2.2.12.2 Detection of lipid droplets

Lipid droplets were visualized by staining with oil red O (sigma Aldrich). LIPG-overexpressing MCF7 cells were treated with HDL or PC-OA or OA/BSA to untreated MCF cells. Oil red O powder was solved in 2-propanol and diluted with water (3:2). Solution was incubated for 30min at room temperature and sterile filtrated before use. After washing with 1x PBS, cells were incubated with oil red O solution for one hour at room temperature. Stained cells were washed with 1x PBS and analyzed using optical microscopy.

2.2.13 Working with immune cells

Natural killer cells (NK cells) belong to the group of lymphocytes but are part of the innate immunity. NK cells were isolated from whole blood samples coming from voluntary healthy donors.

2.2.13.1 Isolation of NK cells from whole blood samples

Isolation of NK cells from whole blood samples begins with extraction of peripheral blood mono-nucleated cells (PBMC). Therefore, 15mL lymphocyte separation medium (LSM/Ficoll, density gradient d= 1,077g/mL; Lonza) per tube were carefully overlayed with 30mL heparinized (100U/mL) whole blood. Gradient centrifugation at 2.200rpm for 25min at room temperature (without using brake) separates components of whole blood (Fig. 2.9). PBMCs (lymphocytes and monocytes) were concentrated in interphase (white layer) between plasma and Ficoll. Plasma was aspirated and PBMC-containing white layer was transferred into a fresh tube. PBMC suspension was washed two times with 1x PBS and centrifugation at 1.500rpm for five minutes at room temperature.

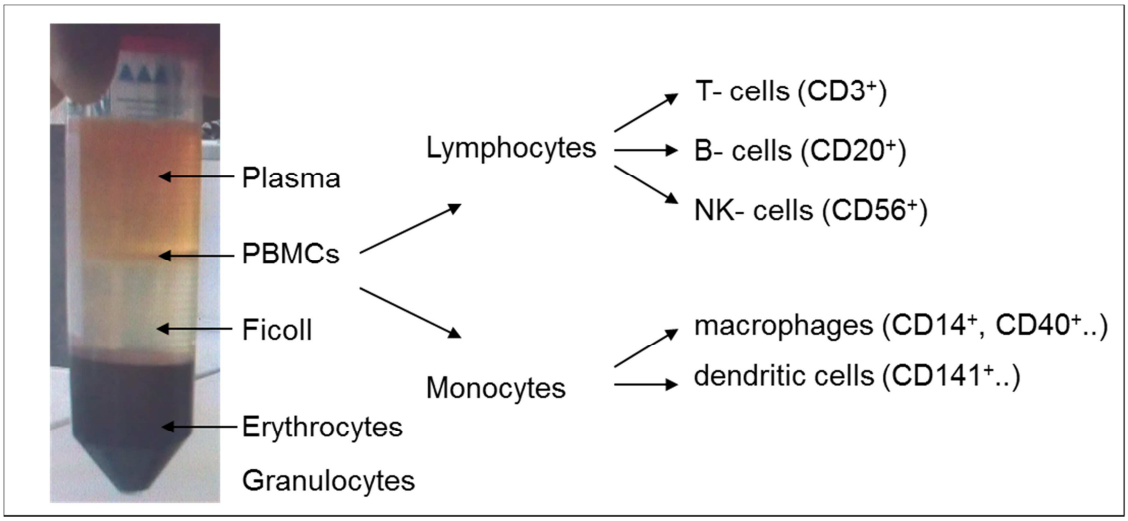

Fig. 2.9: Isolation of PBMCs by gradient centrifugation

After centrifugation, supernatant was removed and pellet was suspended in Dynal buffer (1x PBS + 0.1% BSA) to a concentration of $1x10^8$ cells/mL. NK cells were isolated following manufactures instructions of Dynabeads® Untouched™ Human NK Cells protocol (life technologies). Suspended PBMCs (1mL) were mixed with 200µL heat inactivated fetal bovine serum (hi-FBS) plus 200µL antibody mix and incubated for 20min at 4°C. Antibody mix contained biotinylated mouse IgG antibodies for CD3, CD14, CD36, CDw123, HLA class II DR/DP and CD235a (Glycophorin A) to deplete contaminating cells as T-cells, B-cells, monocytes, dendritic cells, platelets, macrophages, granulocytes and erythrocytes. Cells were washed by adding 4mL isolation buffer and centrifuged at 350xg for eight minutes at 4°C. Cell pellet was suspended in 1mL Dynal buffer and 1mL of pre-washed Dynabeads (uniform, super paramagnetic, polystyrene beads coated with streptavidin) was added. After incubation for 15min at 18°C, cells were suspended in 4mL isolation buffer by pipetting (avoided foaming) and placed in magnet for two minutes (this step was repeated two times). The supernatant contained unbound human NK cells and was transferred into a fresh tube. To remove remaining supernatant, cells were centrifuged at 300xg for ten minutes at room temperature. Supernatant was discarded and cells were suspended with standard media ($1x10^6$ cells/mL in IMDM media; Gibco). To ensure maximal activity of freshly isolated NK cells, cells were stimulated with so called feeder cells (K562mb15-41BBL; 10x 10^6 NK cells + 5x 10^6

feeder cells) and 200U/mL interleukin-2 (IL-2; cytokine stimulated proliferation, differentiation and activation of lymphocytes) for two weeks at 37°C.

2.2.13.2 ^{51}Cr-release assay (killing assay)

Using the ^{51}Cr-release assay the cytotoxic activity of NK cells or the resistance of target cells of NK cell attacks can be quantified. Treated target cells were incubated with radioactive labeled chromium (^{51}Cr) and co-cultured with NK cells. Killer cells damaging target cells and released chromium amount gives a value for killing resistance.

200.000 K-562 (leukemia) suspension cells were incubated over 48h with OA/BSA or BSA alone to internalize fatty acids and accumulate lipids to form lipid droplets. After washing with 1x PBS cells were trypsinated and counted. 5.000 target cells per sample were labeled with 100µCi ^{51}Cr ($Na_2{}^{51}CrO_4$) for one hour at 37°C under soft rotation. Before co-culturing with titrated dilution of NK cell (1:50, 1:25, 1:12.5, 1:6.25) amount target cells were washed two times with standard media. Co-culturing step took four hours at 37°C (Fig. 2.10).

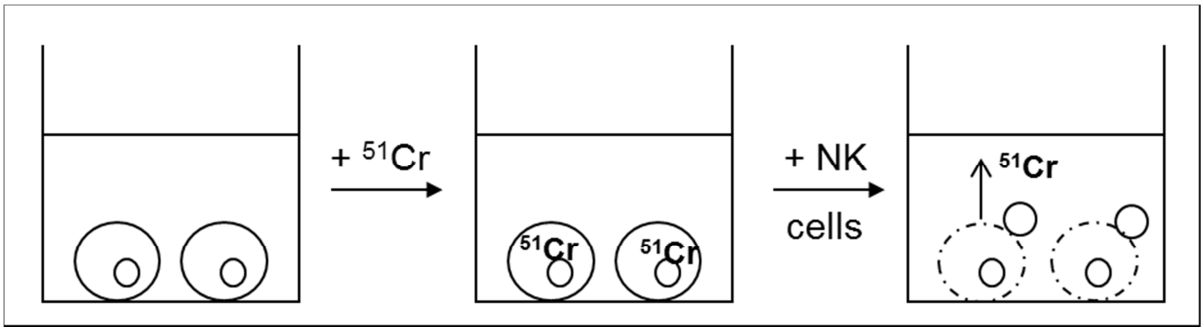

Fig. 2.10: **Schematic illustration of killing assay (^{51}Cr-release assay).** K-562 target cells were labeled with ^{51}Cr for one hour at 37°C. After washing target cells were co-cultured with NK effector cells for four hours at 37°C. NK cells bind and damage target cell membrane which results in ^{51}Cr-release into media supernatant.

Carried along controls were first labeled K-562 cells alone as negative control (spontaneous Cr-release set to 0%) and labeled K-562 cells incubated with 100µL 2% Triton X-100 as positive control (maximal Cr-release set to 100%). While co-culturing effector cells (NK) bind and lyse target cells (K-562) hence ^{51}Chromium

were released into media supernatant. The complete supernatant were sponged up by absorbent cotton and measured by liquid scintillation (gamma counter). Results of the killing assay were specific lysis in [%] calculated software-based directly after measurement by integrating the spontaneous as well as maximal ^{51}Cr-relase control value.

Calculation of specific lysis [%]:

$$\frac{^{51}\text{Cr-release of target (co-cultured cells)} - ^{51}\text{Cr-release of negative control}}{\text{Maximum } ^{51}\text{Cr-release} - ^{51}\text{Cr-release of negative control}}$$

2.2.14 Statistical methods

If not mentioned separately were all experiments done with three independent biological samples. For statistical comparison of control cell situations against treated cells the unpaired T-test was applied. P-values with $p<0.05$ were accepted as significant. All mentioned numeric numbers were mean values and standard error of measurement (SEM).

2.2.14.1 Affymetrix gene array data of breast cancer patients

This study includes four cohorts (Mainz, Rotterdam, Transbig and Yu) which offered breast cancer patient data. Application of the Cox model enables the calculation of associations between LIPG RNA expression (log2 transformated) and prognosis (outcome). The univariate Cox-analysis was applied to evaluate the association between LIPG mRNA expression and metastasis-free survival (hazard ratio >1 poor prognosis, hazard ratio <1 better prognosis). Metastasis-free survival describes the time between diagnosis and appearance of metastasis or patient death. The multivariate Cox-analysis was applied to assess the prognostic power of LIPG mRNA expression independent of established clinical parameters. To visualize survival differences in Kaplan-Meier plots, mRNA expression levels were dichotomized and

survival rates were compared with log-rank tests. Cut-off points show the calculated limits between low and high LIPG expression. Spearman-correlation test were applied to calculate correlations of genes in the different patient subgroups. P-values were calculated. The software SPSS 17.0 (SPSS Inc., Chicago, IL, USA) was used for all analysis.

3. Results

3.1 Induced oncogene ErbB2/HER2- (NeuT) overexpression results in premature senescence in MCF7/NeuT breast cancer cell

The receptor tyrosine kinase HER2/ErbB2 plays a central role in breast cancer development as well as in other epithelial tumors. HER2-transformation potential is based on the transduction of mitogenic and anti-apoptotic signals (Trost et al. 2005). The MCF7/NeuT breast cancer cell line, which allows tetracycline-inducible expression of an oncogenic variant of Erbb2 (NeuT) in MCF7 cells, was previously generated by Trost et al. (2005) in order to study ErbB2-induced tumorigenesis. Furthermore, it was characterized by Spangenberg et al. 2006 and Cadenas et al. 2010.

Initially surprisingly, instead of enhanced proliferation, overexpression of the oncogenic variant of HER2 (NeuT) in MCF7 cells was shown to lead to premature senescence. This senescence-associated cell cycle arrest was accompanied by morphological alterations and upregulation of p21- (WAF1/ CIP1) expression. In this work MCF7/NeuT cells were used to investigate oncogene-induced senescence- (OIS) mediated changes in lipid metabolism.

3.1.1 Oncogene HER2- (NeuT) triggered premature senescence is characterized by morphological alterations and induction of p21 (WAF1/CIP1)

The MCF7/NeuT cell line carries a Tet-On-inducible expression of NeuT, an oncogenic variant of ErbB2. Addition of the tetracycline derivate doxycycline (dox) induces simultaneous overexpression of NeuT- and eGFP via a bidirectional promoter. EGFP, as a reporter, enables an indirect control of the efficiency of induction (number of green positive cells) by fluorescence microscopy.

For verification of NeuT expression MCF7/NeuT cells were cultured with or without dox for the indicated time periods and RNA as well as protein were isolated. Dox-treated MCF7/NeuT cells showed already after six hours increased NeuT mRNA

expression which enhanced further in later time points on RNA as well as on protein level (Fig. 3.1).

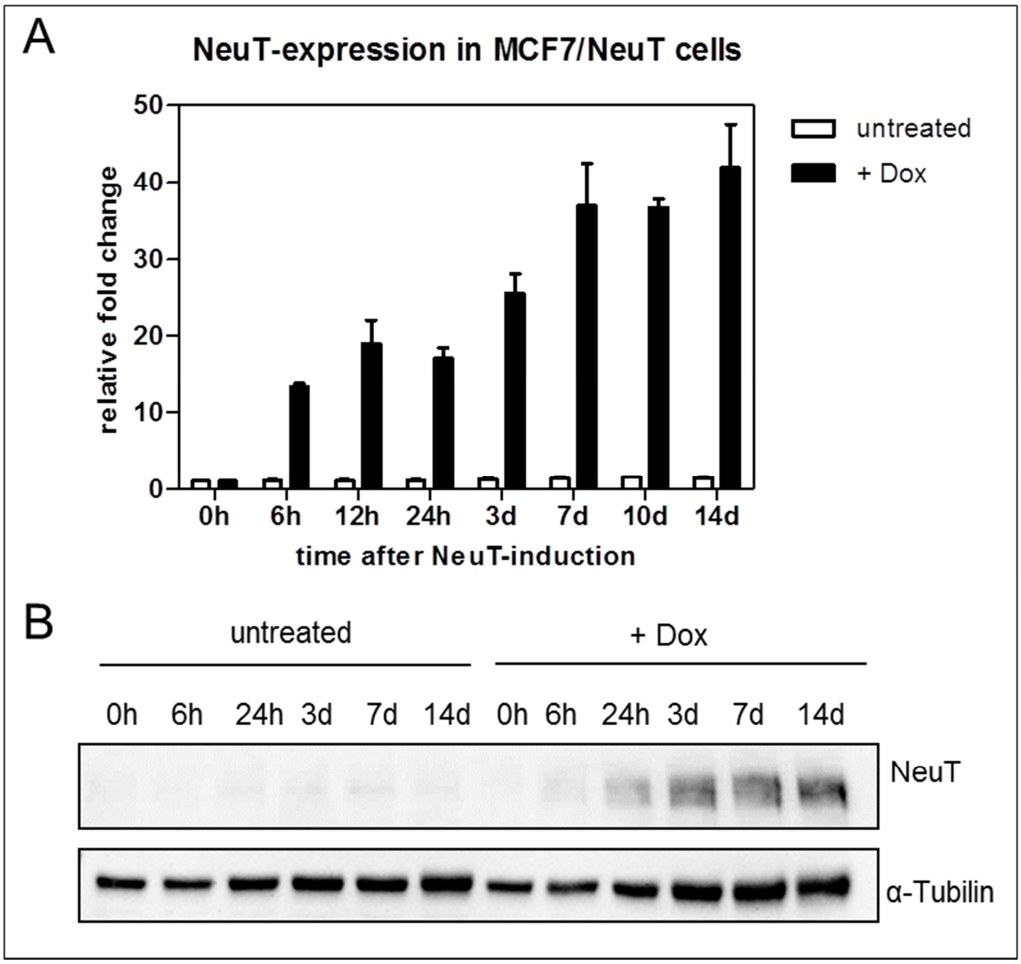

Fig. 3.1: Treatment of MCF7/NeuT cells with doxycycline (dox) triggers ErbB2/NeuT expression. MCF7/NeuT cells were incubated during a 14 days period in presence or absence of dox and NeuT expression was analyzed in a time-dependent manner. (A) ErbB2/NeuT mRNA was analyzed by quantitative real time PCR; as endogenous control TBP (TATA-box binding protein) was used. The results represent mean ± SEM (n=3) (B) Immunoblotting of ErbB2/NeuT protein expression in whole cell lysates; α-tubulin used as loading control. A representative immunoblotting is shown (n=4)

NeuT overexpression causes premature senescence accompanied by phenotypical changes like enlarged and flattened morphology and accumulation of vacuole structures within cytoplasm that became obvious 7d after induction of NeuT (Fig. 3.2).

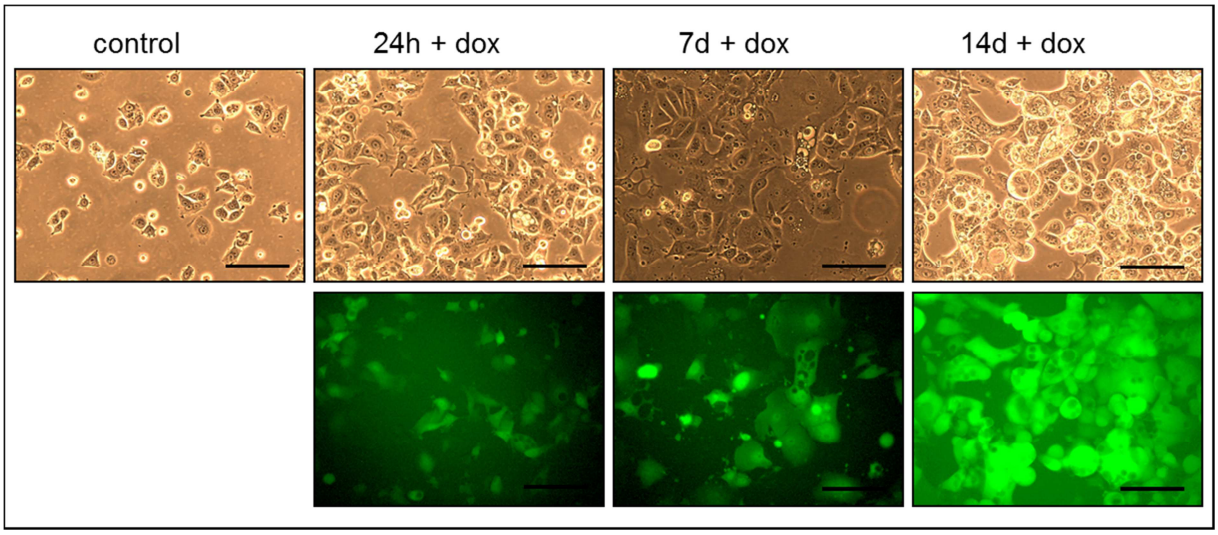

Fig. 3.2: NeuT-mediated senescence is accompanied by morphological changes of MCF7/NeuT cells. Doxycyclin-treated cells showed after three days an enlarged but flattened cell shape accompanied by a strong cytoplasmic vacuolization. Green fluorescence represents eGFP co-expression; scale bar 100µm; representative images are shown

For confirmation of the oncogene-driven cell growth arrest expression of the cyclin-dependent kinase inhibitor (CDKI) p21 (WAF1/ CIP1), an important mediator of cell cycle arrest and premature senescence in breast cancer cells (Okada et al. 2004, Sewing et al. 1997), was analyzed by real time qRT-PCR.

For this purpose MCF7/NeuT cells were cultivated in presence or absence of dox and RNA was collected at different time points. P21 expression on RNA level increased after dox treatment (Fig. 3.3), therefore confirming previous results (Trost et al., 2005).

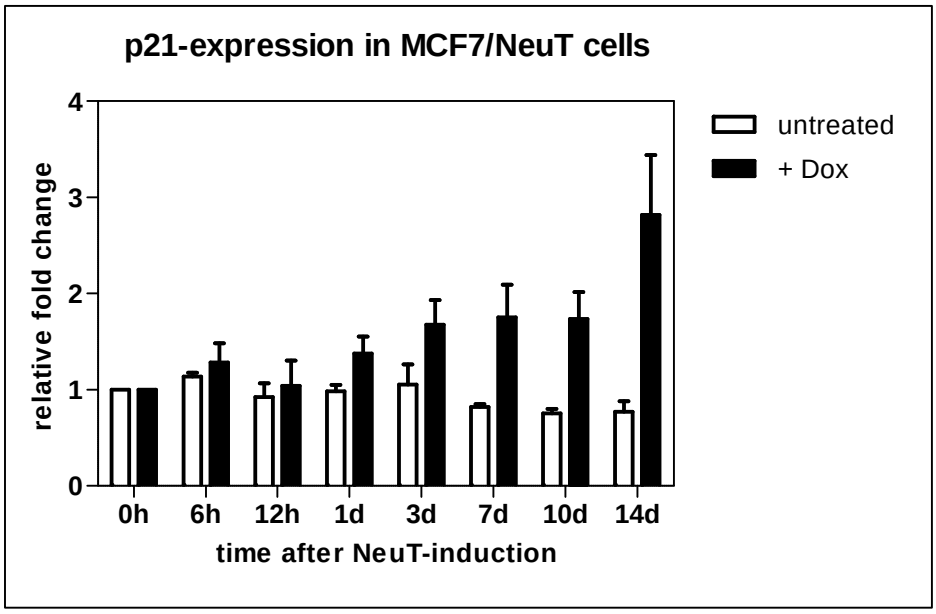

Fig. 3.3: Increased p21- (WAF1/ CIP1) expression in senescent MCF7/NeuT cells. MCF7/NeuT cells incubated during a 14 days period in presence or absence of doxycycline showed enhanced p21 (CIP1/ WAF1) mRNA expression as analyzed by quantitative real time PCR; as endogenous control UBC (ubiquitin C protein) was used. The results represent mean ± SEM (n=3)

3.1.2 ErbB2/NeuT overexpression induces expression changes of genes involved in lipid metabolism

Gene expression alterations triggered by NeuT overexpression in MCF7/NeuT cells were analyzed by Affymetrix gene arrays in a time-dependent manner. A number of genes involved in several processes of lipid metabolism showed considerable alterations in gene expression. Key enzymes were selected for validation by qRT-PCR. Selected lipid metabolism associated enzymes whose expression pattern in MCF7/NeuT cells was confirmed by qRT-PCR are shown in Figure 3.4.

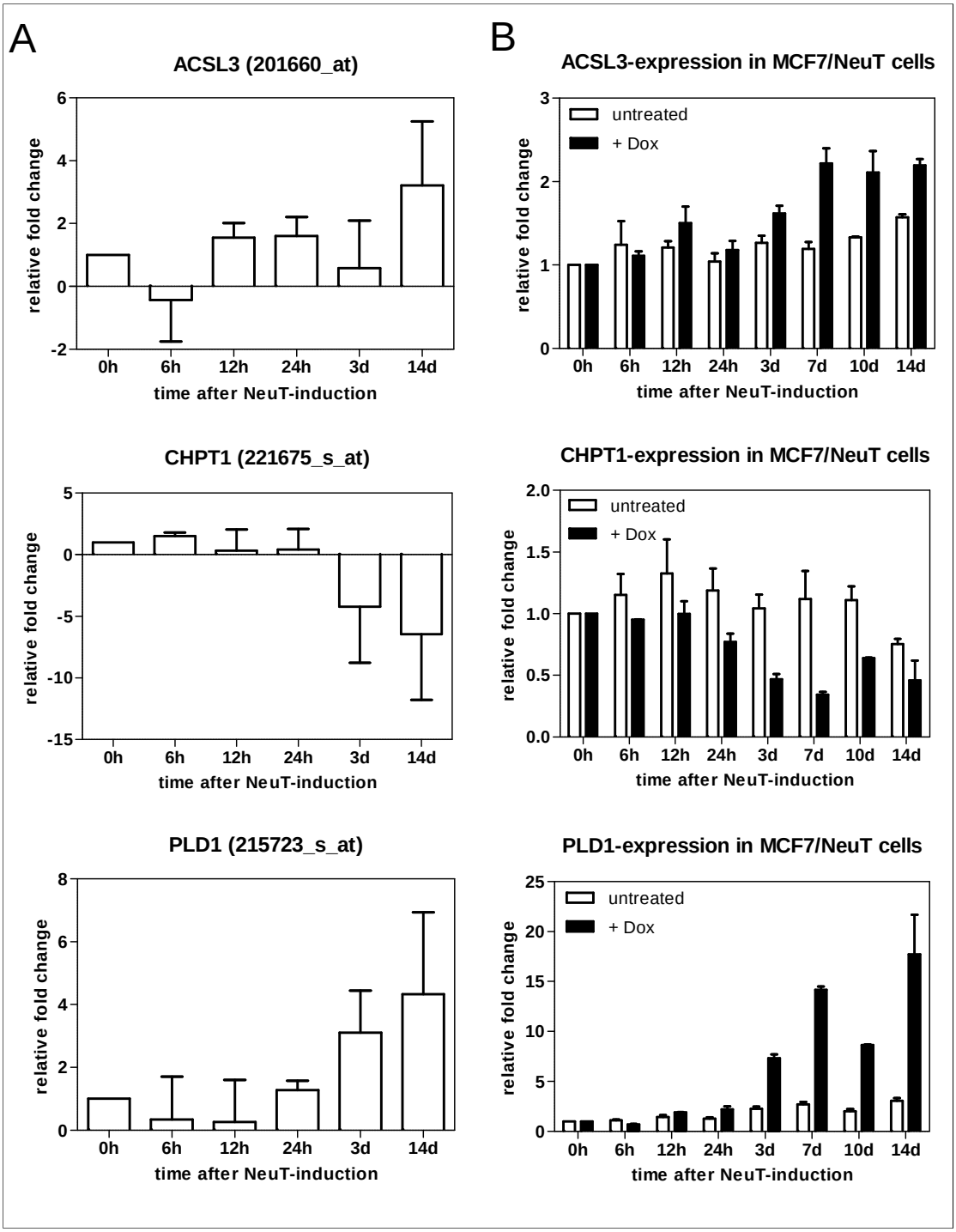
A
ACSL3 (201660_at)
relative fold change
time after NeuT-induction
0h
6h
12h
24h
3d
14d
B
ACSL3-expression in MCF7/NeuT cells
untreated
+ Dox
relative fold change
time after NeuT-induction
0h
6h
12h
24h
3d
7d
10d
14d
CHPT1 (221675_s_at)
relative fold change
time after NeuT-induction
CHPT1-expression in MCF7/NeuT cells
untreated
+ Dox
relative fold change
time after NeuT-induction
PLD1 (215723_s_at)
relative fold change
time after NeuT-induction
PLD1-expression in MCF7/NeuT cells
untreated
+ Dox
relative fold change
time after NeuT-induction

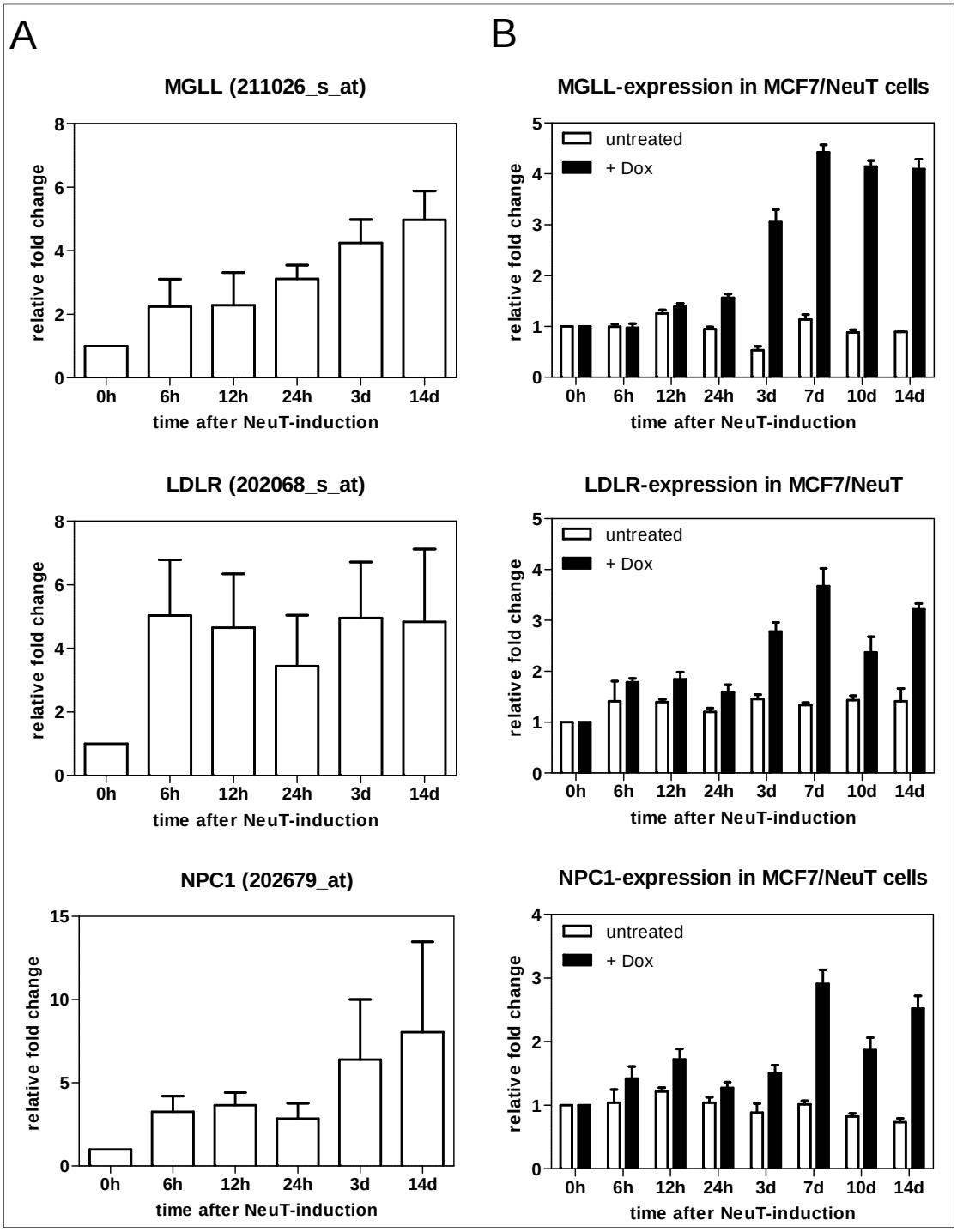
A
B
MGLL (211026_s_at)
relative fold change
0h
6h
12h
24h
3d
14d
time after NeuT-induction
MGLL-expression in MCF7/NeuT cells
untreated
+ Dox
0h
6h
12h
24h
3d
7d
10d
14d
time after NeuT-induction
LDLR (202068_s_at)
LDLR-expression in MCF7/NeuT
NPC1 (202679_at)
NPC1-expression in MCF7/NeuT cells

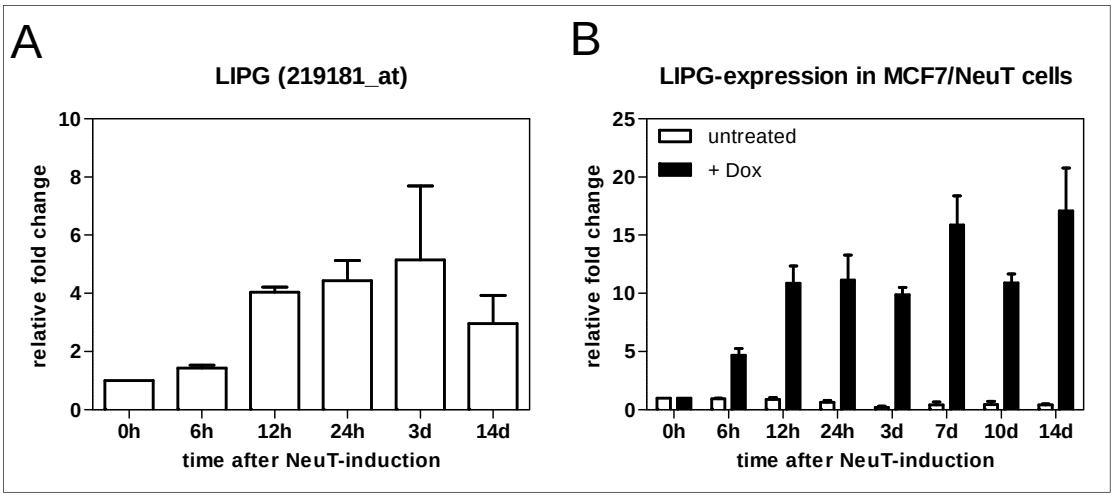

Fig. 3.4: Dox-exposed MCF7/NeuT cells show altered expression of a number of genes involved in lipid metabolism. MCF7/NeuT cells were incubated during a 14 days period in presence or absence of doxycycline; (A) Affymetrix gene array results of seven selected key enzymes of lipid metabolism (B) Confirmation of gene array by qRT-PCR; as endogenous control UBC (ubiquitin C protein) was used. The results represent mean ± SD (n=3)

Acyl-CoA synthase long chain 3 (ACSL3) is important for the activation as well as degradation of long-chain fatty acids and phospholipid remodeling (Soupene and Kuypers 2008). This gene shows an up-regulation of 2.22 ± 0.18 on mRNA level seven days after dox exposure.

Choline phosphotransferase 1 (CHPT1) catalyzes the last step in the *de novo* synthesis of phosphatidylcholine (PC; Kennedy pathway) by transferring phosphocholine from CDP-choline to diacylglycerol and releasing CMP (Henneberry et al. 2000). This gene shows a down-regulation of 0.35 ± 0.02 on mRNA level seven days after dox exposure.

Phospholipase D1 (PLD1) hydrolyses PC to generate phosphatidic acid (PA) and choline (Gomez-Cambronero 2010). This lipase is involved in cell migration, cell signaling, intracellular protein trafficking, membrane remodeling and cell proliferation. PLD1 shows an up-regulation of 14.17 ± 0.32 on mRNA level seven days after dox treatment.

Monoacylglycerol lipase (MAGL or MGLL) releases free fatty acids from monoacylglycerol and generates precursors of pro-tumorigenic signaling molecules which facilitate cell migration, survival, and cancer cell growth (Nomura et al. 2010).

MGLL level is increased in aggressive cancer cells. This lipase displayed an up-regulation of 4.43 ± 0.14 on mRNA level after seven days of dox incubation.

The low-density lipoprotein receptor (LDLR) enables the uptake of cholesterol-carrying lipoproteins by endocytosis (Jeon & Blacklow 2005). This gene shows an up-regulation of 3.67 ± 0.35 on mRNA level seven days after dox exposure.

Niemann-Pick C1 (NPC1) plays a role in intracellular cholesterol trafficking and regulation of cholesterol homeostasis (Ory 2004). NPC1 reveals an up-regulation of 2.91 ± 0.22 on mRNA level seven days after dox exposure.

Lipoprotein lipase G (LIPG) shows phospholipase activity A1 and a low triglyceride lipase activity (Gauster et al. 2005). It binds high density lipoproteins phosphatidylcholine (HDL-PC) as main substrate and cleaves it into lyso-phosphatidylcholine (LPC) and fatty acids. These released fatty acids can be taken up in an autocrine way. LIPG shows an up-regulation of 18.56 ± 0.55 on mRNA level seven days after dox exposure.

Altogether, these expression changes show that a remodeling of lipid metabolism takes place in oncogene-induced senescence in MCF7/NeuT cells. On one hand two proteins involved in uptake of extracellular lipids - LDLR and LIPG - and enzymes known to be involved in phospholipid remodeling - ACSL3 and PLD1 - are upregulated. On the other hand enzymes involved in *de novo* synthesis of phospholipids, such as CHPT1, is downregulated. This indicates that MCF7/NeuT cells may depend on exogenous lipid supply rather than on endogenous lipid synthesis.

3.1.3 NeuT-induced senescence is accompanied by increased LIPG expression

LIPG was among the genes displaying most prominent mRNA expression alterations. LIPG mRNA became immediately induced upon NeuT overexpression and further increased as cells entered the senescence state. This gene attracted our attention because there was no published connection between ErbB2 and LIPG. Interestingly no other member of the triglyceride lipase gene family, such as lipoprotein lipase (LPL; LIPD) and hepatic lipase (HL; LIPC) were shown to be significantly up- or

down-regulated upon NeuT induction in MCF7/NeuT cells (gene array data, data not shown). Therefore, LIPG induction by NeuT seemed to be unique among the members of the TAG lipase family members. Analysis of LIPG protein levels in MCF7/NeuT cells treated with dox in a timely manner confirmed mRNA data. A band of 55kDa corresponding to the full length intracellular LIPG protein could be detected by immunoblotting already after three days of dox incubation (Fig. 3.5).

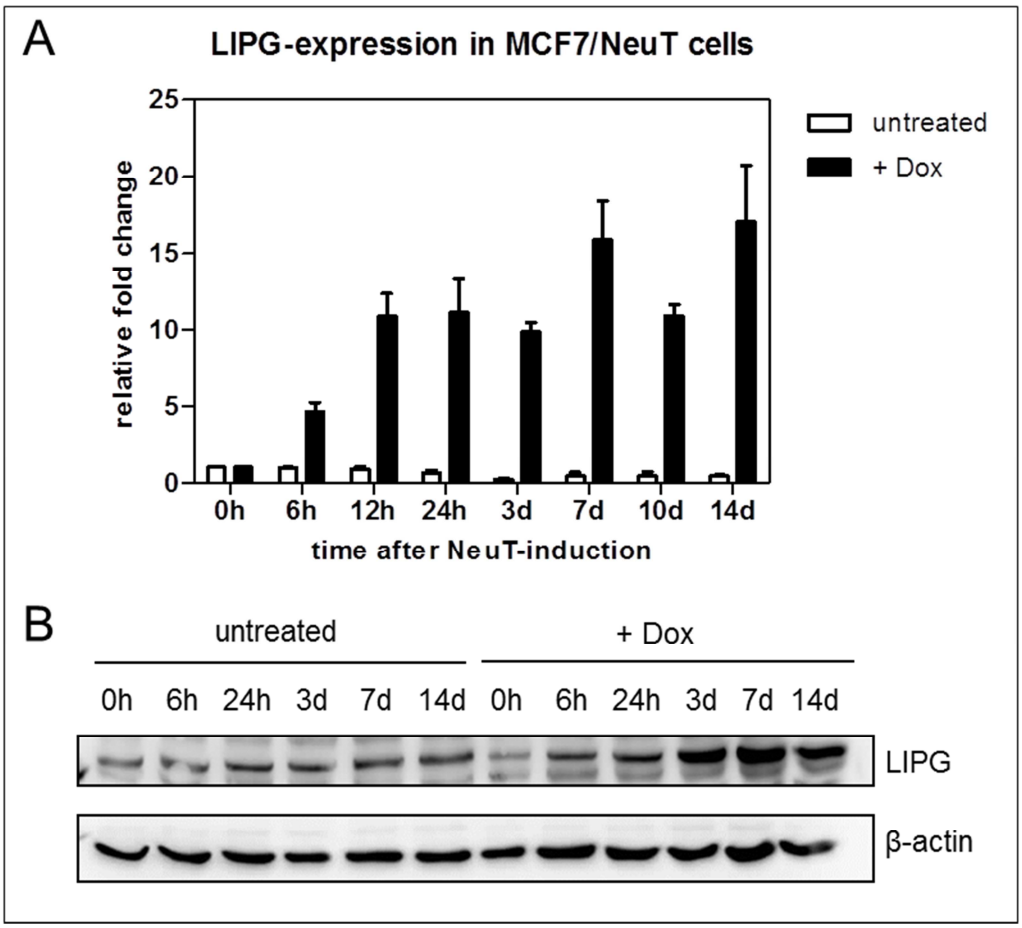

Fig. 3.5: NeuT overexpression in dox-treated MCF7/NeuT cells leads to increased LIPG expression. (A) MCF7/NeuT cells were incubated during a 14 days period in presence or absence of doxycycline; LIPG expression in RNA extracts analyzed by quantitative real time PCR (LIPG; Hs00195812) was increased already after six hours of dox exposure; as endogenous control UBC (ubiquitin C protein) was used. The results represent mean ± SEM (n=3) (B) Immunoblotting of LIPG protein expression in MCF7/NeuT cells treated or untreated with doxycycline showed increased levels of LIPG immunoreactivity (55kDa size) after three days of dox exposure in whole cell protein lysates; β-actin used as loading control. A representative immunoblotting is shown (n=2)

Previous results showing induction of LIPG in MCF7/NeuT cells by real time qRT-PCR (TaqMan primers Hs00195812, spanning exons 8-9) were confirmed by using

the additional TaqMan primers Hs00969502 (exons 1-2) and Hs00969505 (exons 4-5). The human LIPG locus 18q21.1 contains eleven exons (Ishida et al. 2004).

All three used primers displayed the same early LIPG gene expression after six hours and progressively increased expression at longer times of dox exposure in MCF7/NeuT cells (Fig. 3.6).

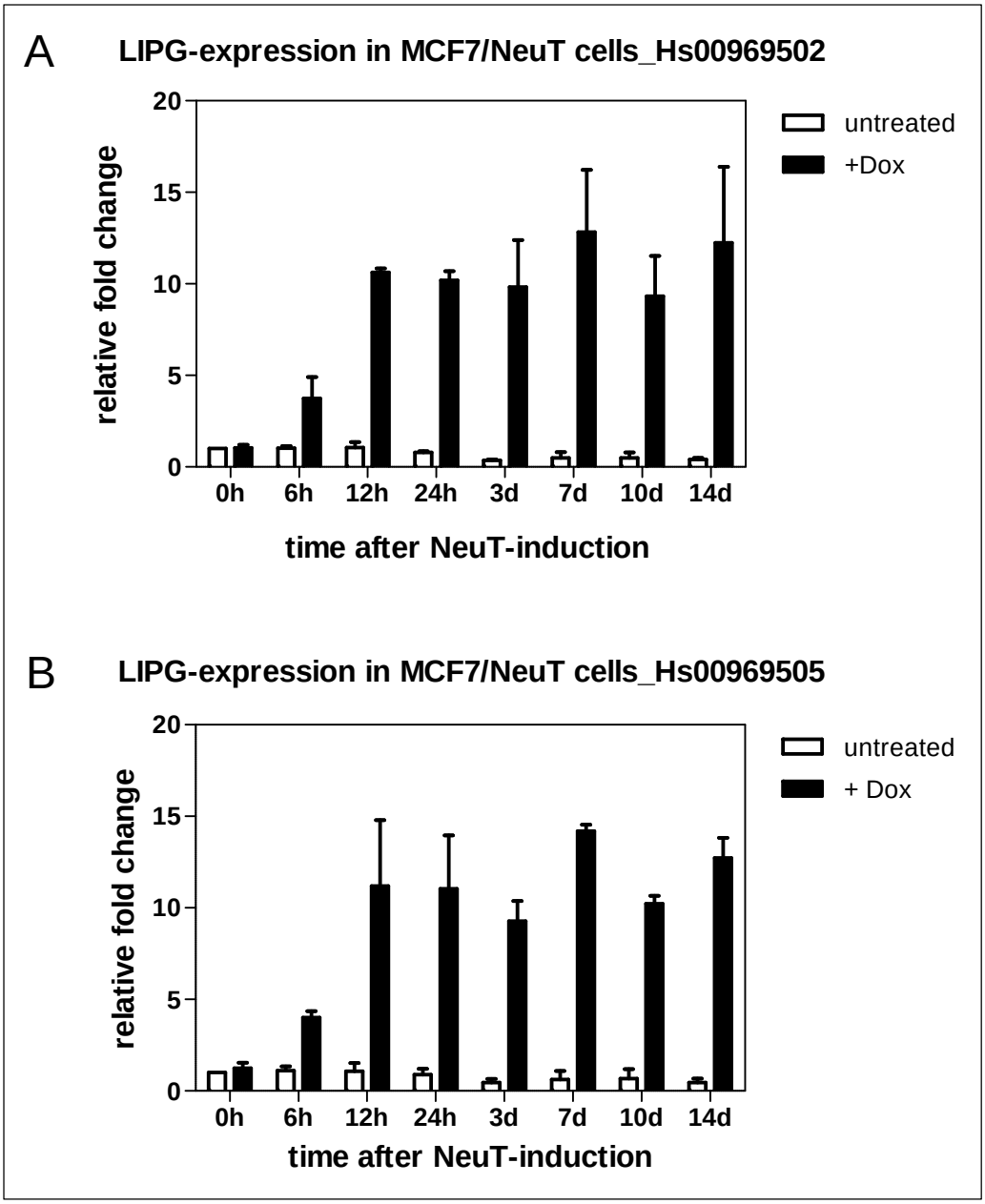

Fig. 3.6: NeuT overexpression in dox-treated MCF7/NeuT cells leads to increased LIPG expression. Confirmation of LIPG mRNA induction by real time qRT-PCR with different primers. (A) MCF7/NeuT cells were incubated during a 14 days period in presence or absence of doxycycline; LIPG expression in RNA extracts was analyzed by quantitative real time PCR using primer (A)

Hs00969502 (Exon 1-2) and (B) Hs00969505 (Exon 4-5); as endogenous control UBC (ubiquitin C protein) was used. The results represent mean ± SEM (n=2)

To ensure that LIPG expression was specifically induced by NeuT overexpression and not by addition of doxycycline we analyzed LIPG on dox-treated MCF7/eGFP control cells. MCF7/eGFP cells lack NeuT and therefore only eGFP responds to the Tet-On system. As shown in Figure 3.7, no induction of LIPG expression was observed in this control cell line. These results indicate a correlation between NeuT-overexpression and LIPG expression and exclude the possibility that LIPG becomes activated by doxycycline.

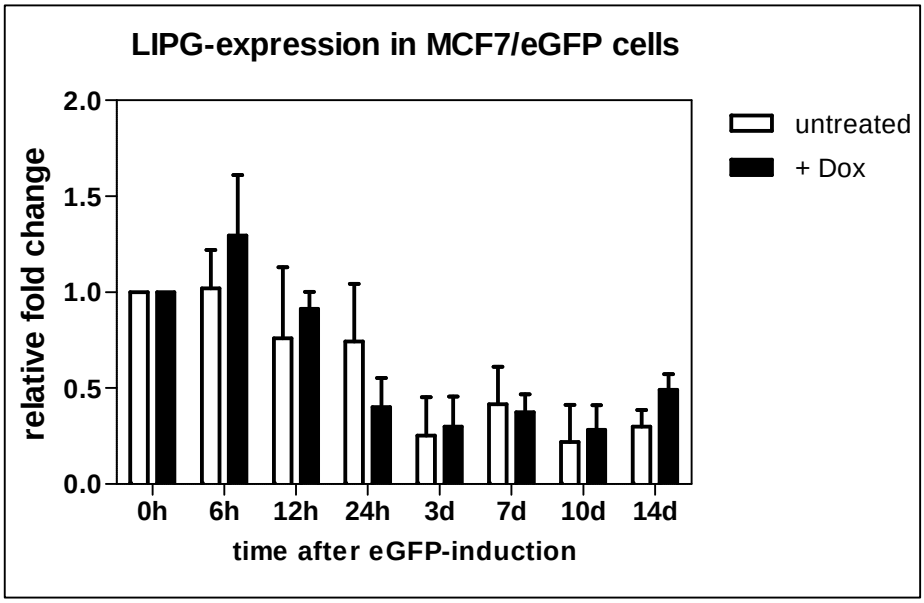

Fig. 3.7: No induction of LIPG expression in MCF7/eGFP-control cells upon dox treatment. MCF7/eGFP cells were incubated during a 14 days period in presence or absence of doxycycline; LIPG expression in RNA extracts was analyzed by quantitative real time PCR; as endogenous control UBC (ubiquitin C protein) was used. The results represent mean ± SEM (n=2)

3.1.4 Senescent MCF7/NeuT cells display an increased mRNA expression of the lipid droplet-coating protein Perilipin 2 (PLIN2) together with elevated cellular triacylglyceride levels

LIPG has been reported to display phospholipase A1 activity and to cleave phosphatidylcholine from HDL as main substrate (Gauster et al. 2005). Released fatty acids can directly be taken up by cells, and become stored in form of

triacylglycerides (TAG) within lipid droplets. To investigate whether induction of LIPG in MCF7/NeuT cells is paralleled by lipid droplet accumulation we analyzed both expression of lipid droplets-associated proteins and the level of triacylglycerides. Among the members of the perilipin family only PLIN2 was shown to be upregulated by NeuT overexpression in the Affymetrix gene array data. Therefore, we measured PLIN2 mRNA by real time qRT-PCR. The PLIN2 protein coats intracellular lipid droplets and is a marker of lipid accumulation. Figure 3.9 illustrates an increase of PLIN2 expression in MCF7/NeuT cells upon NeuT overexpression concomitant with LIPG upregulation.

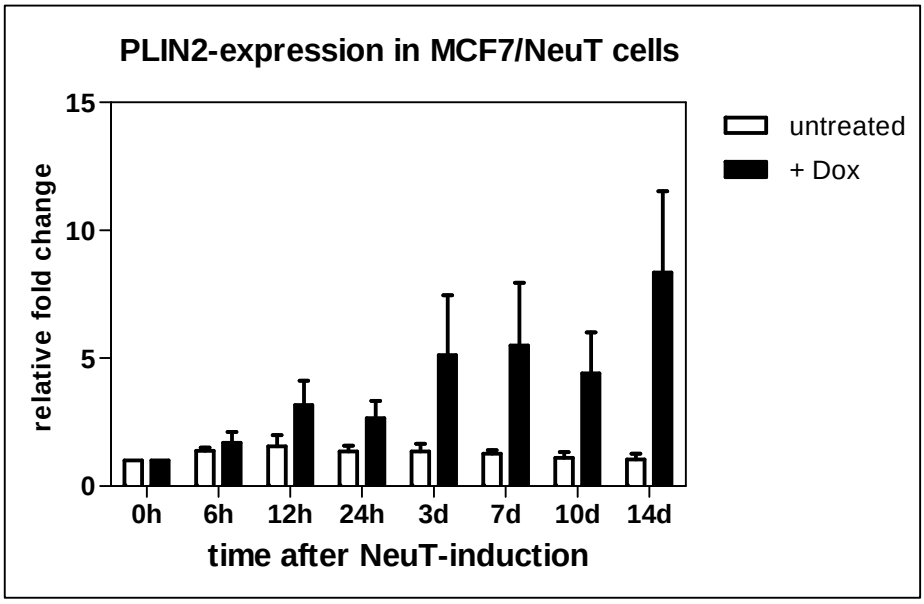

Fig. 3.8: Overexpression of NeuT in dox-treated MCF7/NeuT cells increases Perilipin2 (PLIN2) expression. MCF7/NeuT cells were incubated during a 14 days period in presence or absence of doxycycline; PLIN2 expression in RNA extracts was analyzed by quantitative real time PCR; as endogenous control UBC (ubiquitin C protein) was used. The results represent mean ± SEM (n=3)

Quantification of triacylglycerol (TAG) was performed to confirm lipid accumulation as suggested by the measured PLIN2 expression levels in senescent cells. MCF7/NeuT cells were treated for six days with doxycycline and after lipid extraction the intracellular TAG content was quantified. Senescent MCF7/NeuT cells exhibited a four-fold increase of TAG compared to untreated control cells (Fig. 3.9).

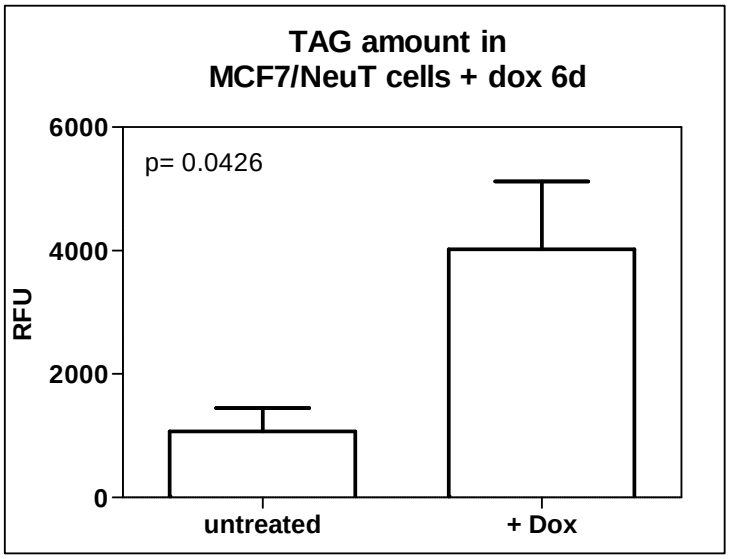

Fig. 3.9: Senescent MCF/NeuT cells show increased amounts of intracellular triglycerides (TAG). After six days of dox exposure senescent cells revealed a four-fold increased triacylglycerol amount compared to untreated cells. Quantification of triacylglycerols was performed with the Triglyceride Quantification Kit (ab65336) from abcam. The results represent mean ± SEM (n=2)

3.1.5 Elevated oxidative stress in senescent cells does not lead to increased LCN2 gene expression

Lipocalin2 (LCN2) displays a variety of functions. It can transport hydrophobic molecules (Grzyb et al. 2006), promote remodeling of intracellular phospholipids (Yang et al. 2012), regulate lipid droplet formation in liver (Asimakopoulou et al. 2014) and is a well-known marker of inflammation (Jha et al.2014). Moreover, oxidative stress has been shown to increase Lipocalin2 (LCN2) levels in H_2O_2-treated HepG2 cells (Roudkenat et al. 2007). Klaunig and Kemanedulis (2004) described that oncogene overexpression can lead to production of reactive oxygen species (ROS). Quantification of ROS by a TBARS (Thiobarbituric acid reactive substances) assay together with upregulation of enzymes that are known to combate ROS, such as TXNRD1 (Cadenas et al. 2010), showed increased oxidative stress in senescent MCF7/NeuT cells induced by ErbB2/NeuT expression. Therefore, the LCN2 RNA level in dox-exposed MCF7/NeuT cells was studied. As shown in Figure 3.10, no LCN2 expression alteration was observed at any time point.

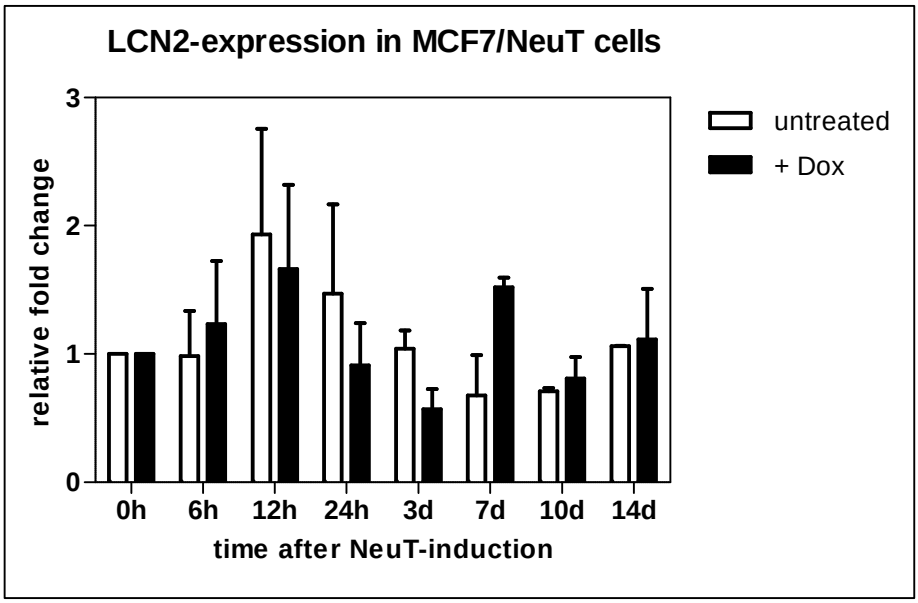

Fig. 3.10: NeuT overexpression in dox treated MCF7/NeuT cells does not result in changes in Lipocalin2 (LCN2) expression. MCF7/NeuT cells were incubated for 14 days in presence or absence of doxycycline; LCN2 expression in RNA extracts was analyzed by quantitative real time PCR; as endogenous control UBC (ubiquitin C protein) was used. The results represent mean ± SEM (n=2)

3.1.6 NeuT oncogene-induced activation of signaling pathways mediating LIPG induction

After onset of NeuT expression in MCF7/NeuT cells several signaling pathways become activated, including the AKT/PI3K-, p38-, MEK1/2- and SAPK/JNK-pathways (Trost et al. 2005, Cadenas et al. 2010) that may lead to changes in gene expression patterns. To study the influence of these pathways on LIPG expression different inhibitors LY294002 (targeting PI3K), SB203538 (p38 MAPK inhibitor), PD98059 (inhibitor of MEK1/2) and SP600125 (JNK inhibitor) (Fig 3.11) were used.

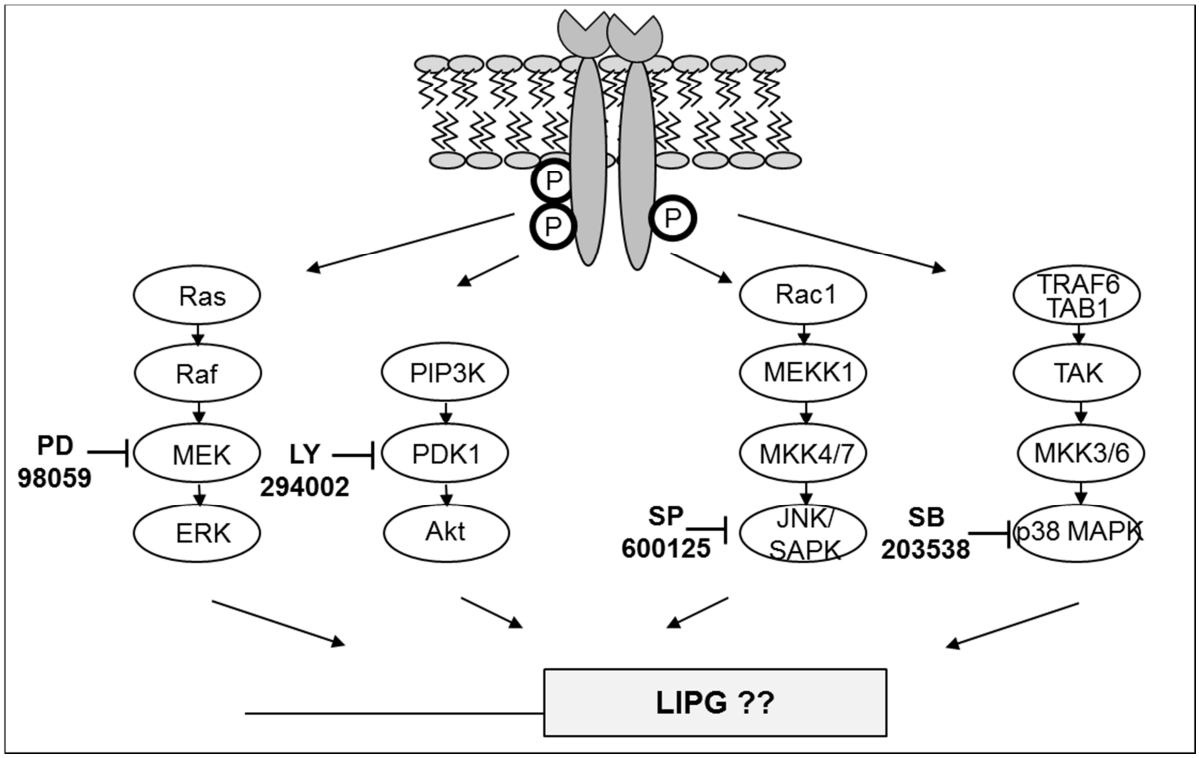

Fig. 3.11: Summary of most important ErbB2-mediated signaling pathways. The aim of the study was to investigate the influence of different inhibitors on LIPG transcription

Up-regulation of LIPG mRNA upon NeuT oncogene overexpression was reduced by the small molecule inhibitors of p38 MAPK (SB203538) (Fig. 3.13) and AKT/PI3K (LY294002) (Fig. 3.12) but not by the PD98059 (Fig. 3.14) nor SP600125 inhibitors (Fig. 3.15).

Already after 24h of dox exposure MCF7/NeuT cells displayed increased LIPG expression on RNA level. Blocking the PI3K/AKT-pathway by the LY294002-inhibitor reduced LIPG gene expression at all investigated time points and more than 14-fold in senescent cells after seven days (Fig. 3.12).

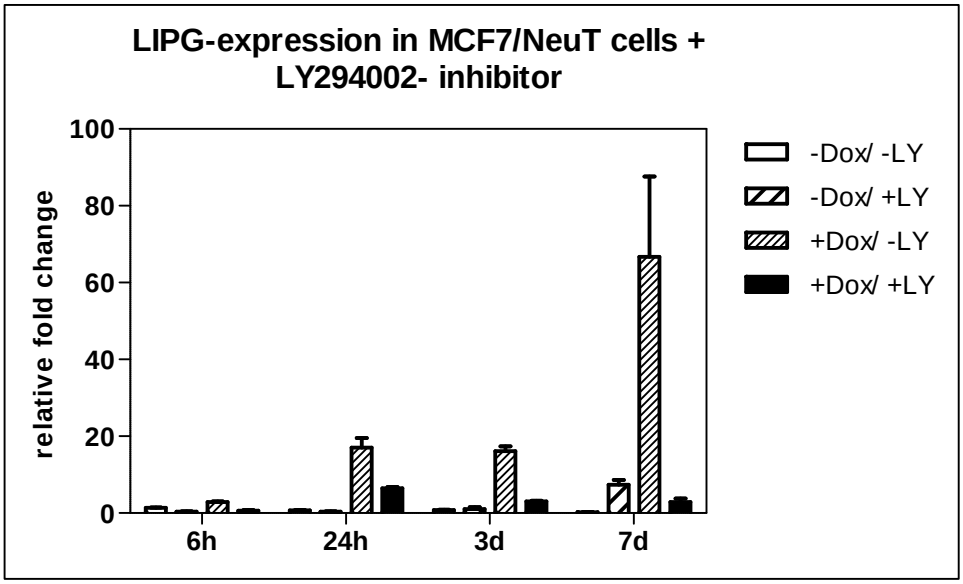

Fig. 3.12: Blocking the AKT/PI3K-pathway by adding the LY294002 inhibitor to MCF7/NeuT cells ± doxycycline affects the induction of LIPG expression. MCF7/NeuT cells were incubated with or without doxycycline in the presence or absence of AKT/ PI3K-pathway inhibitor LY294002 (20µM) up to seven days; LIPG expression in RNA extracts analyzed by quantitative real time PCR; as endogenous control UBC (ubiquitin C protein) was used. The numbers represent mean ± SEM (n=3)

Similarly, addition of p38-pathway inhibitor SB203538 dampened upregulation of LIPG by NeuT at all studied time points (Fig. 3.13).

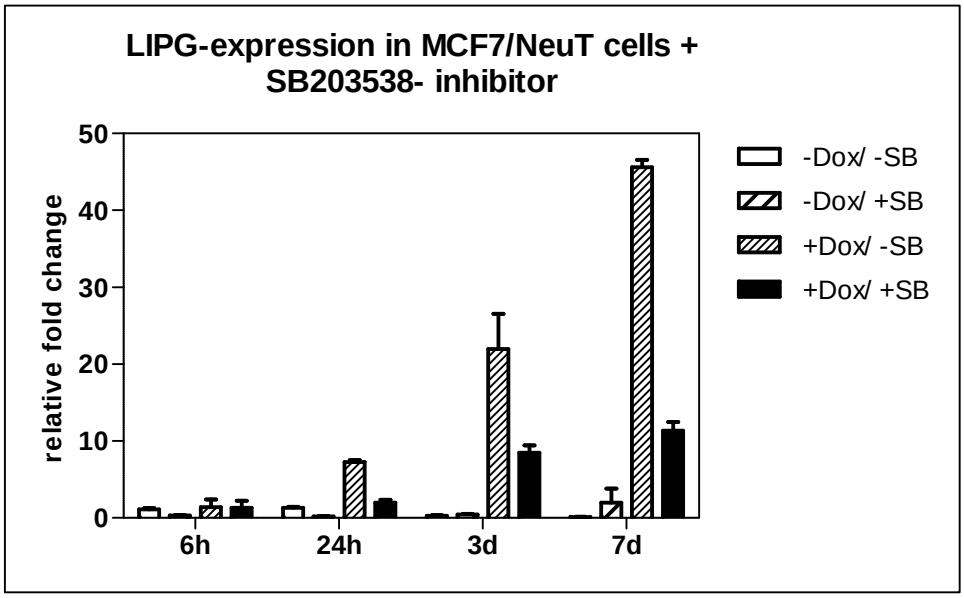

Fig. 3.13: Blocking the p38-pathway by adding SB203538 inhibitor to MCF7/NeuT cells treated with doxycycline prevents the induction of LIPG expression. MCF7/NeuT cells were incubated

with or without doxycycline in the presence or absence of the p38-pathway inhibitor SB203538 (25µM) up to seven days; LIPG expression in RNA extracts analyzed by quantitative real time PCR; as endogenous control UBC (ubiquitin C protein) was used. The bars represent mean ± SEM (n=3)

MEK1/2-inhibitor PD98059 showed no influence on LIPG gene expression after 24h and only a very slight effect after three days incubation of senescent MCF7/NeuT cells. Solely at the time point seven days there was a remarkable reduction of LIPG expression by two-fold (Fig. 3.14).

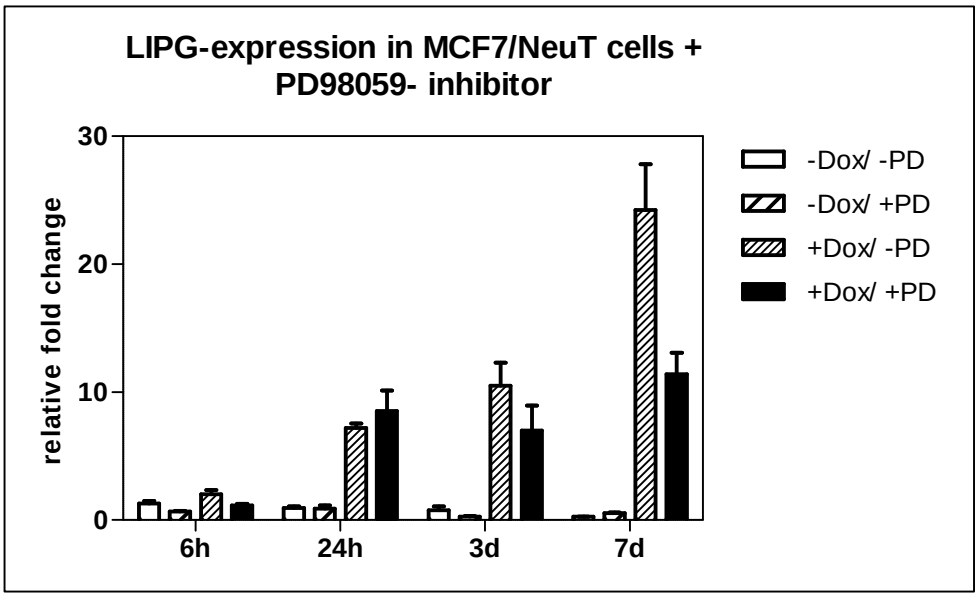

Fig. 3.14: Blocking the MEK1/2-pathway by adding PD98059 inhibitor to MCF7/NeuT cells treated with doxycycline slightly affects the induction of LIPG expression. MCF7/NeuT cells were incubated with or without doxycycline in the presence or absence of the MEK1/2-pathway inhibitor PD98059 (25µM) up to seven days; LIPG expression in RNA extracts analyzed by quantitative real time PCR; as endogenous control UBC (ubiquitin C protein) was used. The bars represent mean ± SEM (n=3)

Similar results were obtained when the SAPK/JNK-pathway inhibitor SP600125 was applied. LIPG expression in MCF7/NeuT cells treated with dox was not altered by blocking SAPK/JNK at the 24h and three day time points, and only slightly reduced at day seven (1.6-fold decreased LIPG level) (Fig. 3.15).

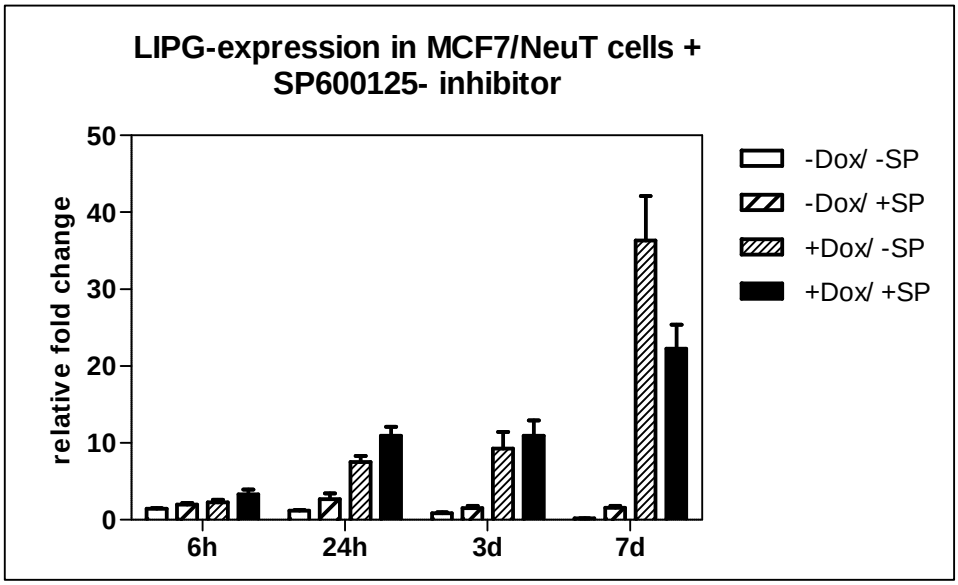

Fig. 3.15: Blocking SAPK/JNK-pathway by adding SP600125 inhibitor to MCF7/NeuT cells ± doxycycline only slightly affects the induction of LIPG expression. MCF7/NeuT cells were incubated with or without doxycycline in presence or absence of the SAPK/JNK-pathway inhibitor SP600125 (25µM) up to seven days; LIPG expression in RNA extracts analyzed by quantitative real time PCR; as endogenous control UBC (ubiquitin C protein) was used. The results represent mean ± SEM (n=3)

In summary, these results showed that p38 MAPK and AKT/PI3K but not MEK1/2- and JNK are underlying signaling pathways involved in NeuT-triggered stimulation of LIPG expression.

3.1.7 LIPG gene expression in additional HER2-overexpressing MCF7 cells

NeuT is an oncogenic variant of ErbB2 that contains a valine to glutamine amino acid exchange in the transmembrane domain at position 664 (Schechter et al. 1984, Bargmann et al. 1986). This mutation has been shown to constitutively stimulate NeuT tyrosine kinase activity (Weiner et al. 1989). LIPG induction by wildtype HER2 (ErbB2) or mutated isoforms has not been reported in other studies. Therefore, we investigated whether LIPG expression is also elevated in MCF7 breast cancer cells stably transfected with the HER2 oncogene. In addition to wildtype HER2, we examined a different HER2 mutant containing an YVMA insertion at codon 776 (YVMA: insertion of four amino acids; Y=tyrosine, V=valine, M=methionine and

A=alanine). This YVMA insertion results in a higher constitutive auto-phosphorylation of HER2 resulting in enhanced tyrosine kinase activity (Greulich et al. 2012, Wang et al. 2006). Real time qRT-PCR analysis was performed to investigate LIPG expression in the MCF7/HER2wt and in the MCF7/HER2-YVMA cells. However no significant higher levels of LIPG mRNA could be observed in these two cell lines compared to the parental MCF7 cells (not shown). This shows that HER2 overexpression is not necessary associated with upregulation of LIPG.

3.2 LIPG overexpression in MCF7 breast cancer cells

In order to investigate whether LIPG influences the lipid content in breast cancer cells we first overexpressed LIPG in MCF7 cells. The transfection was done with a non-liposomal reagent (Roche). Figure 3.16a illustrates the dramatic increase in the mRNA expression level of LIPG in transfected cells, with 15.000-fold increase compared to empty vector control cells. Representative bright field and confocal microscopic images of full media (FM, untreated), empty vector (EV, control) and LIPG-overexpressing cells (LIPG-OE) were shown in Figure 3.16b/c. No phenotypical changes were recognizable between control and LIPG-OE cells.

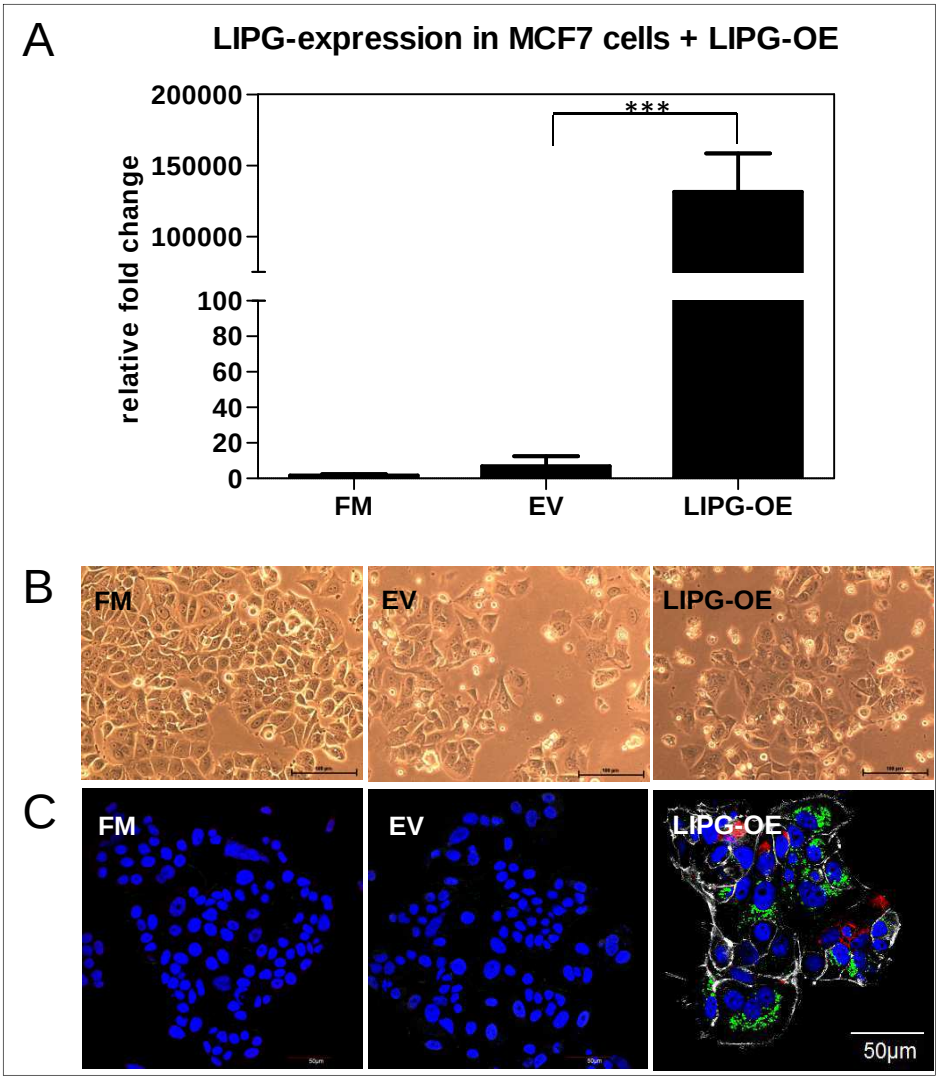

Fig. 3.16: LIPG overexpression (OE) in MCF7 cells. (A) LIPG mRNA levels are increased 48 hours after transfection with 1500ng of a FLAG-tagged LIPG-OE vector with the X-tremeGENE HP DNA transfection reagent (Roche); LIPG expression in RNA extracts was analyzed by quantitative real time PCR; as endogenous control UBC (ubiquitin C protein) was used. The bars represent mean ± SEM (n=3) (B) Representative bright field microscopic images of full media (FM, untreated), EV (empty vector control) and LIPG-OE (overexpressing) cells; scale bar 100µm; (C) Confocal microscopic images of fixed MCF7 cells labelled with fluorescent LIPG (anti-FLAG, red), nuclei (DAPI, blue) and lipid droplets (Bodipy 493/503; green); scale bar 20µm, representative images are shown

To control the efficiency of LIPG overexpression on protein level also immunoblotting was done. The protein LIPG is intracellularly synthetized with a size of 55kDa. After glycosylation and transport to the cell membrane it acquires a size of 68kDa. Furthermore, LIPG becomes secreted into the media and becomes cleaved and thus inactivated by pro-protein convertases into the fragments of 40kDa and 28kDa.

To demonstrate proper localization of the overexpressed LIPG, whole cell protein lysates, as well as membrane-bound protein and extracellular fractions were prepared.

As described by Gauster et al. 2005 we could confirm that LIPG-overexpressing MCF7 breast cancer cells produced intracellular LIPG which can be found also on cell surface and released into the supernatant. In the whole cell lysates a small 55kDa protein band was detectable (corresponding to the immature LIPG), accompanied by a strong 68kDa glycosylated LIPG protein together with the cleaved 40kDa product were detected. In the fraction corresponding to the cell-surface attached LIPG (prepared by heparine release) only a strong 68kDa band was observed. The cell supernatant contained the 68kDa released LIPG protein together with the 40kDa cleaved product (Fig. 3.17).

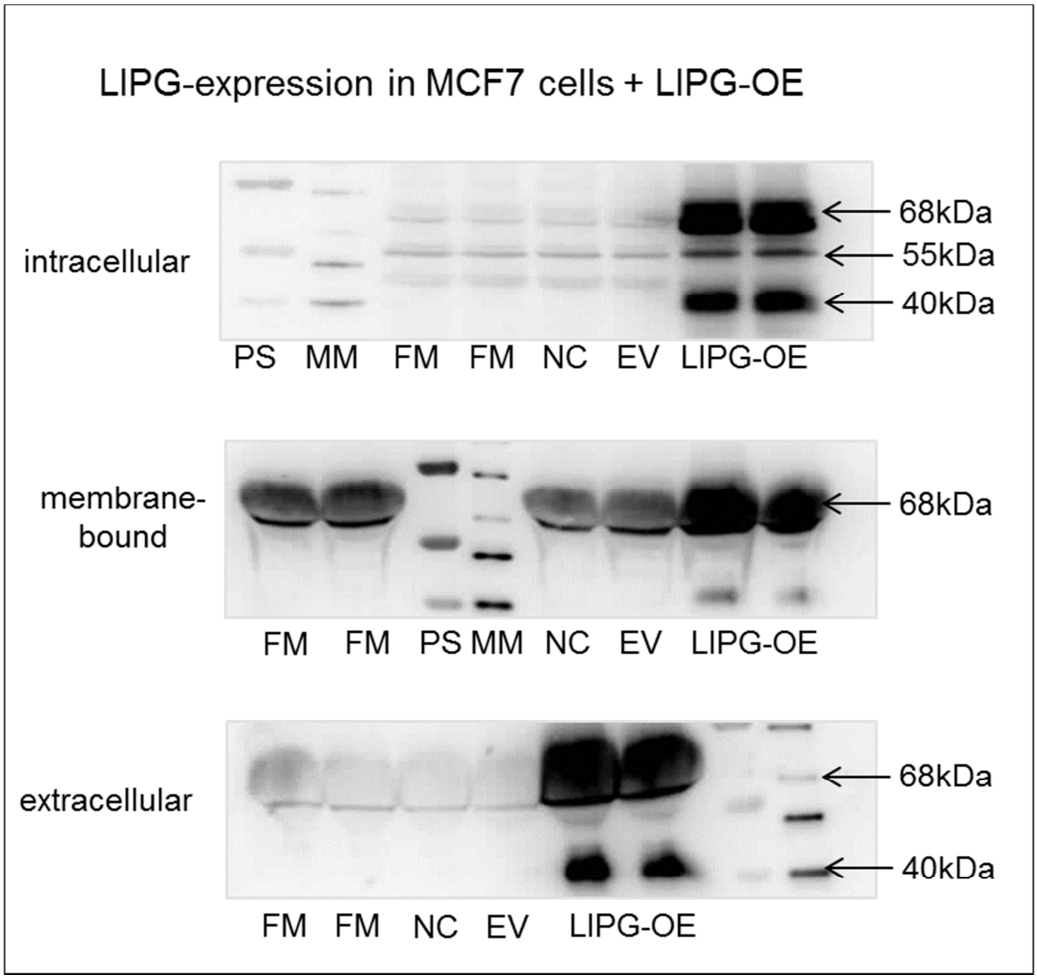

Fig. 3.17: LIPG overexpression (OE) in MCF7 cells results in increased LIPG protein levels in all three subcellular fractions (intracellular, membrane-bound and extracellular). The comparison of full media (FM, untreated) and empty vector (EV, control) with LIPG-overexpressing (LIPG-OE) cells

illustrates a strong 68kDa protein band in all three compartments. A representative immunoblot is shown (n=3)

3.2.1 Induction of LIPG in MCF7 breast cancer cells is accompanied by increased triacylglyceride levels

The literature has reported a high phospholipase A1 and low triglyceride lipase activity of LIPG (Strauss et al. 2002). Accordingly, the addition of high-density lipoprotein (HDL) as the main substrate of LIPG to LIPG-overexpressing cells is expected to result in the release of fatty acids from the phosphatidylcholine contained in HDL particles and subsequent cellular uptake and incorporation into cellular lipid stores, such as triacylglycerides (TAG). Because we were restricted by the great variability of HDL quality that is commercially available we also explored the ability of exogenously added phosphatidylcholine (PC) to serve as a LIPG substrate in cell culture. For this purpose we added vesicles of PC esterified with oleic acid (1,2-dioleoyl-sn-glycero-3-phosphocholine; DOPC; PC-OA, Avanti). After overexpression of LIPG for 48h cells were serum-starved and incubated with HDL or PC-OA for further 48h. Subsequently, lipids were extracted for quantification of the accumulated TAG amount by using the Triglyceride Quantification Kit (abcam).

Serum-starved LIPG-overexpressing cells that were incubated for 48h with 800µg HDL accumulated 2.5-fold more TAG than control cells (Fig. 3.18a). Lipid droplets staining by oil red O and immunofluorescence (Bodipy) confirmed the TAG quantification results (Fig. 3.18b/c). Only LIPG-overexpressing cells were able to incorporate HDL-derived fatty acids leading to lipid accumulation.

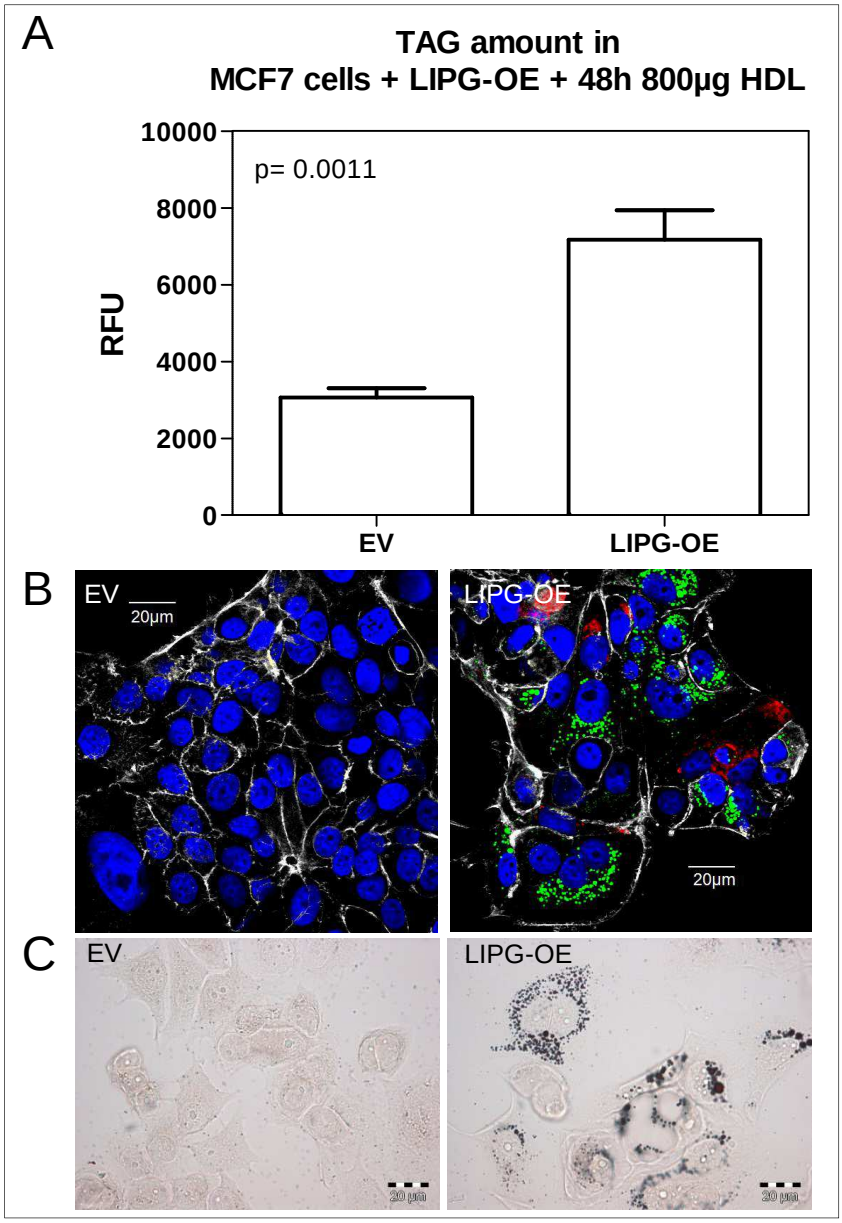

Fig. 3.18: LIPG-overexpressing MCF7 cells incubated with HDL show increased lipid accumulation. After 48 hours transfection with 1500ng LIPG-FLAG expression vector and X-tremeGENE HP DNA transfection reagent (Roche) cells were incubated with serum-free media supplemented with 800µg high density lipoprotein (HDL) for further 48h. (A) Quantification of cellular triacylglycerol (TAG) levels after lipid extraction by using Triglyceride Quantification Kit (ab65336) from abcam. The results represent mean ± SEM (n=3); (B) Confocal microscopic images of fixed MCF7 cells after transfection and culture with HDL as described above labelled with fluorescent LIPG (anti-FLAG, red), nuclei (DAPI, blue), actin cytoskeleton (Rhodamine Phalloidin, grey) and lipid droplets (Bodipy 493/503, green); scale bars are 20µm; representative images are shown; (C) Representative bright field microscopic images of empty vector (EV, control) and LIPG-OE (overexpressing) cells stained with triglyceride dye oil red O. Only LIPG-overexpressing cells are able to incorporate HDL and show increased cellular triglycerides; scale bar 20µm

LIPG-overexpressing cells fed with PC-OA had a twelve-fold increased TAG accumulation compared to empty vector (EV) cells (Fig. 3.19). Staining of lipid droplets with oil red O and immunofluorescence (Bodipy) also confirmed the results of the TAG quantification.

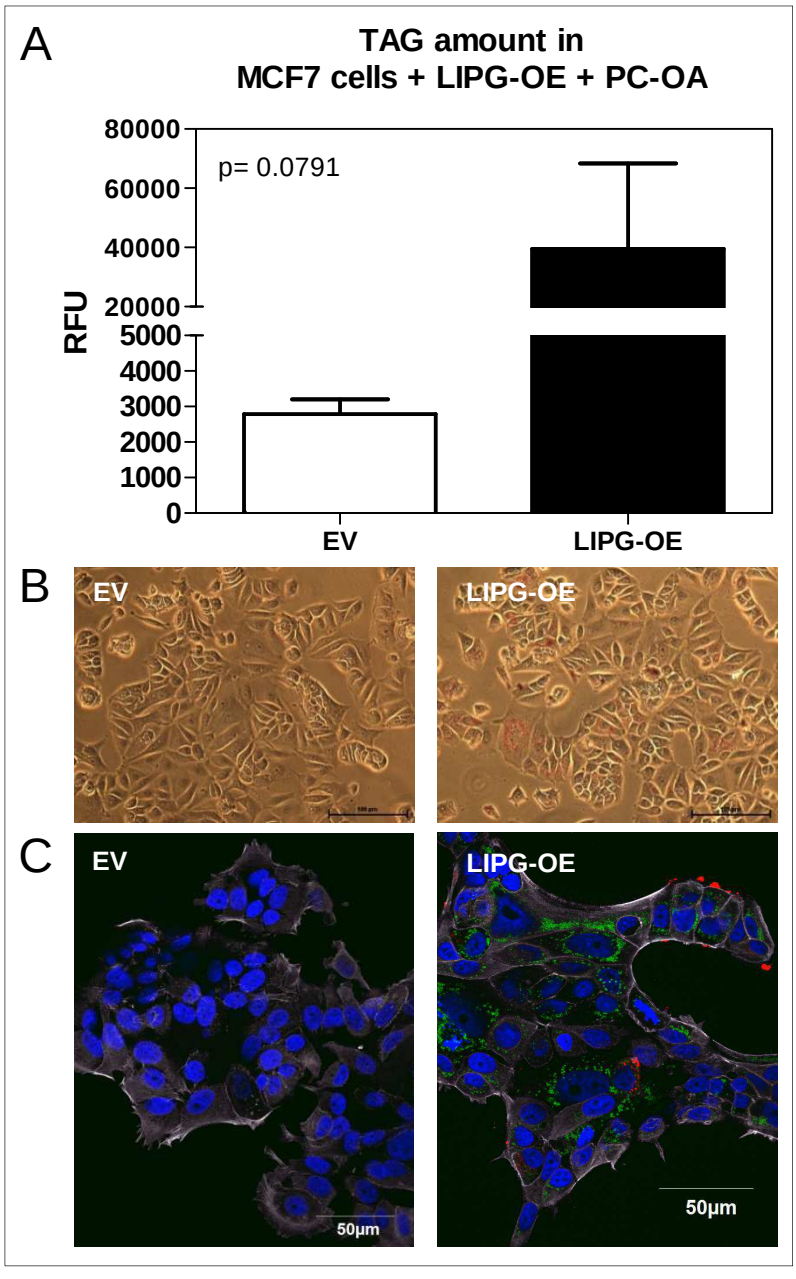

Fig. 3.19: LIPG-overexpressing MCF7 cells incubated with PC-OA (DOPC, 1,2-dioleoyl-sn-glycero-3-phosphocholine, Avanti) show increased cellular triglyceride levels. After 48 hours transfection with 1500ng LIPG-FLAG expression vector and X-tremeGENE HP DNA transfection reagent (Roche) cells were incubated with serum-free media supplemented with 800µg PC-OA for further 48h. (A) Quantification of triacylglycerol (TAG) amount by using Triglyceride Quantification Kit

(ab65336) from abcam. The results represent mean ± SEM (n=3); (B) Representative bright field microscopic images of empty vector (EV, control) and LIPG-OE (overexpressing) cells stained with

triglyceride dye oil red O. Only LIPG- overexpressing cells are able to incorporate oleic acid released from PC-OA into TAG; scale bar 100µm; representative images are shown; (C) Confocal microscopic images of fixed MCF7 cells labelled with fluorescent LIPG (anti-FLAG, red), nuclei (DAPI, blue), cytoskeleton actin (Rhodamine Phalloidin, grey) and lipid droplets (Bodipy 493/503, green); scale bars are 50µm; representative images are shown

In addition to PC-OA also feeding of LIPG-overexpressing cells with phosphatidylcholine containing other fatty acid species, such as stearic acid in 1,2-distearoyl-sn-glycero-3-phosphocholine (DSPC; PC-SA) and palmitic acid in 1,2-dipalmitoyl-sn-glycero-3-phosphocholine (DPPC; PC-PA), was tested. As illustrated in Figure 3.20 adding these PC species does not result in accumulation of intracellular in lipid droplets.

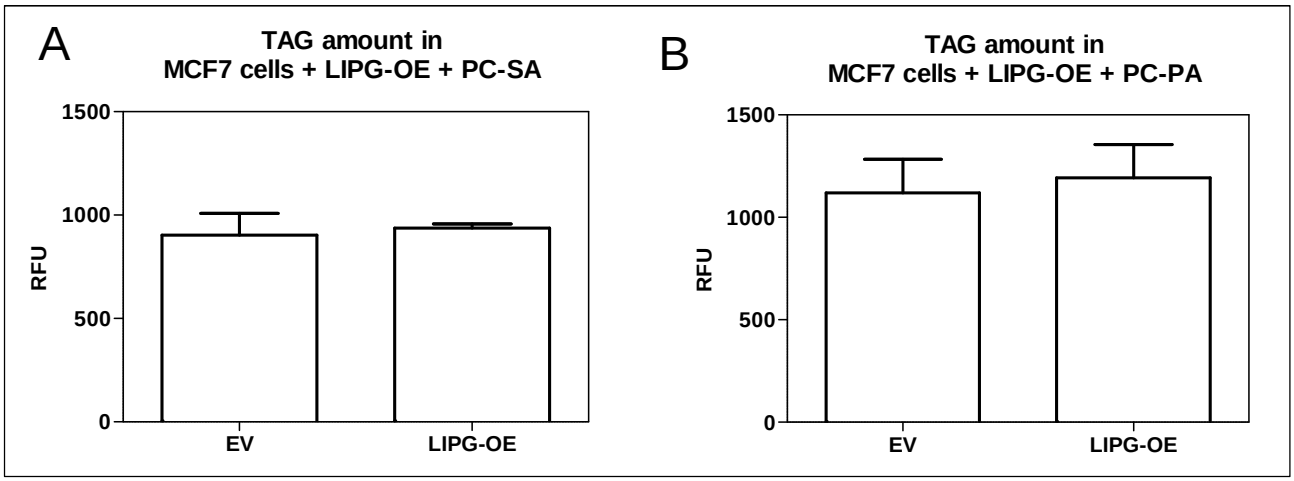

Fig. 3.20: LIPG-overexpressing MCF7 cells incubated with PC-SA (DSPC, 1,2-distearoyl-sn-glycero-3-phosphocholine, Avanti) and PC-PA (DPPC, 1,2-dipalmitoyl-sn-glycero-3-phosphocholine, Avanti) show no increased TAG levels. After 48 hours transfection with 1500ng LIPG-FLAG expression vector and X-tremeGENE HP DNA transfection reagent (Roche) cells were incubated with serum-free medium supplemented with 800µg (A) PC-SA or (B) PC-PA for further 48h. Quantification of triacylglycerol (TAG) amount by using Triglyceride Quantification Kit (ab65336) from abcam. The numbers represent mean of biological replicates ± SEM (n=1)

To make sure that the increased TAG amount is dependent on addition of LIPG substrates cells were transfected with EV or LIPG-OE and incubated in serum-free media without any additional substrates. Quantification of TAGs demonstrated the need of a LIPG-specific substrate like HDL or PC-OA to accumulate intracellular

lipids (Fig. 3.21) since LIPG overexpression alone (without HDL or PC-OA) does not lead to increased TAG levels.

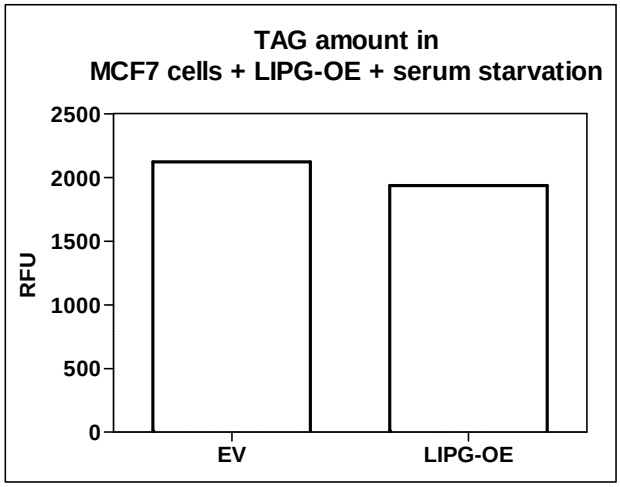

Fig. 3.21: LIPG-overexpressing MCF7 cells did not show lipid accumulation under serum-free conditions without substrate. After 48 hours transfection with 1500ng LIPG-FLAG expression vector and X-tremeGENE HP DNA transfection reagent (Roche) cells were serum-starved for further 48h. Quantification of triacylglycerol (TAG) levels was performed by the Triglyceride Quantification Kit (ab65336) from abcam. The numbers represent (n=1)

3.2.2 Induction of LIPG is accompanied by expression of the lipid droplet-coating protein PLIN2 and of LCN2

TAG quantification demonstrates increased lipid accumulation in LIPG-overexpressing cells fed with LIPG main substrates. These results could be confirmed by measuring the RNA level of the lipid droplet coating protein PLIN2 (Fig. 3.22). Under both conditions, fed with HDL or PC-OA, LIPG-overexpressing cells always display an increased PLIN2 expression (two-fold fed with HDL and three-fold with PC-OA).

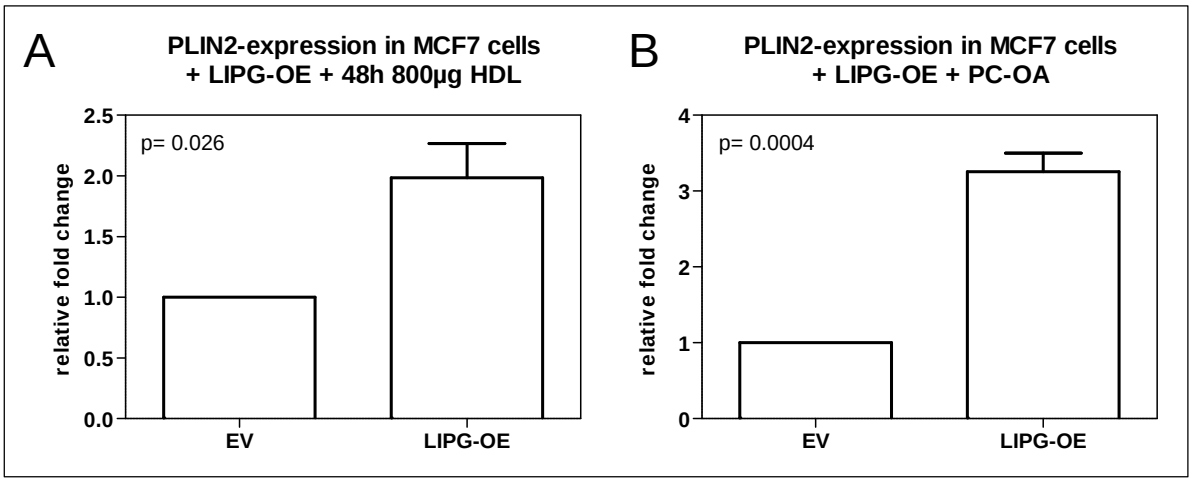

Fig. 3.22: LIPG-overexpressing MCF7 cells incubated with either (A) HDL or (B) PC-OA show increased Perilipin2 (PLIN2) expression, a marker for lipid droplets. After 48 hours LIPG-OE with 1500ng vector-DNA and X-tremeGENE HP DNA transfection reagent (Roche) cells were incubated with serum starved media supplemented with 800µg high density lipoprotein (HDL) or 800µg PC-OA (DOPC, 1,2-dioleoyl-sn-glycero-3-phosphocholine, Avanti) for further 48h. (A; B) PLIN2 expression in RNA extracts analyzed by quantitative real time PCR; as endogenous control UBC (ubiquitin C protein) was used. The numbers represent mean ± SEM (n=3)

Because Lipocalin2 (LCN2) has been shown to regulate lipid droplet formation in liver (Asimakopoulou et al. 2014) we also tested LCN2 gene expression in HDL and PC-OA treated LIPG-overexpressing cells. We observed a 1.8-fold increase in LCN2 expression in cells fed with 800µg HDL and two-fold elevation in the PC-OA-fed ones compared to controls (Fig. 3.23).

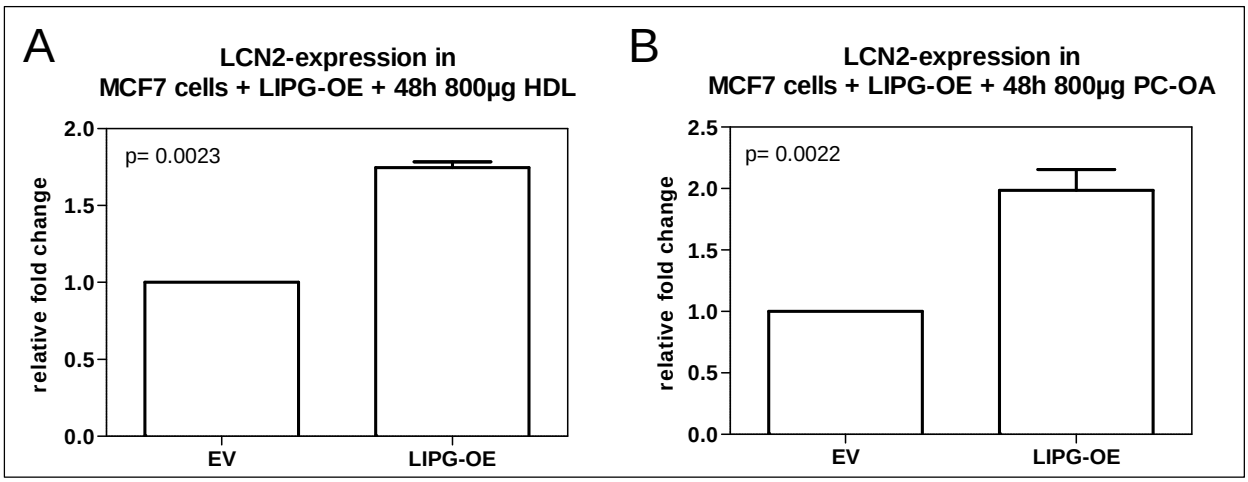

Fig. 3.23: LIPG-overexpressing MCF7 cells incubated with either (A) HDL or (B) PC-OA show enhanced Lipocalin2 (LCN2) expression. After 48 hours transfection with 1500ng LIPG-FLAG expression vector and X-tremeGENE HP DNA transfection reagent (Roche) cells were incubated with serum-free medium supplemented with 800µg high density lipoprotein (HDL) or 800µg PC-OA (DOPC, 1,2-dioleoyl-sn-glycero-3-phosphocholine, Avanti) for further 48h. (A; B) LCN2 expression in RNA

extracts was analyzed by quantitative real time PCR; as endogenous control UBC (ubiquitin C protein) was used. The results represent mean ± SEM (n=3)

The overexpression of LIPG without any substrates was not sufficient to enhance LCN2 mRNA expression, as shown in Figure 3.24.

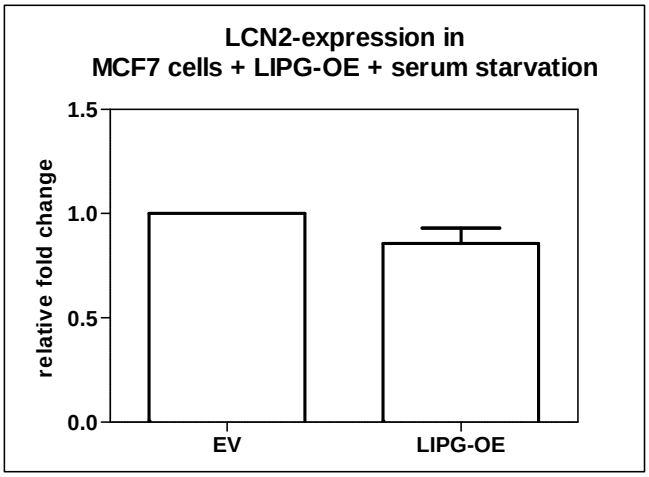

Fig. 3.24: LIPG-overexpressing MCF7 cells did not show elevated LCN2 expression in absence of LIPG substrate. After 48 hours transfection with 1500ng LIPG-FLAG expression vector and X-tremeGENE HP DNA transfection reagent (Roche) cells were serum-starved for further 48h. LCN2 expression in RNA extracts analyzed by quantitative real time PCR; as endogenous control UBC (ubiquitin C protein) was used. The numbers represent mean of technical duplicates ± SEM (n=1)

Rodvold et al. (2012) described that LCN2 induces epithelial to mesenchymal transition (EMT) in MCF7 cells. Several EMT markers exist like twist (increases EMT), snai1 (Zinc finger protein; no expression change under EMT), Nedd9 (neural precursor cell expressed, developmentally down-regulated; up-regulated by EMT), vim (vimentin; up-regulated by EMT) and CDH1 (E-cadherin; down-regulated by EMT). Therefore, we studied whether LCN2 induction in LIPG-transfected cells promotes EMT. For this purpose we analyzed expression of the aforementioned EMT markers. QRT-PCR measurements of LIPG-overexpressing cells fed with 800µg HDL show no detectable expression changes of these five mentioned genes (Fig. 3.25). These results suggest no correlation between LIPG overexpression-mediated lipid accumulation and EMT.

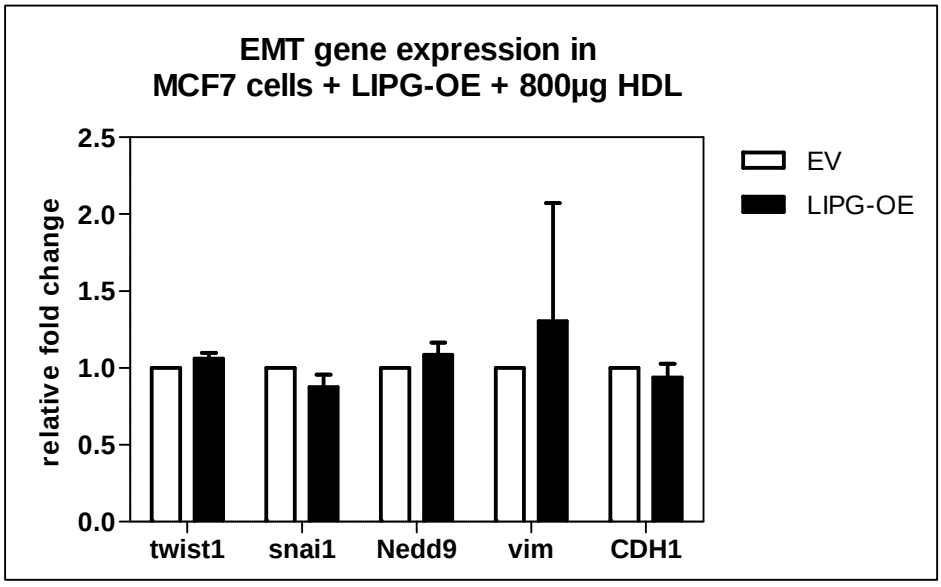

Fig. 3.25: LIPG-overexpressing MCF7 cells incubated with 800µg HDL did not show expression alterations of genes involved in epithelial to mesenchymal transition (EMT). After 48 hours transfection with 1500ng LIPG-FLAG expression vector with the X-tremeGENE HP DNA transfection reagent (Roche) cells were incubated with serum-free media supplemented with 800µg high density lipoprotein (HDL) for further 48h. Expression of genes involved in EMT was analyzed by quantitative real time PCR; as endogenous control UBC (ubiquitin C protein) was used. The results represent mean ± SEM (n=3)

3.2.3 Incubation of MCF7 cells with oleic acid results in intracellular lipid droplet accumulation

Blood serum contains 33% oleic acid as a free fatty acid (Patil and Magar 1959) source. As a control experiment parental MCF7 cells were incubated over 48h with oleic acid previously complexed with its carrier bovine serum albumin (OA/BSA) or BSA alone to confirm their capability to take up fatty acids independently of LIPG expression. This resulted in a 100-fold increase in cellular TAG in OA/BSA-treated cells compared to control BSA-alone treated cells (Fig. 3.26a). Lipid droplet staining with oil red O and Bodipy confirmed the dramatic lipid accumulation quantified by the TAG kit (Fig. 3.26b/c).

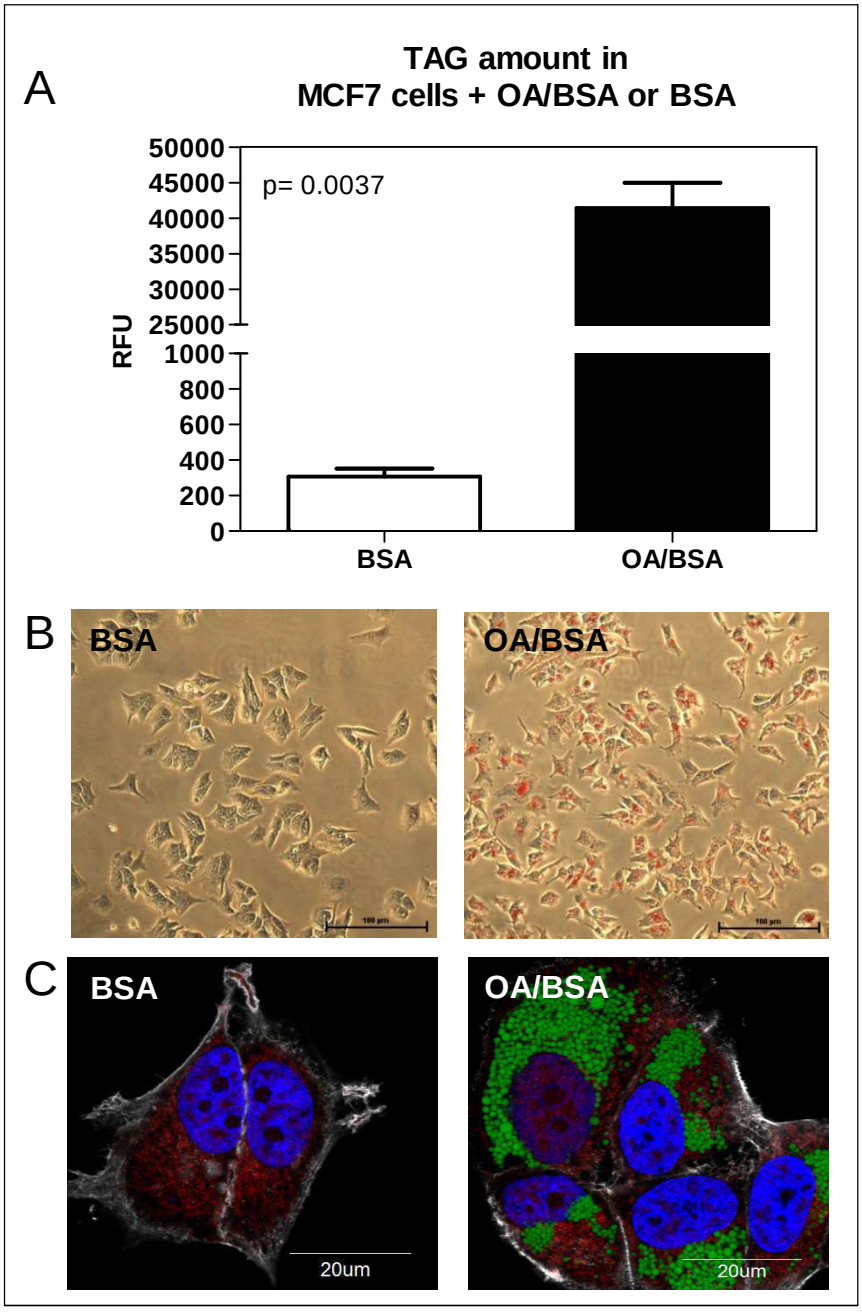

Fig. 3.26: Increased cellular triglyceride accumulation in MCF7 cells treated with oleic acid (OA) complexed to bovine serum albumin (BSA) compared to BSA-only treated cells. (A) Serum starved MCF7 cells incubated for 48h with 800µg oleic acid bound on BSA exhibit huge increased triacylglycerol (TAG) level compared with BSA-treated control cells. Quantification of triacylglycerol levels was done by using Triglyceride Quantification Kit (ab65336) from abcam. The results represent mean ± SEM (n=3); (B) Representative bright field microscopic images of serum starved MCF7 cells incubated for 48h with 800µg oleic acid bound on BSA or BSA alone stained with triglyceride dye oil red O. MCF7 cells are able to incorporate oleic acid and show lipid accumulation; scale bar 100µm; representative images are shown; (C) Confocal microscopic images of fixed MCF7 cells labeled for nuclei (DAPI, blue), cytoskeleton actin (Rhodamine Phalloidin, grey), lipid droplets (Bodipy 493/503, green) and PLIN2 (ADFP 647nm, red); scale bars are 200µm; representative images are shown

Furthermore, LIPG-overexpressing and empty vector-transfected MCF7 cells were also incubated with OA/BSA or BSA alone to study whether LIPG expression increases fatty acid uptake and thus result in higher cellular lipid accumulation levels. Treatment with OA/BSA but not with BSA, resulted in an equally increased TAG accumulation in LIPG-overexpressing and in empty vector transfected cells (Fig. 3.27). This shows that MCF7 breast cancer cells are able to incorporate exogenous fatty acids into TAG when added to the cells irrespectively of LIPG, but as seen in previous experiments, only LIPG expression renders them capable of using HDL and PC-OA as a fatty acid source.

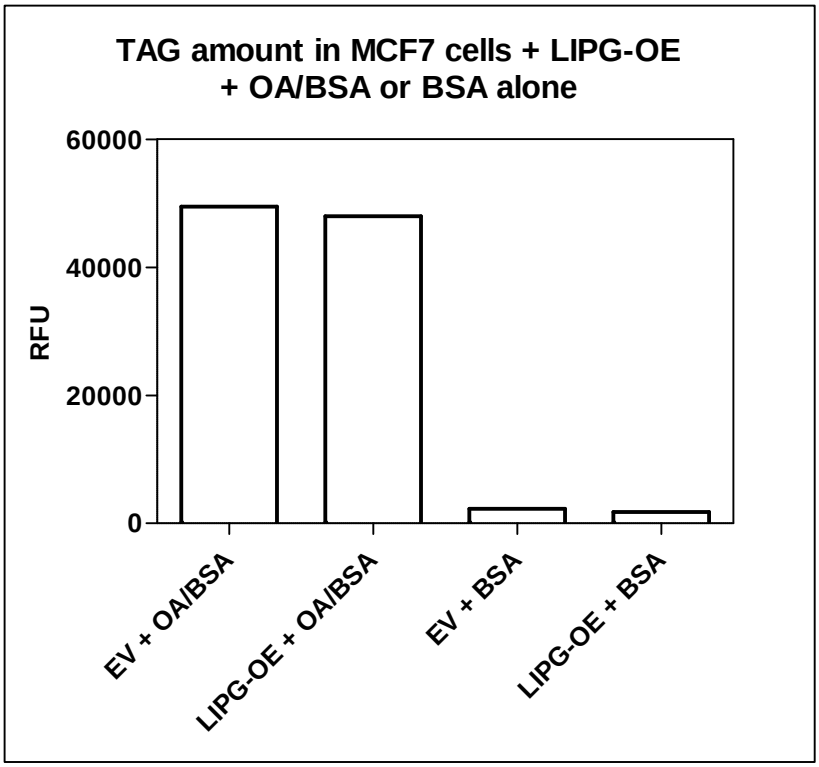

Fig. 3.27: The ability to incorporate oleic acid bound on BSA into TAG is independent of LIPG. LIPG-overexpressing and empty vector transfected MCF7 cells were incubated for 48h with 800µg oleic acid bound on BSA or BSA alone as control. Cellular TAG amounts were quantified with the Triglyceride Quantification Kit (ab65336) from abcam. The results represent n=1

QRT-PCR analysis of PLIN2 expression confirmed the TAG quantification and lipid droplets visualization shown in Figure 3.27. Incubation of MCF7 cells with OA/BSA or BSA alone led to a five-fold increase in PLIN2 expression (Fig. 3.28a). Also LCN2 displayed a four-fold upregulation after OA/BSA treatment compared to BSA control cells (Fig. 3.28b).

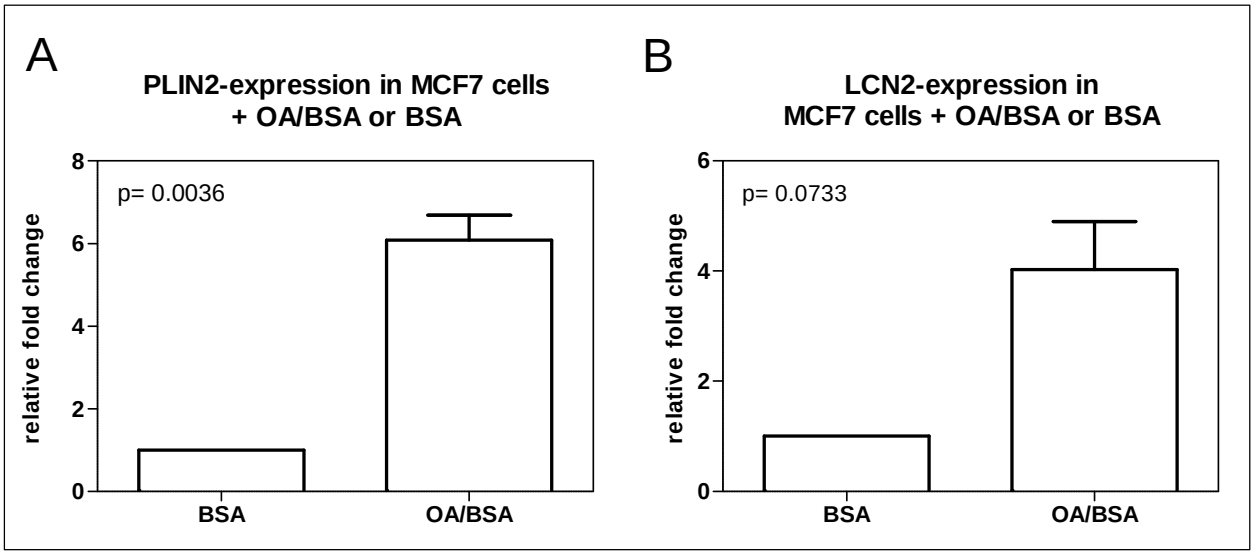

Fig. 3.28: MCF7 cells incubated with oleic acid (OA)/bovine serum albumin (BSA) for 48h exhibit an increased PLIN2- (A) and LCN2- (B) expression level compared to BSA-treated control cells. Gene expressions in RNA extracts were analyzed by quantitative real time PCR; as endogenous control UBC (ubiquitin C protein) was used. The results represent mean ± SEM (n=3)

3.2.4 MCF7 cells with increased lipid accumulation display survival advantages under starvation conditions

Proliferation assays were performed under harsh starvation conditions to elucidate advantages of elevated intracellular lipid content. MCF7 cells were fed with OA or solvent (DMSO) for 48h, followed by incubation in medium without glucose and serum (starvation period). The number of living cells was recorded by a CASY cell counter.

MCF7 cells incubated with 200µg OA/DMSO showed in all three experiments over ten days of harsh starvation conditions an increased number of living cells, indicating a survival advantage of lipid droplet-rich cells compared to the control cells (Fig.

3.29). The living cell number was measured at the beginning of the starvation period (=0h start) and after 10d of starvation. 73.4% of the OA-treated cells survived the starvation period, whereas only 20% of the control cells were viable.

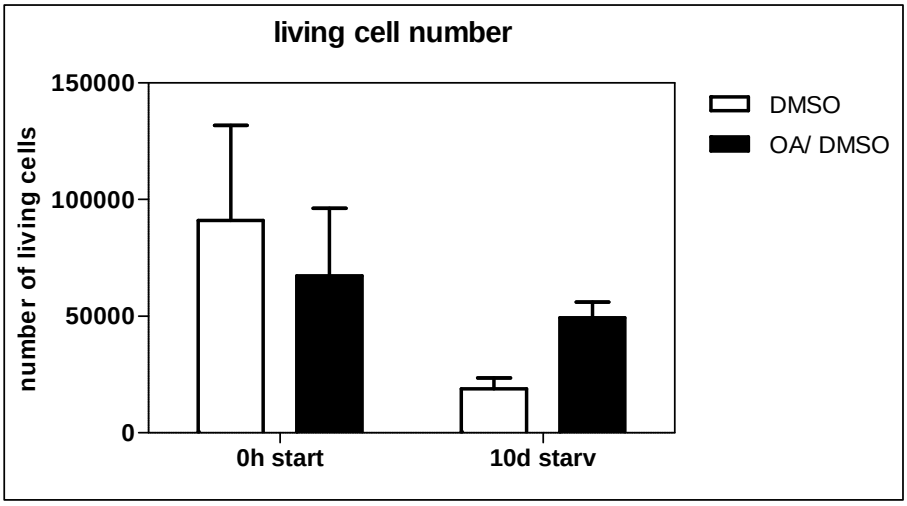

Fig. 3.29: Intracellular lipid accumulation after oleic acid (OA)/DMSO incubation confers MCF7 cells survival advantage under starvation conditions. MCF7 cells were incubated with 200µg OA/DMSO or 200µg DMSO alone with serum starved media to enables intracellular lipid accumulation. After 48h media was removed, washed and incubated with serum starved media without glucose (0g/L starv). The experiment shows the living cell number after 48h of OA/DMSO or DMSO incubation (0h start) and after 10d of harsh starvation; The numbers represent mean ± SEM (n=3)

In order to test the survival behavior of LIPG-transfected cells we performed a proliferation assay with LIPG-overexpressing cells fed with 800µg or 400µg PC-OA. LIPG-overexpressing cells did not show any alterations in proliferation behavior compared to empty vector control (Fig. 3.30). TAG quantification measurements confirmed increased lipid accumulation (ten-fold, data not shown) in LIPG-overexpressing cells but it seemed not to be sufficient to implicate survival advantages under starvation conditions.

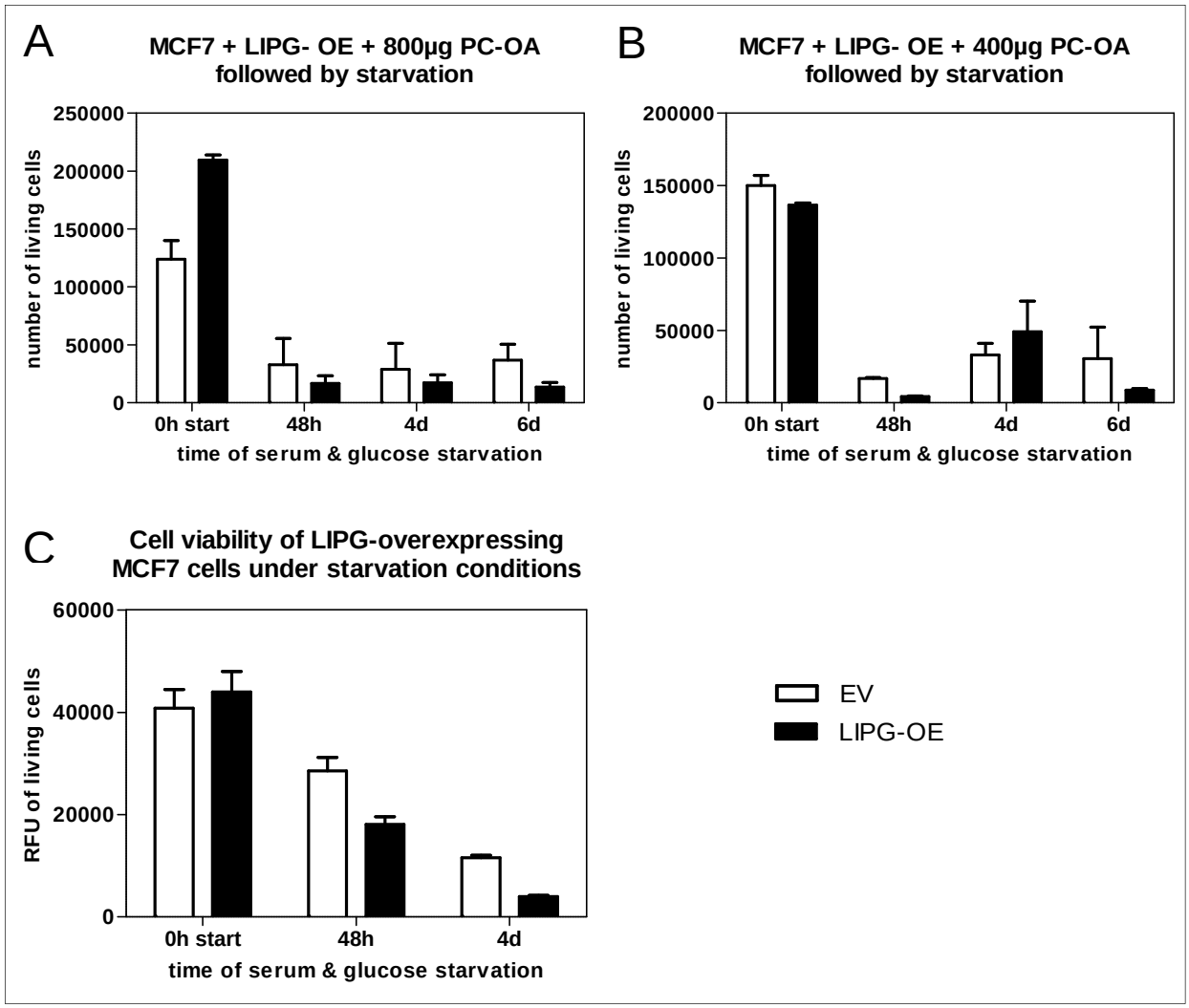

Fig. 3.30: Intracellular lipid accumulation after LIPG overexpression and PC-OA exposure in MCF7 cells did not confer survival advantage under starvation conditions. MCF7 cells were transfected under following conditions: EV (empty vector, control) and LIPG-OE (overexpression) for 48h. Cells were washed and incubated with serum starved media (A,C) + 800µg or (B) 400µg PC-OA. After 48h media was removed, washed and incubated with serum starved media without glucose (0g/L starv). (A,B) experiments show the living cell number in total over the mentioned time points; each experiment contains the mean of biological duplicates ± SEM. (C) shows the cell viability measured by CellTiter-Blue®Cell Viability assay (Promega) over the mentioned time points; The numbers represent mean ± SEM (n=3)

3.3 Effect of intracellular lipid accumulation on immunosurveillance

As reported before, LIPG overexpression triggers intracellular lipid accumulation. Moreover, we could show that lipid droplets confer a survival advantage upon nutrient shortage. In a next step we aimed to explore the possibility that intracellular lipid accumulation in cancer cells confers resistance to killing by immune cells.

For this purpose we tested the ability of natural killer (NK) cells to kill target cells which carry increased intracellular lipid content compared to control cells. The ^{51}Chromium-release killing assay with leukemia cells line K-562 as target cells is well established at the Immunology group (Prof. Dr. C. Watzl) at IfADo and was chosen for the experimental set-up. K-562 cells were incubated with OA/BSA to achieve intracellular lipid accumulation or with BSA alone (control). Natural killer cells (NK cells) were isolated from whole blood samples of healthy donors and co-cultured with ^{51}Cr-labeled K-562 target cells (OA/BSA and BSA-treated) to perform the killing assay.

Figure 3.31a displays the killing efficiencies of OA/BSA-treated and control K-562 cells in the ^{51}Chromium (Cr) release assay (killing assay). The y-axis shows the specific lysis [%] and the x-axis the effector (NK cells) to target (K-562 cells) ratio (e:t). The release of ^{51}Chromium from K-562 cells cultured in media alone (without co-culturing with NK cells) is referred as spontaneous value and set to 0%. The release of ^{51}Chromium from target cells treated with Triton X-100 was the maximal value and set to 100%. These controls underlie the calculation of the specific lysis [%]. K-562 cells previously incubated for 48h with OA/BSA to induced intracellular lipid accumulation showed less killing compared to BSA control. Figure 3.31b shows the results of the TAG quantification in OA/BSA and BSA-treated K-562 cells. All OA/BSA incubated cells revealed a high lipid accumulation compared to BSA alone treated control cell.

These results indicate that fat accumulation in cancer cells may partially inhibit natural killer cell-mediated cytotoxicity and thus contribute to tumor escape from the immune system.

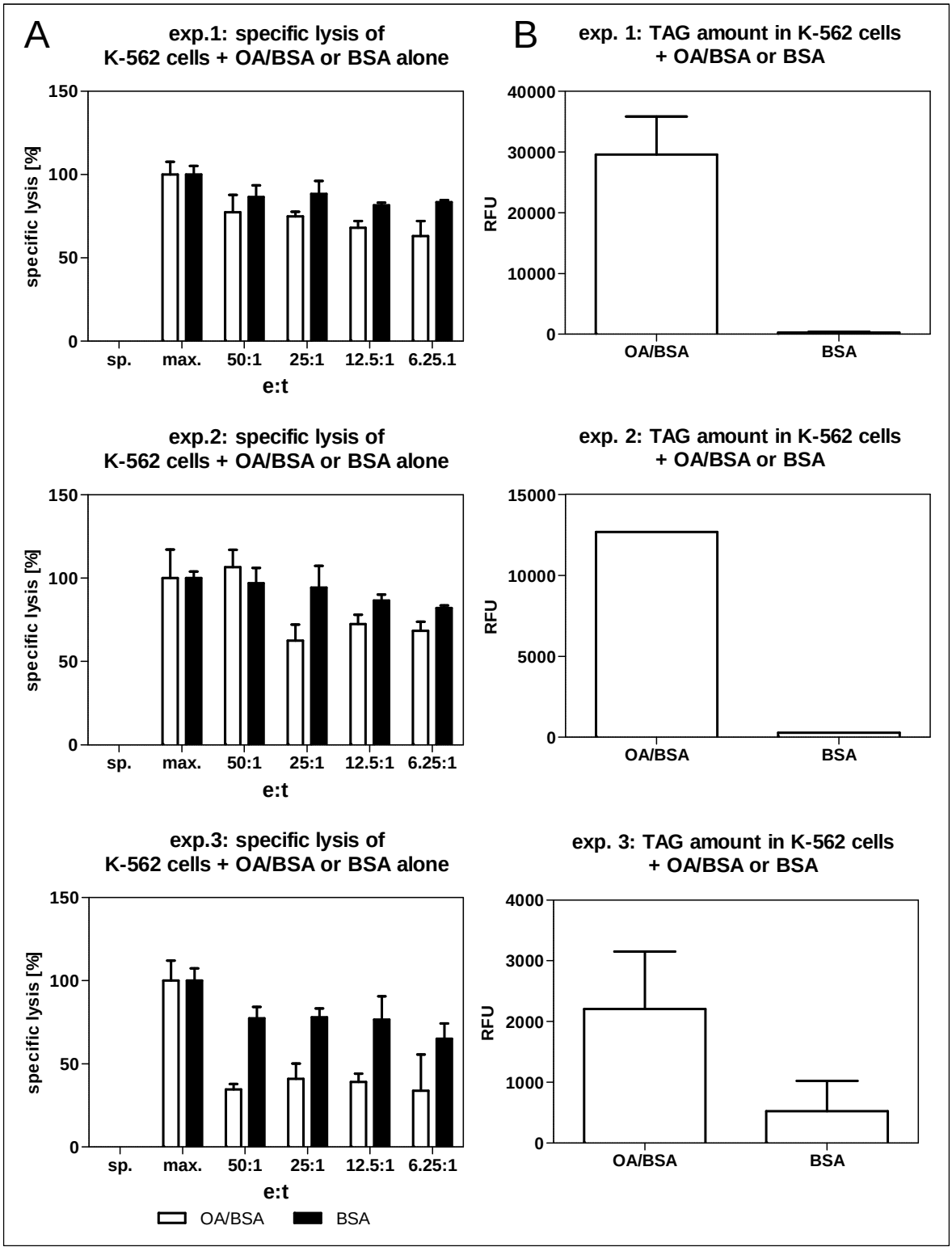

Fig. 3.31: K-562 cells incubated for 48h with oleic acid (OA)/bovine serum albumin (BSA) are less killed compared to BSA-treated control cells. Leukemia suspension K-562 cells incubated for 48h with 800µg oleic acid bound on BSA or only with BSA as control. (A) ^{51}Chromium (Cr) release assay (killing assay) with natural killer cells indicates less killing of OA/BSA-treated cells compared to BSA control cells. Shown are three independent experiments each performed as biological triplicates; (B) Quantification of TAG amount by using Triglyceride Quantification Kit (ab65336) from abcam to control lipid accumulation

3.4 LIPG is induced after blockage of intracellular fatty acid synthesis

The previous results could show that increased LIPG expression enhances intracellular lipid accumulation via lipolysis and uptake of exogenous lipid sources. Because cancer cells are usually capable of synthetizing fatty acids *de novo* (Zaidi et al. 2013), we tested the hypothesis that LIPG may be induced if fatty acid synthesis (FAS) is impaired.

5-(tetradecyloxy)-2-furoic acid (TOFA) is an inhibitor of the acetyl-CoA carboxylase (ACACA) resulting in blocking the *de novo* fatty acid synthesis. MCF7 cells were incubated for 24h or 48h with 6µM TOFA and LIPG expression was analyzed by qRT-PCR. Figure 3.32 illustrates a significant increase in LIPG expression in TOFA-treated cells compared to control cells. This result suggests that LIPG may be induced to compensate a decreased capacity of fatty acid synthesis.

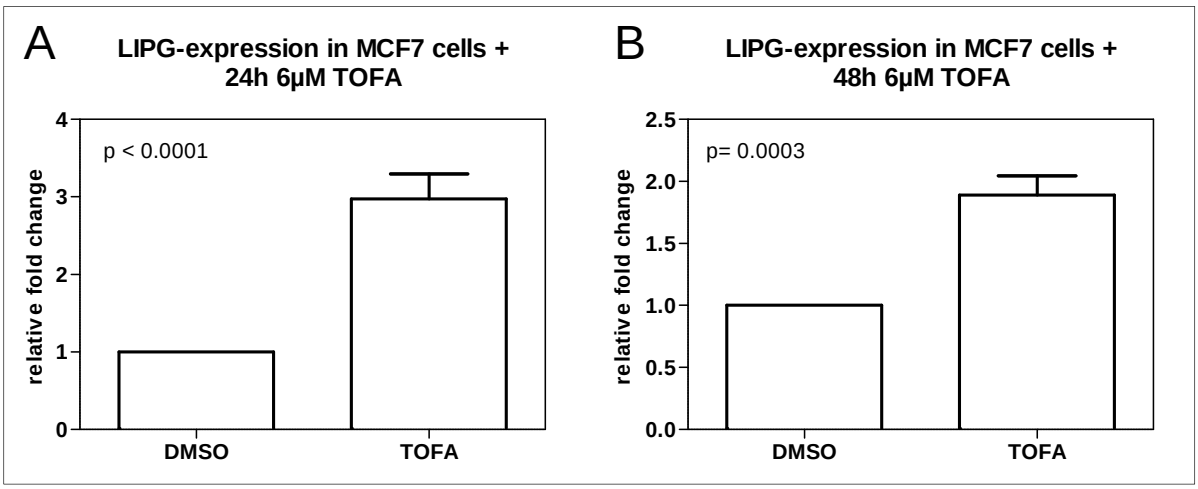

Fig. 3.32: Blocking the *de novo* fatty acid synthesis in MCF7 cells by TOFA results in increased LIPG expression. MCF7 cells were incubated over 24h (A) or 48h (B) with 6µM 5-(tetradecyloxy)-2-furoic acid (TOFA) to inhibit acetyl-CoA carboxylase (ACACA) and prevent *de novo* fatty acid synthesis. LIPG gene expression in RNA extracts was analyzed by quantitative real time PCR; as endogenous control UBC (ubiquitin C protein) was used. The numbers represent mean ± SEM (n=3)

Due to the fact that LIPG is upregulated in case of a blocked endogenous fatty acid synthesis we tested whether LIPG overexpression and its function as a fatty acid "supplier" could confer a survival advantage under these conditions. For this purpose LIPG-overexpressing and empty-vector transfected cells fed with 800µg PC-OA for 48h were incubated with 6µM TOFA in serum starved media for further 48h. We

checked the mitochondrial membrane potential by using tetramethylrhodamine ethyl ester perchlorate (TMRE). Mitochondrial membrane potential driven accumulation of TMRE within inner membrane region indicates healthy functioning mitochondria. In case of depolarization (changes in membrane potential towards more positive potential) or inactive mitochondria results in decreased membrane potential and fail to sequester TMRE (loss of dye at latest less fluorescence). Figure 3.33 illustrates that LIPG-overexpressing cells treated with PC-OA incorporated significantly (p=0.001) more (1.6-fold) TMRE compared to MCF7 cells transfected with empty vector and incubated with PC-OA. That implies that LIPG-mediated lipid supply promotes mitochondrial survival in case of intracellular fatty acid depletion.

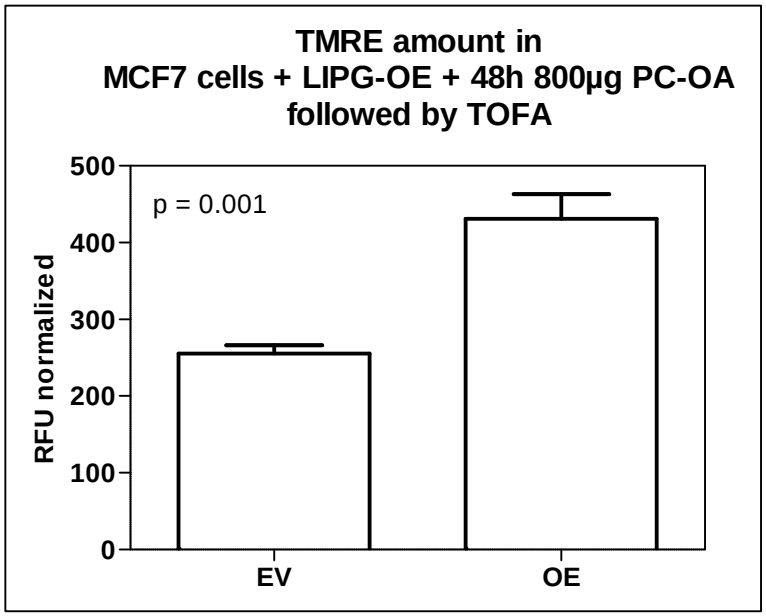

Fig. 3.33: Blocking the *de novo* fatty acid synthesis by TOFA in LIPG- overexpressing MCF7 cells fed with PC-OA resulted in increased TMRE amount. MCF7 cells were incubated over 48h with 6µM 5-(tetradecyloxy)-2-furoic acid (TOFA) to inhibit acetyl-CoA carboxylase (ACACA) and prevent *de novo* fatty acid synthesis in serum starved media after transfection with either LIPG- or empty vector control-DNA both fed with 800µg PC-OA for 48h. LIPG overexpression enables lipid accumulation by incubation with PC-OA and maintains the mitochondrial function in case of intracellular fatty acid depletion. The numbers represent mean ± SEM (n=3)

3.5 Increased LIPG expression in MCF7 cells incubated with cobalt chloride ($CoCl_2$)

Cobalt chloride ($CoCl_2$) has hypoxia-mimicking effect under normoxic conditions and induces generation of reactive oxygen species (ROS) in different cell types (Oh et al. 2014). Recently, it has been reported that lipid droplets protect against ROS and support survival in hypoxia-reoxygenation (Bensaad et al. 2014). Moreover, it could be shown that lipid droplet formation under these conditions was due to fatty acid uptake while *de novo* lipid synthesis is repressed (Bensaad et al. 2014). Therefore we explored the possibility that LIPG plays a role in lipid uptake under oxidative stress conditions. For this purpose, MCF7 cells were incubated with different concentrations of $CoCl_2$ for 24h to induce oxidative stress. Expression of LIPG as well as of PLIN2, as a lipid droplet marker, was analyzed by real time qRT-PCR. In this thesis we had the opportunity to obtain already isolated RNA from $CoCl_2$ treated-MCF7 cells, kindly provided by Rosemarie Marchan, Joanna Stewart and Michaela Lesjak. Interestingly, both genes LIPG and PLIN2 showed a $CoCl_2$-concentration dependent increase on mRNA levels (Fig. 3.34a/b). LIPG revealed a ten-fold enhanced expression accompanied by 2.5-fold PLIN2 expression increase. This suggested that $CoCl_2$ induces formation of lipid droplets and that LIPG may be involved in this process by promoting lipolysis of extracellular lipoproteins and subsequent uptake of fatty acids. Oxidative stress upon $CoCl_2$ exposure was measured by analyzing expression of antioxidant proteins (Fig. 3.34c/d). Thioredoxiin reductase (TXNRD1) is required for reducing thioredoxin (TXN), which in turn is necessary for repair of oxidized proteins. Interestingly, at the highest concentrations of $CoCl_2$ the TXN-inhibitor thioredoxin interacting protein (TXNIP) was downregulated. Upregulation of TXNRD1 and downregulation of TXNIP have been shown to occur in our model of MCF7/NeuT induced senescence (Cadenas et al. 2010), which is also accompanied by high levels of ROS (Cadenas et al. 2010). This concomitant upregulation of the thioredoxin activator and downregulation of its inhibitor is meant increased availability of active, reduced thioredoxin in the cell. Moreover, these gene expression alterations in MCF7/NeuT cells are also associated to upregulation of LIPG and PLIN2 as well as by accumulation of intracellular lipid droplets. This shows that LIPG is induced upon conditions of acute oxidative stress

associated with uptake of extracellular lipids, both in a model of oncogene-induced senescence and toxicity by chemical hypoxia.

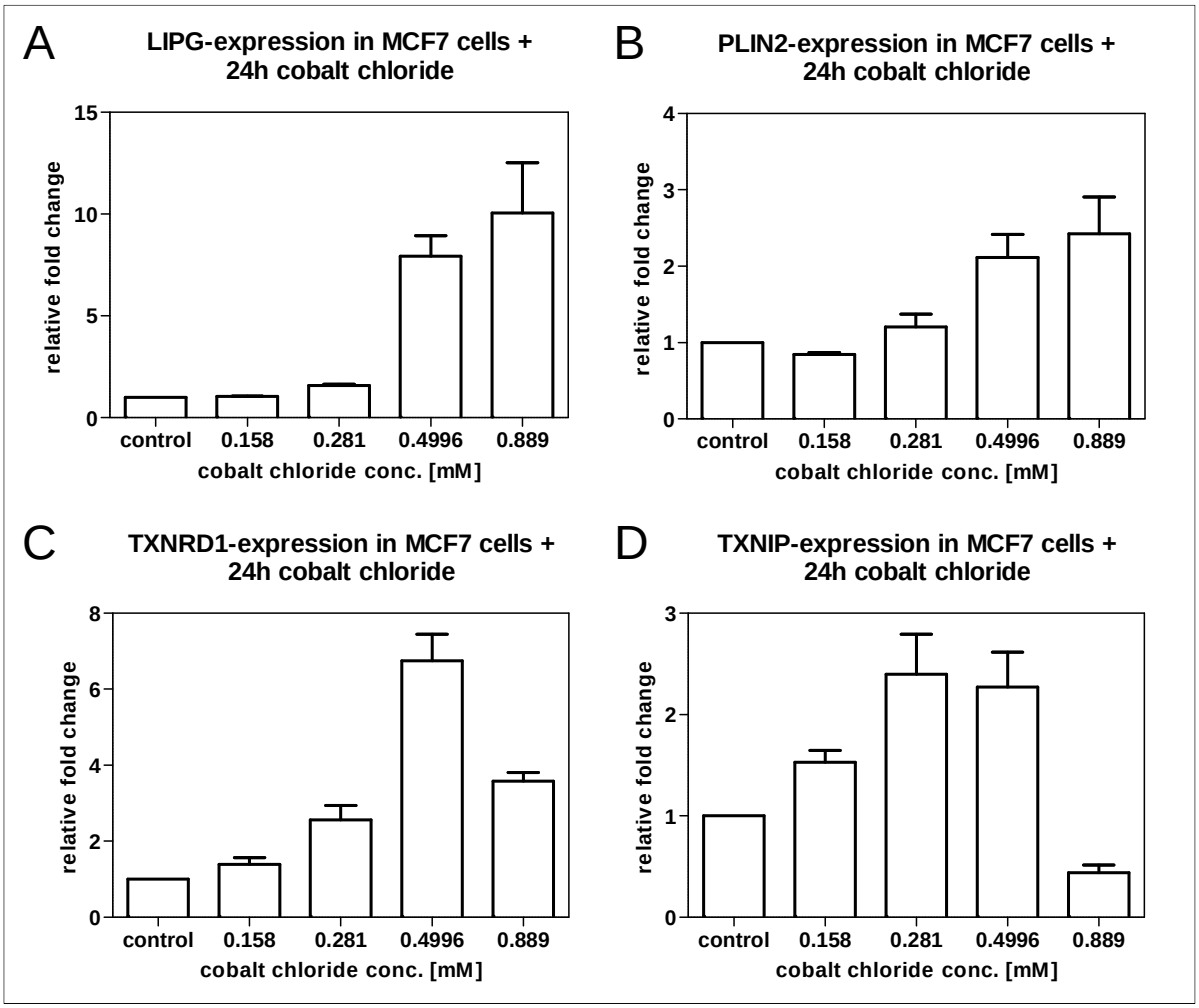

Fig. 3.34: Hypoxic-mimicking effect of $CoCl_2$ induces huge LIPG- and weak PLIN2 expression in MCF7 cells. MCF7 cells were incubated with different cobalt chloride ($CoCl_2$) concentrations over 24h. LIPG (A), PLIN2 (B), TXNRD1 (C) and TXNIP (D) gene expression in RNA extracts was analyzed by quantitative real time PCR; as endogenous control UBC (ubiquitin C protein) was used. The numbers represent mean ± SEM (n=3)

3.6 Endogenous LIPG expression in different cancer cell lines

In addition to breast cancer cells we investigated LIPG expression in cell lines derived from other tumors, including endometrial, liver and ovarian cancer. For this purpose real time qRT-PCR analysis of endogenous LIPG expression in available cDNA samples was performed.

LIPG expression in the different cell lines was normalized to LIPG expression level in MCF7/NeuT cells. Figure 3.35 shows that the highest endogenous LIPG expression was detected in the MDA-MB-468 breast cancer cell line, in the AN3-CA endometrial cancer cell line, in the SFL004 liver cancer cell line and in the OVCAR-3 ovarian cancer cells. This observation suggested in general higher expression of LIPG in more aggressive, metastazing cells lines.

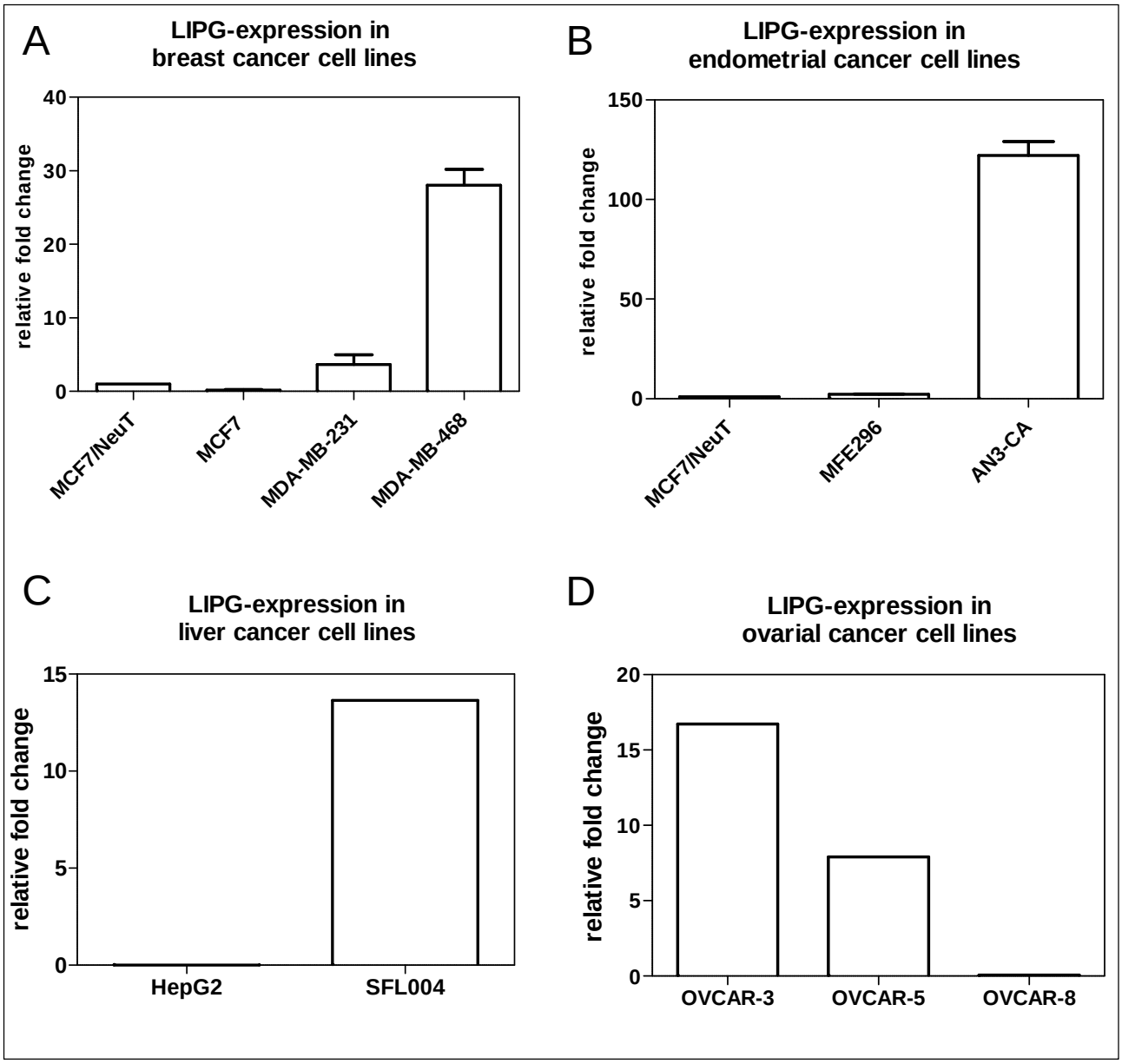

Fig. 3.35: LIPG expression is higher in more aggressive cancer cell lines. RNA extracts were analyzed by quantitative real time PCR to compare LIPG expression in different cancer cell lines; As an endogenous control UBC (ubiquitin C protein) was used and LIPG expression level in MCF7/NeuT cells was taken as a reference. (A) Among the breast cancer cell lines MCF7, MDA-MB-231 and MDA-MB-468, MDA-MB-468 cells showed the highest endogenous LIPG expression compared to the other cell lines. The numbers represent mean ± SEM (n=3) (B) Among the endometrial cell lines MFE296

and AN3-CA, AN-3CA exhibited a 125-fold higher LIPG expression level compared to the other cell lines. The numbers represent mean ± SEM (n=3) (C) Liver cancer HepG2 and SFL004 cell lines, whereas SFL004 showed a 14-fold elevated endogenous LIPG expression. The numbers represent one biological experiment (D) Ovarial cancer OVCAR-3, OVCAR-5 and OVCAR-8 cell lines. OVCAR-3 cells indicated the highest LIPG expression level compared to the other cell lines. The numbers represent one biological experiment

3.7 Transient reduction of LIPG gene expression by siRNA *in vitro*

Small interfering RNAs (siRNA) enable the transient reduction of expression of genes of interest. In order to explore the consequences of LIPG downregulation LIPG knock down experiments were performed. Cells were incubated for 72h with either a specific LIPG-siRNA or a control-siRNA (negative control; NC), which is non-specific. Different siRNA concentrations and transfection conditions were tested in order to generate a robust maximal LIPG knock down efficiency. Knock down efficiencies were controlled by quantitative real time PCR and immunoblotting. We aimed to achieve a knock down efficiency of at least 80%. MDA-MB-468 cells were chosen for the experiment, since, as shown in Figure 3.35, they exhibit a high endogenous LIPG expression level compared to other tested breast cancer cell lines.

In this thesis ten different LIPG-siRNAs were tested combined with five chemical transfection reagents as well as electroporation. Figure 3.36 illustrates a representative knock down result. Mostly knock down experiments showed on RNA level a tolerable efficiency between 50%-80% reduction. Checking the protein amount of LIPG by immunoblotting no knock down success could be registered. Conditioned by the inefficient transient LIPG reduction no knock down experiments could be performed.

During the knock down experiments different problems were encountered. On one hand liposome-based transfection reagents were shown to influence LIPG expression. Therefore, five different transfection reagents as well as electroporation were tested. On the other hand a satisfactory knock down efficiency could not be achieved. Ten different LIPG-siRNA oligos were tested that resulted in a reduction of LIPG mRNA levels of 50-80%. However, reduction of LIPG protein levels was not observed with any of the siRNA oligos.

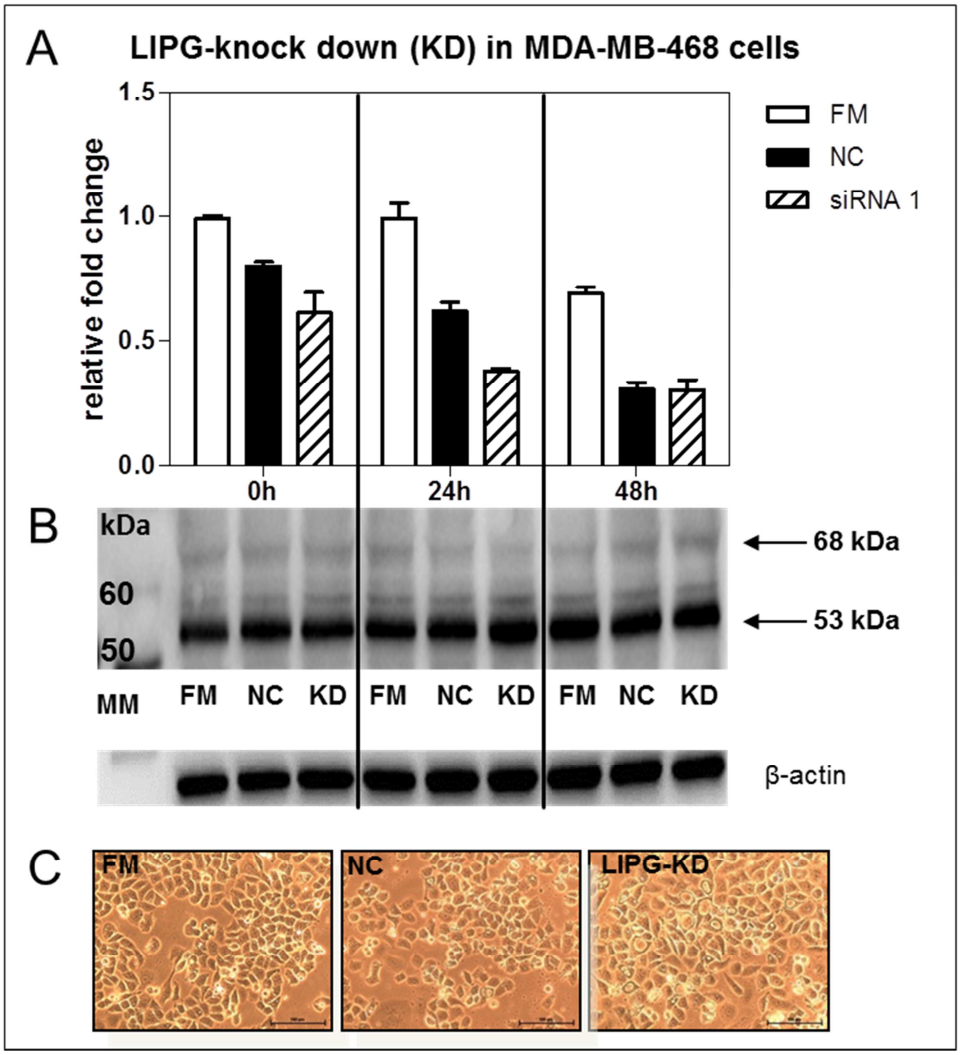

Fig. 3.36: LIPG-knock down using siRNAs in MDA-MB-468 cells did not lead to LIPG protein reduction. MDA-MB-468 cells were transfected with siRNA against LIPG and non-specific siRNA (NC) as negative control. (A) LIPG expression was analyzed by quantitative real time PCR to control knock down efficiency at different time points: directly after transfection, 24h- and 48h- post-transfection; as endogenous control UBC (ubiquitin C protein) was used. The numbers represent mean of one representative knock down (performed in duplicates); (B) Immunoblotting of LIPG expression in MDA-MB-468 cells to detect knock down efficiency on protein level; protein collection of whole cell lysate; β-actin used as loading control. A representative immunoblot is shown; (C) Representative bright field microscopy images of cells after LIPG knock down by siRNA

3.8 The role of LIPG in human breast carcinoma

In order to investigate LIPG expression in human breast tumors and its possible contribution to tumor progression we investigated first a collection of homogenous lymph node-negative untreated (no chemotherapy) breast cancer patients. The main study cohort (Mainz GSE11121) comprises 200 node-negative breast cancer patients. Additional investigated node-negative untreated cohorts included Rotterdam (GSE2034, n=286), Transbig (GSE6532, n=84 & GSE7390, n=196) and Yu (GSE5327, n=58).

Histograms of LIPG expression in the four cohorts showed a bimodal distribution of LIPG mRNA. The majority of tumors displayed low LIPG levels and a limited subset of tumors appeared to express high levels of LIPG mRNA (Fig. 3.37), suggesting that LIPG in breast cancer represents a rare event.

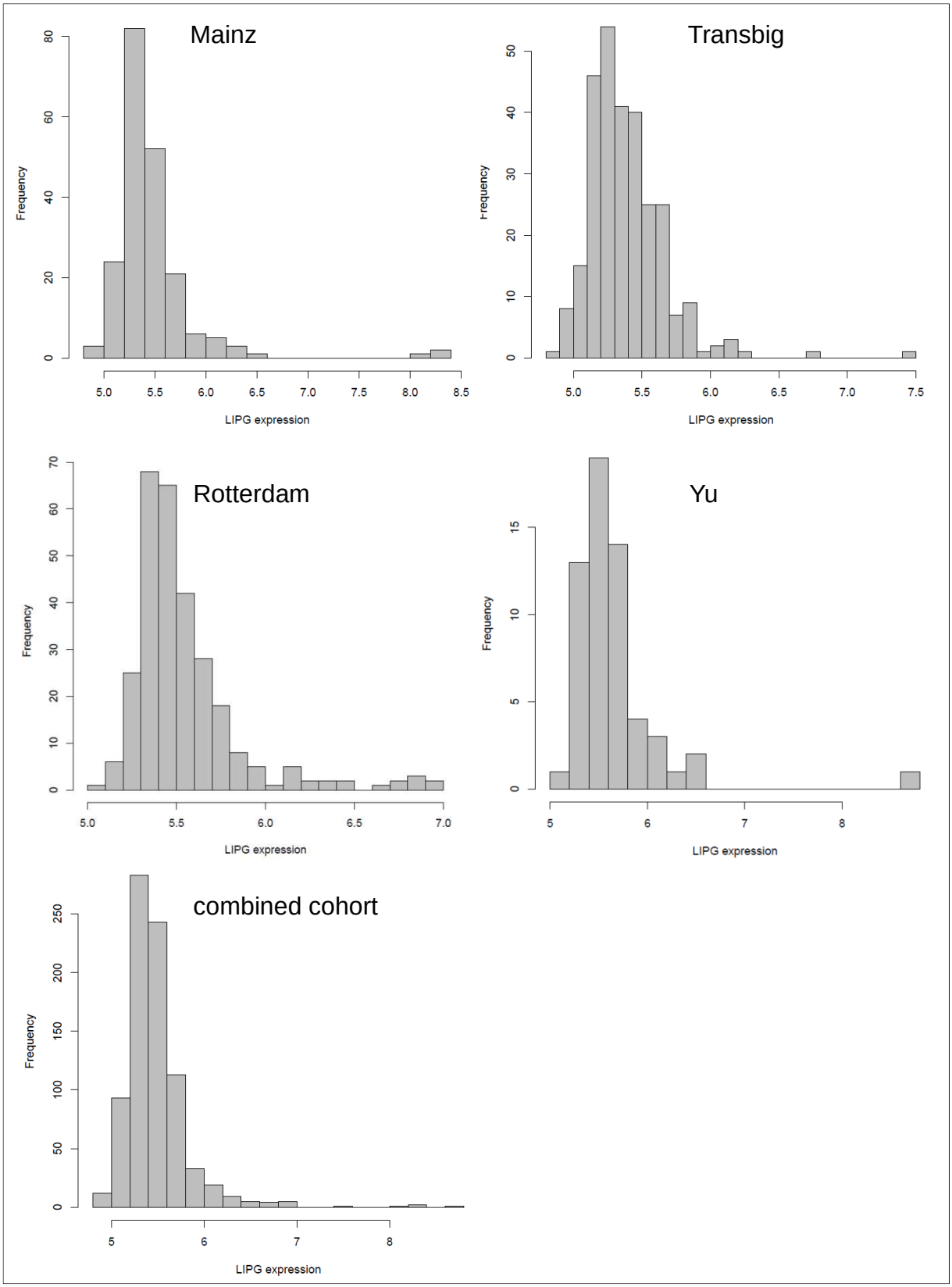

Fig. 3.37: Histograms of LIPG expression in four different cohorts. All cohorts show a bimodal distribution of LIPG expression with only a small population displaying high LIPG mRNA levels

LIPG mRNA expression in breast tumors was validated by quantitative real time PCR (qRT-PCR). Ten samples of the Mainz cohort (two samples with high, four samples with moderate and four samples with low LIPG expression) were available for the analysis. The qRT-PCR results could confirm the Affymetrix gene array data (Fig. 3.38)

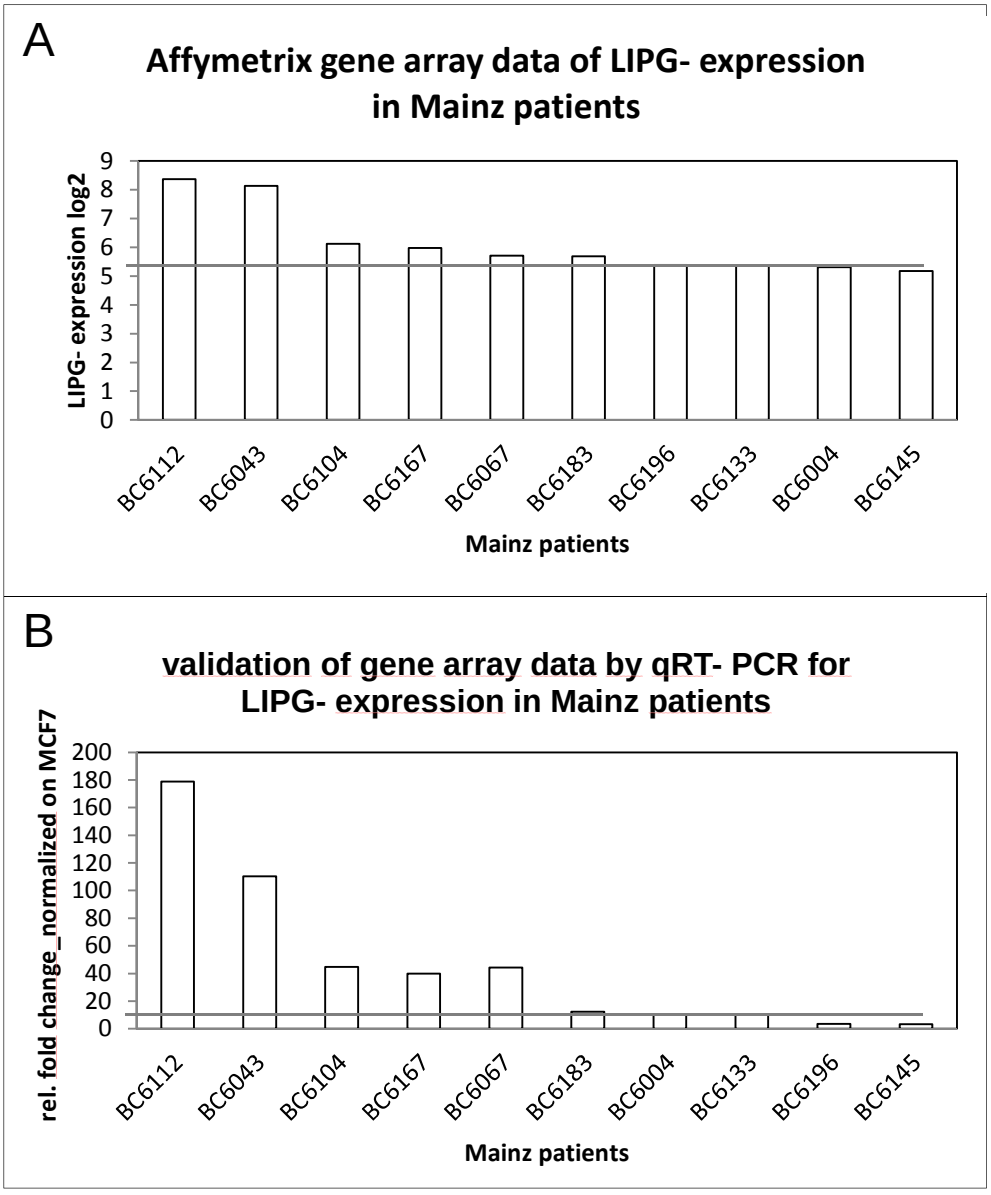

Fig. 3.38: LIPG expression in ten breast cancer patients of Mainz cohort. (A) Affymetrix gene array data of LIPG expression of two breast cancer patients with increased LIPG level, four with moderate level and four patients with lower LIPG expression level; numbers represent n=1; (B) Validation of Affymetrix gene array data by quantitative real time PCR from RNA extracts of selected breast cancer patients; normalized on LIPG level in MCF7 cells; as endogenous control UBC (ubiquitin C protein) was used; numbers represent n=1

3.8.1 Uni- and multivariate Cox model for LIPG in untreated, node-negative cohorts

As shown in Figure 3.37 all studied cohorts of untreated patients exhibited a similar distribution of LIPG expression with only a few outliers showing high expression of LIPG. Due to the limited number of LIPG-expressing tumors it was not possible to use LIPG mRNA expression as a continuous variable to investigate survival associations in Cox models. A 98% quantile cut-point (CP=6.451), quantile plus interquartile range, discriminated n=4 outliers with strong LIPG expression in the Mainz cohort, n=8 in the Rotterdam cohort, n=2 in the Transbig cohort and n=3 in the Yu cohort.

Based on this dichotomization we performed an univariate Cox-analysis to investigate the correlation between LIPG expression and survival. A significant association of LIPG-high expression with worse prognosis (HR>1; p value <0.05) was observed in the Mainz (HR=6.42, p=0.002), the Transbig (HR=22.52, p=0.003) and the combined cohort (HR=2.49, p=0.011) (Tab. 3.1). These results are illustrated in the Kaplan-Meier curves (Fig. 3.39).

To investigate the relationship between LIPG expression and metastasis-free survival considering the impact of other clinical parameters (age, histological grade, pTstage, HER2 and ER-status) we performed a multivariate Cox-analysis (calculation of independence) (Tab. 3.1-3.6). In the combined cohort increased LIPG expression was associated with worse prognosis independently of the clinico-pathological factors.

Tab. 3.1: Univariate Cox-analysis

univariate Cox-analysis (LIPG >6.451)		
cohorts	**hazard ratio**	**p-value**
Mainz	6.42	0.002
Rotterdam	1.11	0.853
Transbig	22.52	0.003
Yu	2.55	0.373
combined	2.49	0.011

Tab. 3.2: Multivariate Cox-analysis for Mainz cohort

multivariate Cox-analysis (LIPG >6.451) in Mainz cohort		
clinical parameter	**hazard ratio**	**p-value**
LIPG	3.53	0.064
age > 50years	0.93	0.816
stage II + III	0.91	0.759
grade III	4.66	<0.001
ER +	1.64	0.201
HER2 +	1.5	0.248

Tab. 3.3: Multivariate Cox-analysis for Rotterdam cohort

multivariate Cox-analysis (LIPG >6.451) in Rotterdam cohort		
clinical parameter	**hazard ratio**	**p-value**
LIPG	1.13	0.847
ER +	1.01	0.966
HER2 +	1.02	0.953

Tab. 3.4: Multivariate Cox-analysis for Transbig cohort

multivariate Cox-analysis (LIPG >6.451) in Transbig cohort		
clinical parameter	**hazard ratio**	**p-value**
LIPG	20.59	0.007
age > 50years	1.10	0.691
stage II + III	1.65	0.042
grade III	0.94	0.814
ER +	0.66	0.149
HER2 +	0.91	0.803

Tab. 3.5: Multivariate Cox-analysis for Yu cohort

multivariate Cox-analysis (LIPG >6.451) in Yu cohort		
clinical parameter	**hazard ratio**	**p-value**
LIPG	2.25	0.441
HER2 +	0.43	0.429

Tab. 3.6: Multivariate Cox-analysis for combined cohort

multivariate Cox-analysis (LIPG >6.451) in combined cohort		
clinical parameter	**hazard ratio**	**p-value**
LIPG	4.53	0.005
age > 50years	1.03	0.892
stage II + III	1.18	0.374
grade III	1.72	0.012
ER +	0.93	0.752
HER2 +	1.17	0.527

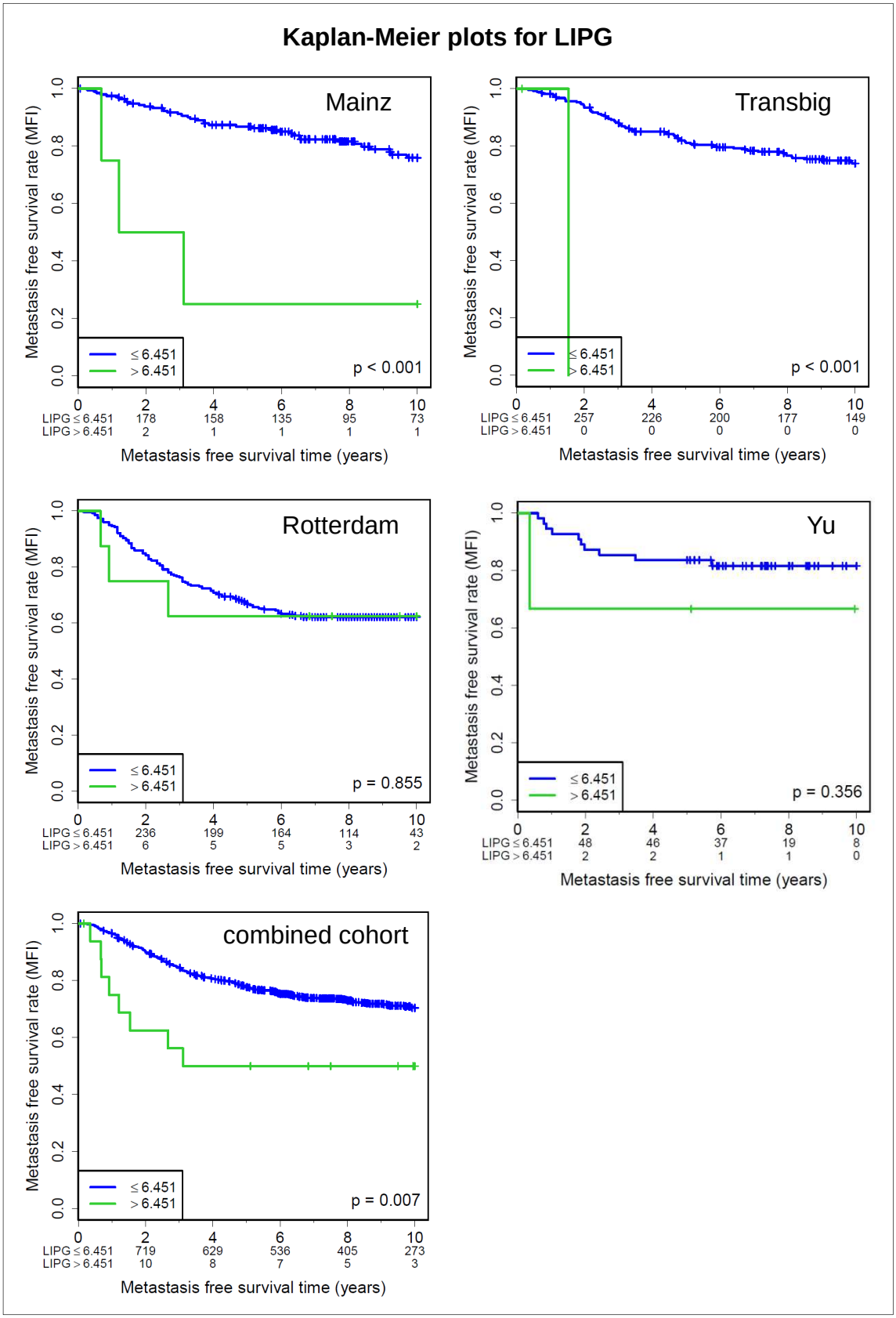

Fig. 3.39: Association of LIPG and metastatic-free survival (MFS) visualized by Kaplan-Meier plots. Increased LIPG expression is significantly associated with worse prognosis (shorter metastatic free survival) in Mainz (p<0.001), Transbig (p<0.001) and in the combined cohort (p=0.007)

3.8.2 Increased LIPG-expression is associated with negative estrogen receptor status and grade III

For studying the association of LIPG with clinical parameters (age, histological grade, pTstage, HER2 and ER-status) contingency tables for each clinical parameter after dichotomization of LIPG expression (low 98% and high 2% LIPG; CP=6.451) for available cohort data were generated (Tab. 3.7-3.11). In the Mainz, the Rotterdam and in the combined cohort a significant association of LIPG expression (LIPG>6.451) with negative estrogen receptor (ER) status was shown. In the Mainz cohort and in the combined cohort LIPG-high tumors also displayed predominantly grade III. No associations were found with a positive HER2 status, pT stage or age.

Tab. 3.7: Correlation of LIPG expression with clinical parameters in Mainz cohort

Mainz (GSE11121, n=200)				
clinical parameter		**LIPG ≤6.451**	**LIPG >6.451**	**p-value**
histological grade	grade I + II	151	0	0.0033
	grade III	45	4	
pT stage	stage I	97	1	0.6215
	stage II + III	99	3	
age	age ≤ 50 years	47	2	0.2522
	age > 50 years	149	2	
ER status	ER -	34	4	0.0011
	ER +	162	0	
HER2 status	HER2 -	167	2	0.1143
	HER2 +	29	2	

Tab. 3.8: Correlation of LIPG expression with clinical parameters in Rotterdam cohort

Rotterdam (GSE2034, n=286)				
clinical parameter		**LIPG ≤6.451**	**LIPG >6.451**	**p-value**
ER status	ER -	70	7	0.0005
	ER +	208	1	
HER2 status	HER2 -	229	8	0.3588
	HER2 +	49	0	

Tab. 3.9: Correlation of LIPG expression with clinical parameters in Transbig cohort

Transbig (GSE6532, n=84 & GSE7390, n=196)				
clinical parameter		**LIPG ≤6.451**	**LIPG >6.451**	**p-value**
histological grade	grade I + II	164	1	1
	grade III	99	1	
pT stage	stage I	148	1	1
	stage II + III	130	1	
age	age ≤ 50 years	157	1	1
	age > 50 years	121	1	
ER status	ER -	77	2	0.0848
	ER +	191	0	
HER2 status	HER2 -	244	1	0.2348
	HER2 +	34	1	

Tab. 3.10: Correlation of LIPG expression with clinical parameters in Yu cohort

Yu (GSE5327, n=58)				
clinical parameter		**LIPG ≤6.451**	**LIPG >6.451**	**p-value**
HER2 status	HER2 -	44	3	1
	HER2 +	11	0	

Tab. 3.11: Correlation of LIPG expression with clinical parameters in the combined cohort

combined cohort				
clinical parameter		**LIPG ≤6.451**	**LIPG >6.451**	**p-value**
histological grade	grade I + II	315	1	0.0143
	grade III	144	5	
pT stage	stage I	245	2	0.4379
	stage II + III	229	4	
age	age ≤ 50 years	204	3	1
	age > 50 years	270	3	
ER status	ER -	181	13	<0.0001
	ER +	616	4	
HER2 status	HER2 -	684	14	0.7344
	HER2 +	123	3	

Due to the fact that increased LIPG expression in tumors was predominantly associated with negative ER status and high grade we explored association of LIPG expression with prognosis in these breast cancer subgroups in the combined cohort separately, as illustrated by Kaplan-Meier plots (Fig. 3.40).

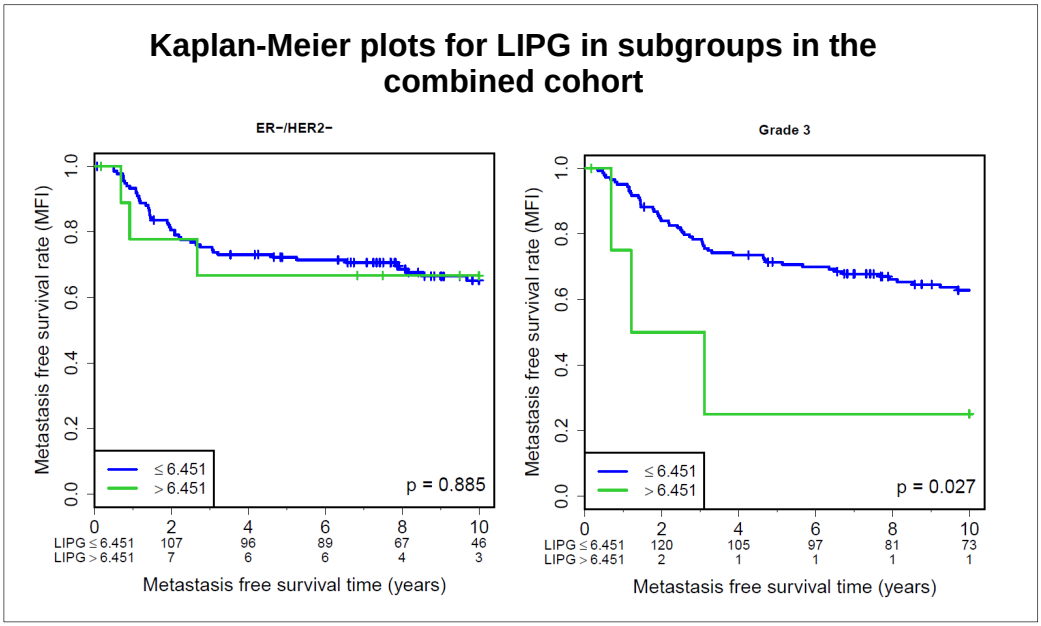

Fig. 3.40: Association of LIPG and metastatic-free survival (MFS) visualized by Kaplan-Meier plots in ER-/HER2- and grade III subgroups in combined cohort. Grade III tumors with high LIPG expression showed a shorter metastatic-free survival (MFS) than grade III tumors with low/ no LIPG

significant in the combined cohort. ER-/Her2- tumors with high LIPG expression showed no association with MFS

3.9 Perilipin2 (PLIN2) expression in human breast carcinoma and its correlation with LIPG-expression

Previous *in vitro* experiments revealed increased PLIN2 expression as a result of LIPG overexpression in MCF7 breast cancer cells fed with HDL or PC-OA, accompanying intracellular TAG accumulation. Therefore, we investigated a possible co-expression of PLIN2 with LIPG in the aforementioned breast cancer cohorts (Affymetrix gene array data (U133A_2.0, probe set 209122_at).

Scatter plots illustrating the relationship between LIPG- and PLIN2 expression (Fig. 3.41) and showed no linear correlation between LIPG and PLIN2; however, the majority of LIPG-high breast tumors also seemed to have increased PLIN2 expression.

To further explore the hypothesis that LIPG-high tumors are also PLIN2-high we generated contingency tables (Tab. 3.12). An 80%-quantile cut-point (CP=10.203) was chosen to select tumors with high PLIN2 expression (in Mainz cohort n=34, Transbig n=54, Rotterdam n=55 and Yu n=22). In the Mainz and in the combined cohort a significant correlation between high PLIN2 (>10.203) and high LIPG (>6.451) was found.

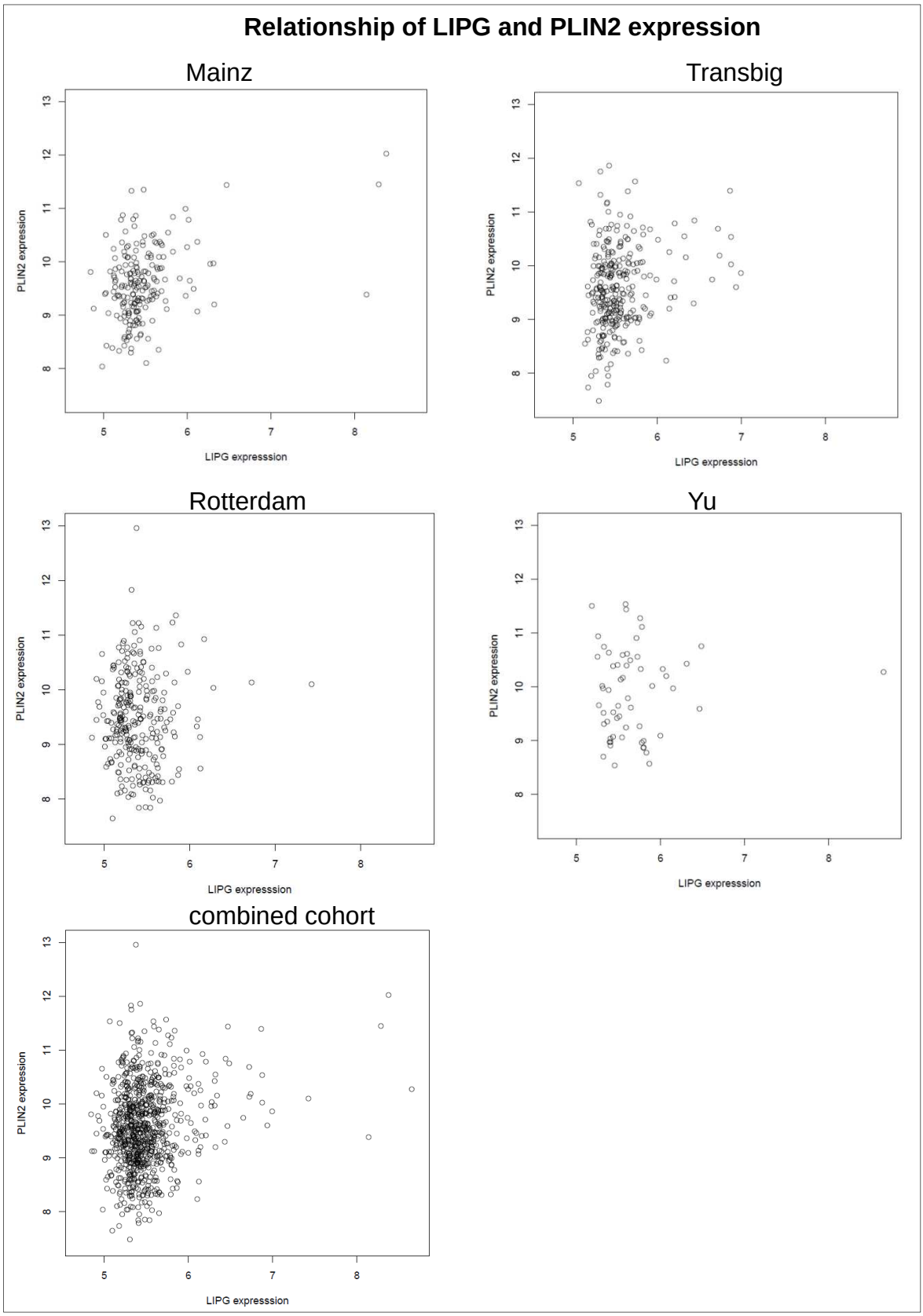

Fig. 3.41: Relationship between LIPG- and PLIN2 expression in breast tumors by scatterplots. Scatterplots did not illustrate a linear correlation between LIPG and PLIN2. Majority of tumors with high LIPG expression also express high PLIN2

Tab. 3.12: Contingency tables showing a possible correlation between LIPG- and PLIN2 expression

Contingency tables for LIPG and PLIN2				
cohorts		**PLIN2 ≤10.203**	**PLIN2 >10.203**	**p-value**
Mainz	LIPG ≤6.451 LIPG >6.451	165 1	31 3	0.0161
Rotterdam	LIPG ≤6.451 LIPG >6.451	226 5	52 3	0.1839
Transbig	LIPG ≤6.451 LIPG >6.451	224 2	54 0	0.1000
Yu	LIPG ≤6.451 LIPG >6.451	35 1	20 2	0.3194
combined	LIPG ≤6.451 LIPG >6.451	650 9	157 8	0.0102

LIPG and PLIN2 mRNA expression in ten breast tumors was validated by qRT-PCR in the Mainz cohort. As shown in Fig. 3.42 not all LIPG-high tumors exhibited also increased PLIN2 expression.

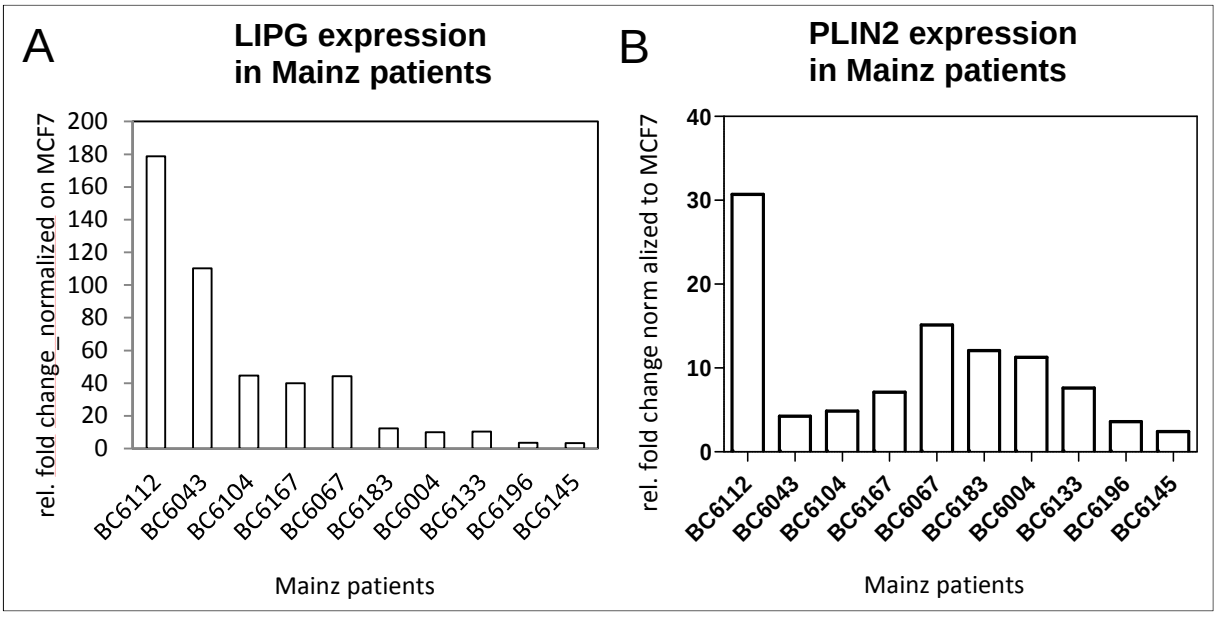

Fig. 3.42: Comparison of RNA analysis extracts for LIPG- (A) and PLIN2- (B) expression by qRT-PCR in some breast cancer patients from Mainz cohort, normalized on LIPG- (A) respectively

PLIN2- (B) level in MCF7 cells. Not all LIPG-high tumors showed also increased PLIN2 expression. As endogenous control UBC (ubiquitin C protein) was used; numbers represent n= 1 (see Fig.3.38)

Partial co-expression of PLIN2 and LIPG in breast cancer tumors suggests that - as observed *in vitro* - high levels of LIPG may induce expression of PLIN2 via enhanced lipid droplet synthesis. Since LIPG is associated with shorter MFS it was investigated whether PLIN2 also associates with MFS itself. Histograms in the four cohorts showed a normal distribution of PLIN2 expression (Fig. 3.43). Therefore, we could use PLIN2 mRNA expression as a continuous variable for studying its association with metastasis-free survival with the uni- and multivariate Cox model.

A significant association of PLIN2-high expression with worse prognosis (HR>1; $p<0.05$) was observed in the Mainz (HR=3.15, $p<0.001$), the Rotterdam (HR=1.7, $p=0.019$) and the combined cohort (HR=1.67, $p<0.001$) (Tab. 3.13).

The multivariate Cox-analysis showed no association of PLIN2 with survival independently of the clinico-pathological variables age, grade, stage, ER status and HER2 status (Tab. 3.14-3.18).

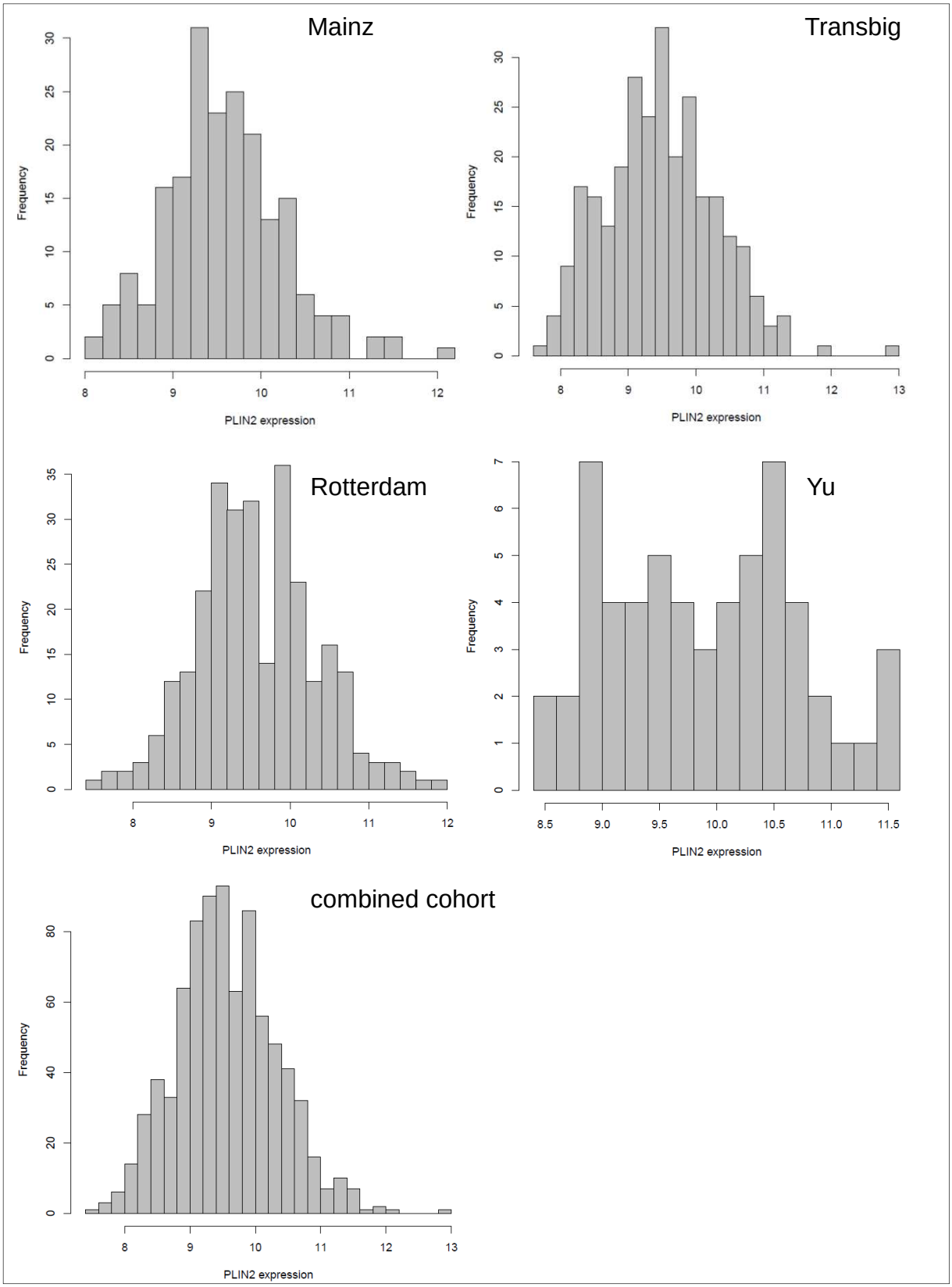

Fig. 3.43: Histograms of PLIN2 expression in four different cohorts. Mainz and Rotterdam cohorts show a normal modal distribution of PLIN2 expression whereas Transbig and Yu cohorts exhibit a weak bimodal distribution

Tab. 3.13: Univariate Cox-analysis for PLIN2

univariate Cox-analysis for PLIN2		
cohorts	**hazard ratio**	**p-value**
Mainz	3.15	< 0.001
Rotterdam	1.70	0.019
Transbig	1	0.994
Yu	3.34	0.054
combined	1.67	< 0.001

Tab. 3.14: Multivariate Cox-analysis for Mainz cohort

multivariate Cox-analysis in Mainz cohort		
clinical parameter	**hazard ratio**	**p-value**
PLIN2	1.92	0.057
age > 50years	0.88	0.713
stage II + III	0.95	0.882
grade III	3.93	<0.001
ER +	1.54	0.236
HER2 +	1.64	0.157

Tab. 3.15: Multivariate Cox-analysis for Rotterdam cohort

multivariate Cox-analysis in Rotterdam cohort		
clinical parameter	**hazard ratio**	**p-value**
PLIN2	1.81	0.013
ER +	1.19	0.459
HER2 +	1.08	0.771

Tab. 3.16: Multivariate Cox-analysis for Transbig cohort

multivariate Cox-analysis in Transbig cohort		
clinical parameter	**hazard ratio**	**p-value**
PLIN2	0.67	0.224
age > 50years	1.14	0.594
stage II + III	1.63	0.043
grade III	0.96	0.881
ER +	0.57	0.050
HER2 +	0.96	0.908

Tab. 3.17: Multivariate Cox-analysis for Yu cohort

multivariate Cox-analysis in Yu cohort		
clinical parameter	**hazard ratio**	**p-value**
PLIN2	3.07	0.083
HER2 +	0.63	0.666

Tab. 3.18: Multivariate Cox-analysis for combined cohort

multivariate Cox-analysis in combined cohort		
clinical parameter	**hazard ratio**	**p-value**
PLIN2	1.15	0.546
age > 50years	1.08	0.698
stage II + III	1.21	0.318
grade III	1.71	0.014
ER +	0.91	0.672
HER2 +	1.20	0.455

Kaplan-Meier curves of dichotomized PLIN2 mRNA expression levels (low 80% and high 20% PLIN2; CP=10.203) (Fig. 3.44) showed that tumors with high PLIN2

expression were significant associated with worse prognosis (shorter MFS) in Mainz (p<0.001), Rotterdam (p=0.018), Yu (p=0.041) and in the combined cohort (p<0.001).

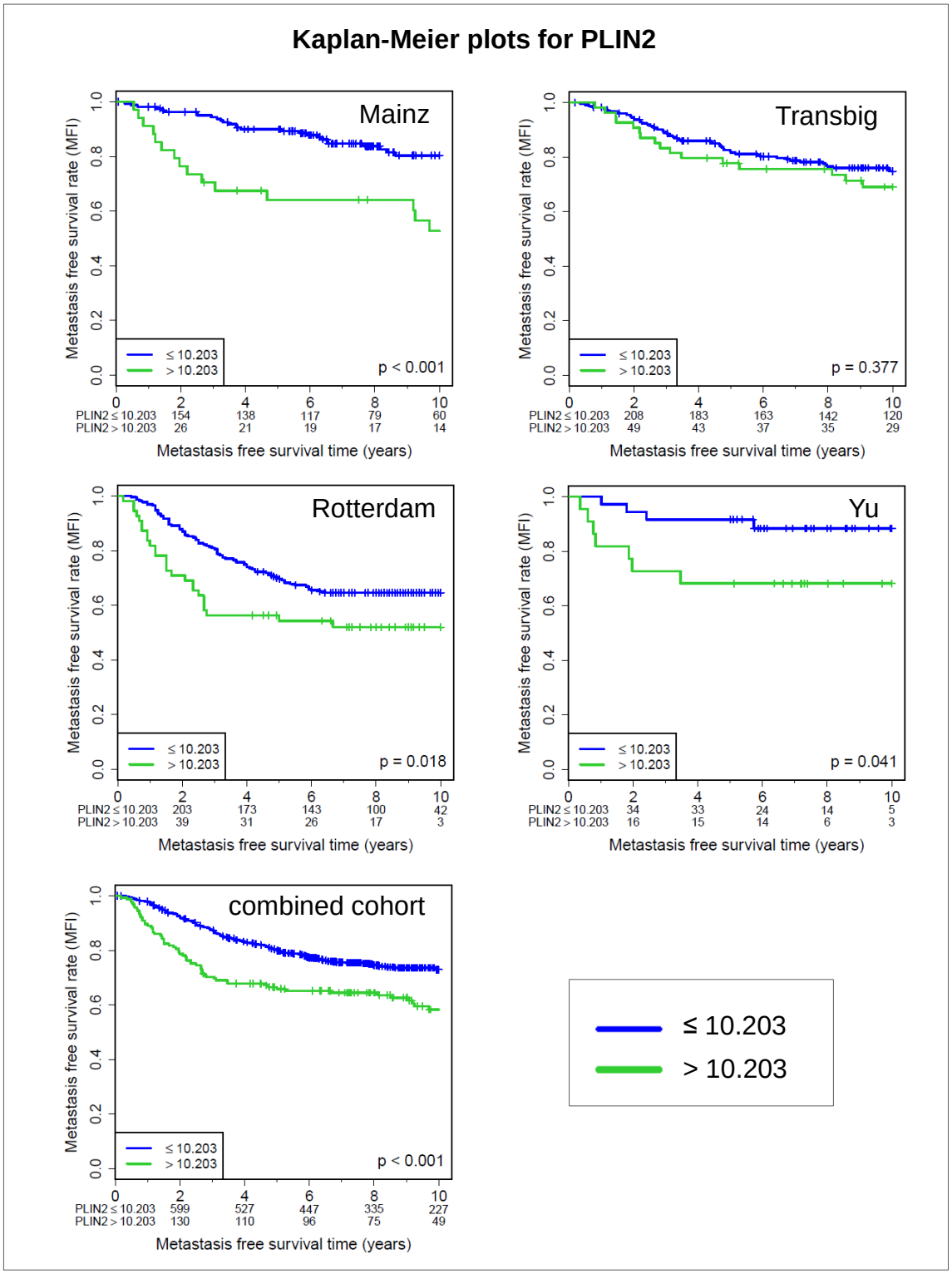

Fig. 3.44: Association of PLIN2 with metastasis-free survival (MFS) visualized by Kaplan-Meier plots. Increased PLIN2 expression (>80%) is significantly associated with worse prognosis (shorter metastasis free survival) in Mainz (p<0.001), Rotterdam (p=0.018), Yu (p=0.041) and in the combined cohort (p<0.001)

As done for LIPG, the association of PLIN2 with clinical parameters (age, histological grade, pTstage, HER2 and ER-status) (Tab. 3.19-3.23) was studied. In the Mainz cohort a significant association of higher PLIN2 expression with grade III and negative ER status was shown, in Rotterdam PLIN2 associated significantly with negative ER status, in the Transbig with grade III, stage II + III and with negative ER status, and in the Yu cohort with negative HER2 status. In the combined cohort PLIN2 significantly associated with grade III, stage II + III and with negative ER status.

Tab. 3.19: Correlation of PLIN2 expression with clinical parameters in the Mainz cohort

Mainz (GSE11121, n=200)				
clinical parameter		**PLIN2 ≤10.203**	**PLIN2 >10.203**	**p-value**
histological grade	grade I + II	140	11	<0.0001
	grade III	26	23	
pT stage	stage I	84	14	0.3507
	stage II + III	82	20	
age	age ≤ 50 years	40	9	0.8273
	age > 50 years	126	25	
ER status	ER -	23	15	0.0002
	ER +	143	19	
HER2 status	HER2 -	143	26	0.1914
	HER2 +	23	8	

Tab. 3.20: Correlation of PLIN2 expression with clinical parameters in the Rotterdam cohort

Rotterdam (GSE2034, n=286)				
clinical parameter		**PLIN2 ≤10.203**	**PLIN2 >10.203**	**p-value**
ER status	ER -	46	31	<0.0001
	ER +	185	24	
HER2 status	HER2 -	190	47	0.6920
	HER2 +	41	8	

Tab. 3.21: Correlation of PLIN2 expression with clinical parameters in the Transbig cohort

Transbig (GSE6532, n=84 & GSE7390, n=196)				
clinical parameter		**PLIN2 ≤10.203**	**PLIN2 >10.203**	**p-value**
histological grade	grade I + II	147	18	<0.0001
	grade III	65	35	
pT stage	stage I	129	20	0.0097
	stage II + III	97	34	
age	age ≤ 50 years	124	34	0.2904
	age > 50 years	102	20	
ER status	ER -	46	33	<0.0001
	ER +	172	19	
HER2 status	HER2 -	199	46	0.6465
	HER2 +	27	8	

Tab. 3.22: Correlation of PLIN2 expression with clinical parameters in the Yu cohort

Yu (GSE5327, n=58)				
clinical parameter		**PLIN2 ≤10.203**	**PLIN2 >10.203**	**p-value**
HER2 status	HER2 -	26	21	0.0387
	HER2 +	10	1	

Tab. 3.23: Correlation of PLIN2 expression with clinical parameters in the combined cohort

combined cohort				
clinical parameter		**PLIN2 ≤10.203**	**PLIN2 >10.203**	**p-value**
histological grade	grade I + II	287	29	<0.0001
	grade III	91	58	
pT stage	stage I	213	34	0.0093
	stage II + III	179	54	
age	age ≤ 50 years	164	43	0.2360
	age > 50 years	228	45	
ER status	ER -	115	79	<0.0001
	ER +	536	84	
HER2 status	HER2 -	558	140	1
	HER2 +	101	25	

As done for LIPG, we investigated the association of PLIN2 with metastasis-free survival in the negative ER-negative status and grade III subgroups. As shown in the Kaplan-Meier plots (Fig. 3.45), high expression of PLIN2 (CP=10.203) was not significantly associated with shorter MFS in these subtypes.

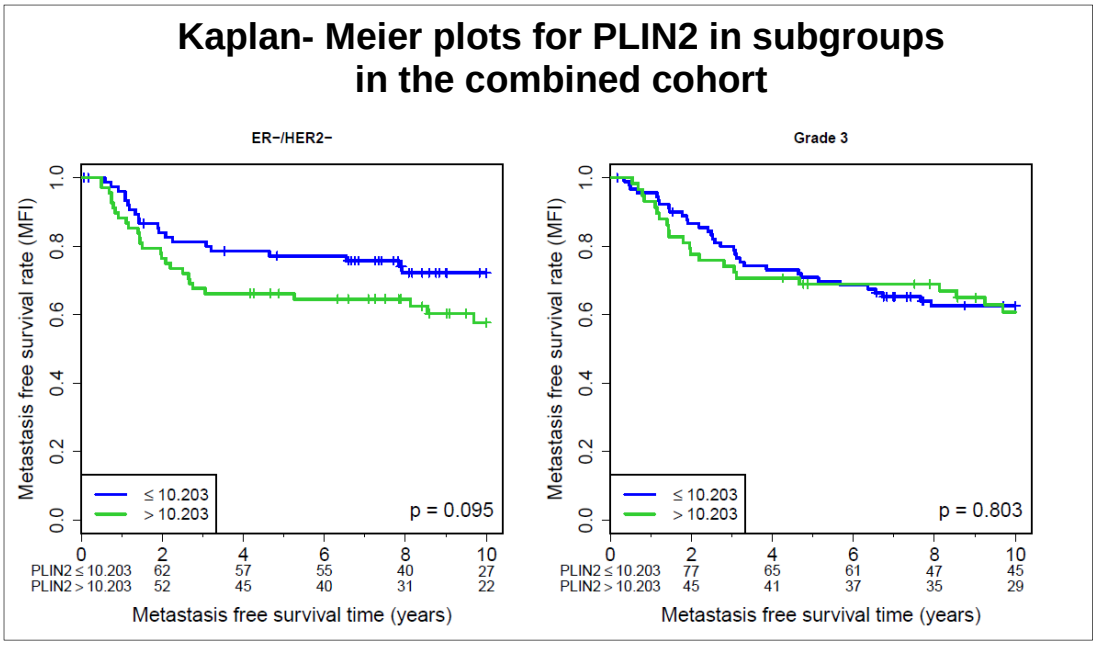

Fig. 3.45: Association of PLIN2 with metastasis-free survival (MFS) visualized by Kaplan-Meier plots in ER-negative and grade III subgroups. High PLIN2 expression did not associate significantly with MFS in these subtypes

3.10 Correlation of LIPG expression and different metabolic genes in the Mainz cohort

The previous results show that the majority of the LIPG-expressing tumors are high grade tumors, have an ER-negative status, and express PLIN2 to a certain degree. In order to get an insight into some metabolic properties shared by LIPG-high tumors scatter plots were generated to visualize co-expression (as determined by Affymetrix gene arrays) of LIPG and other genes involved in different metabolic processes in Mainz patients (Fig. 3.46a-f). Based on the results obtained in the experimental part of the work: 1) Expression of LIPG in a context of oncogene-induced senescence, characterized by oxidative stress; 2) Expression of LIPG in $CoCl_2$-induced chemical hypoxia, also characterized by oxidative stress and by an hypoxia-related expression signature, 3) Expression of LIPG upon conditions of reduced fatty acid synthesis capacity, we searched for surrogates of oxidative stress, hypoxia, fatty acid and lipid droplet metabolism. The following graphs show on the x-axis LIPG expression level. The red vertical line marks the 98% cut-point (CP=6.451) discriminating the four outliers in the Mainz cohort with LIPG expression >6.451. The y-axis displays expression of different selected metabolic genes with the corresponding median shown as a blue horizontal line. Each point displays one breast cancer patient from the Mainz cohort (n=200).

In order to investigate if LIPG is highly expressed in tumors that have a lower capacity to synthetize fatty acids the correlation of LIPG expression with genes involved in *de novo* fatty acid synthesis was investigated (Fig. 3.46a). The enzyme fatty acid synthase (FASN) catalyzes the formation of fatty acids from malonyl-CoA (Mullen and Yet 2015). Three out of four patients with LIPG >6.451 also express higher levels of FASN. Acetyl-coenzyme A carboxylase (ACACA) catalyzes ATP-dependent carboxylation of acetyl-CoA to form malonyl-CoA (Wang et al. 2010). High expression of ACACA in LIPG-high tumors is only partial and Affymetrix gene array probe set-dependent. These results do not seem to support the hypothesis, that LIPG becomes induced when the endogenous fatty acid synthesis is compromised. On the other hand it is known that fatty acid synthesis is regulated by post-translational modifications (phosphorylation) of acetyl-CoA carboxylase rather than on the level of transcription.

To study whether LIPG-high tumors display oxidative stress, as shown in our experimental work, the correlation of LIPG expression with genes involved in the anti-oxidant response, such as TXNRD1, TXN and TXNIP was studied. Interestingly, LIPG-high tumors showed high levels of TXNRD1 and TXN mRNA but low levels of TXNIP mRNA. This suggests that LIPG expression *in vivo* may be relevant in a context of oxidative stress (Fig. 3.46b).

Because oxidative stress is known to occur under prolonged hypoxia (LeGrand and Aw 1996), the correlation of LIPG expression with genes involved in hypoxic processes was investigated. Figure 3.46c shows correlation of LIPG expression with markers of hypoxia. Hypoxia inducible factor 1 alpha (HIF-1α) triggers the transcription of hypoxia-inducible genes and is involved in several biological processes (Enns and Ladiges 2012). All four LIPG >6.451 patients correlate with increased HIF-1α expression. Pyruvate dehydrogenase kinase 1 (PDK1) phosphorylates and inactivates pyruvate dehydrogenase (PDH) therefore limiting the generation of acetyl-CoA from pyruvate, which becomes converted to lactate by lactate dehydrogenase A (LDHA). Three out of four tumors with increased LIPG expression show elevated PDK1 expression. Vascular endothelial growth factor a (VEGFa) is an angiogenic factor induced by HIF-1α (Bensaad et al. 2014). All four tumors with elevated LIPG-expression display VEGFa expression higher than the median. These results suggest that LIPG-high tumors have characteristics of hypoxia-driven tumors with a high glycolytic and angiogenic capacity.

Since we could show experimentally that LIPG promotes lipid droplet formation, the relationship between LIPG and genes involved in TAG formation in Mainz patients was also studied, and shown in Figure 3.46d. Acylglycerophosphate acyltransferases (AGPAT) participate in the synthesis of phosphatidic acid (Yamashita et al. 2014). Most LIPG >6.451 patients also express increased AGPAT levels. The enzyme Lipin1 (LPIN1) encodes for a magnesium-ion-dependent phosphatidic acid phosphohydrolase which catalyzes dephosphorylation of phosphatidic acid to yield diacylglycerol (Jiang et al. 2015). All four patients with LIPG expression about the chosen cut-point show LPIN1 levels higher than the median. Diacylglycerol acyltransferase (DGAT) triggers the final step in the sn-glycerol-3-phosphate pathway resulting in TAG formation (Liu et al. 2012). Three out of four with high LIPG exhibit

also high DGAT expression. Lipocalin 2 (LCN2), a member of the innate immune system associated with inflammation processes as a pro-inflammatory molecule, has lately been shown to be involved in control of intracellular lipid droplet formation (Asimakopoulou et al. 2014). LIPG-high tumors also showed enhanced LCN2 mRNA levels. All together, these findings suggest that LIPG-high tumors are characterized by enhanced triglyceride synthesis, probably from fatty acids derived from LIPG-mediated extracellular lipolysis. The low-density lipoprotein receptor (LDLR) enables the uptake of cholesterol-carrying lipoproteins by endocytosis (Jeon and Blacklow 2005). Fatty acid binding protein 7 (FABP7) is essential for fatty acid uptake and their intracellular transport (Bensaad et al. 2014). Increased LIPG expression correlates with enhanced LDLR- and FABP7 expression.

Monoacylglycerol lipase (MAGL or MGLL) regulates free fatty acid levels and builds a diverse lipid network enriched in pro-tumorigenic signaling molecules which facilitates cell migration, survival, and cancer cell growth (Nomura et al. 2010). Three out of four LIPG >6.451 patients also show increased MGLL expression (Fig. 3.46e)

A further interesting finding was that LIPG-expressing tumors displayed quite low levels of the pro-protein convertase PCSK5 (Fig. 3.46f). As previously mentioned, secreted active 68kDa LIPG protein is cleaved and inactivated by pro-protein convertases (pPC) into fragments of 40kDa and 28kDa size and PCSK5 (PC6) has been shown to specifically inactivate LIPG (Gauster et al. 2005). The finding that tumors with high LIPG expression in the Mainz cohort exhibit low PCSK5 expression is interesting because it suggests that LIPG-high/ PCSK5-low tumors may have not only increased levels of LIPG mRNA but also higher levels of active LIPG protein.

A

Relationship of LIPG expression and genes involved in *de novo* fatty acid synthesis

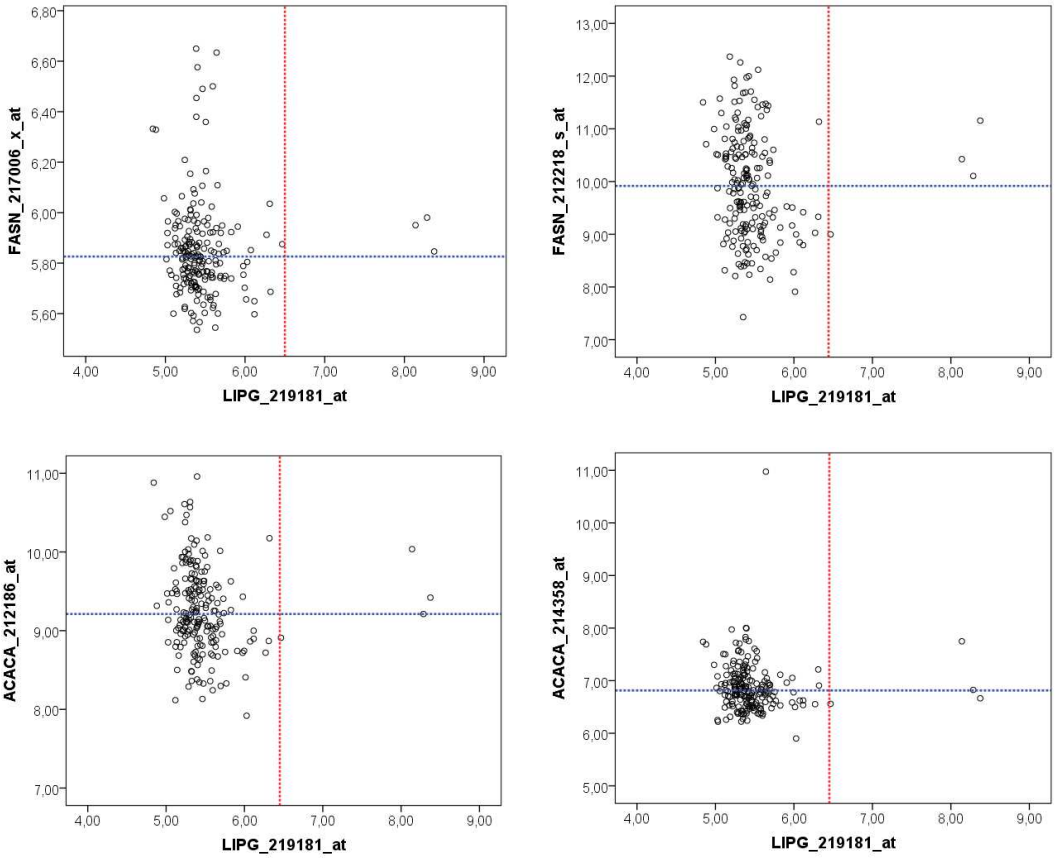

B

Relationship of LIPG expression and genes involved in anti- oxidant response

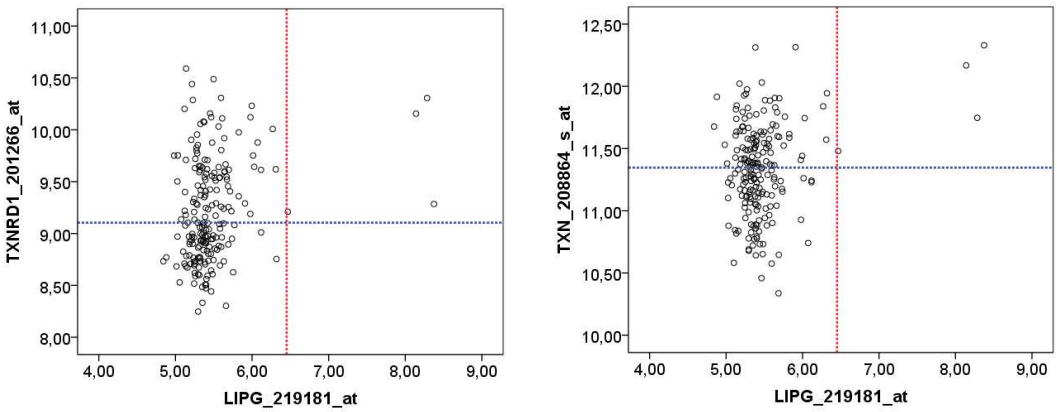

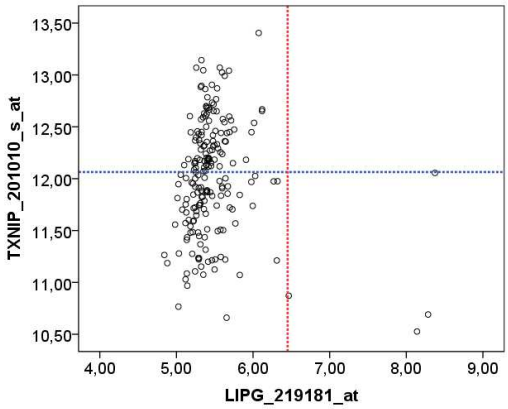

C

Relationship of LIPG expression and genes involved in hypoxic processes

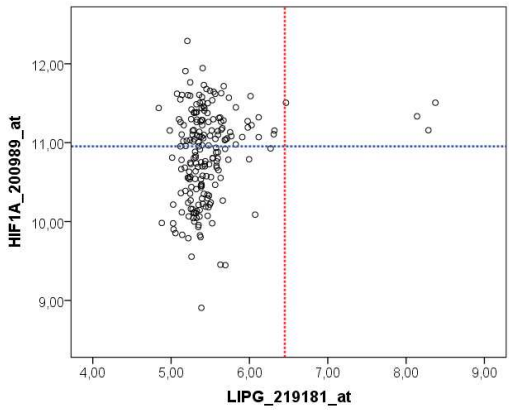

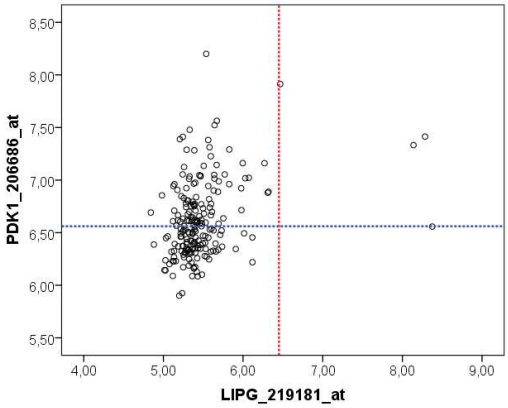

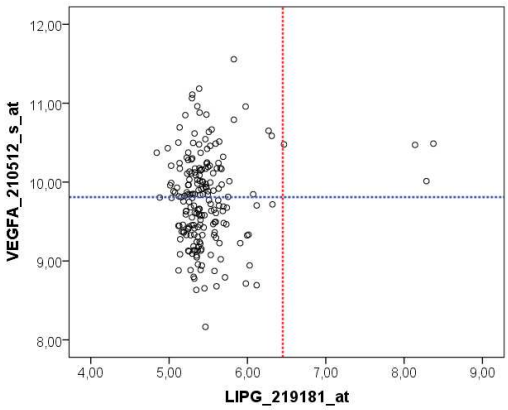

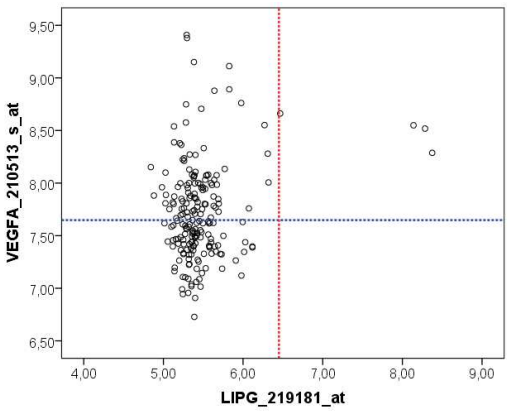

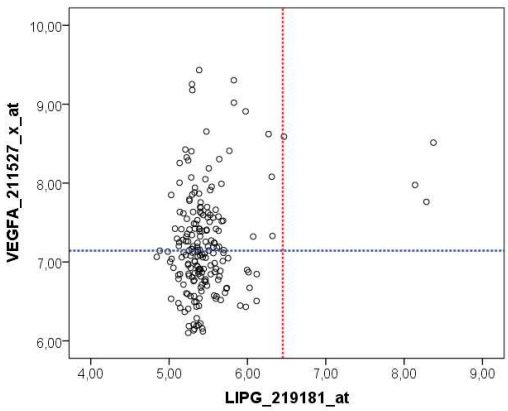

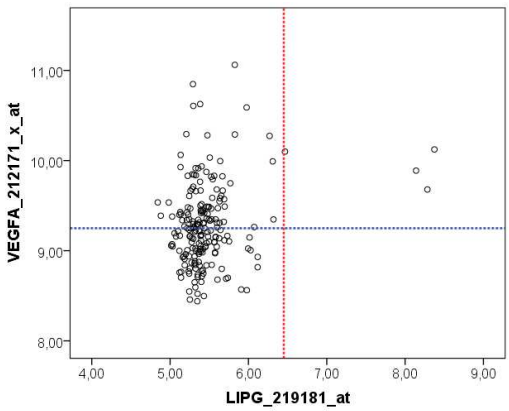

D **Relationship of LIPG expression and genes involved in TAG formation**

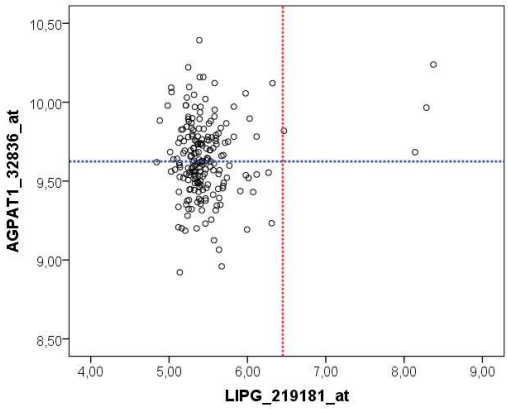

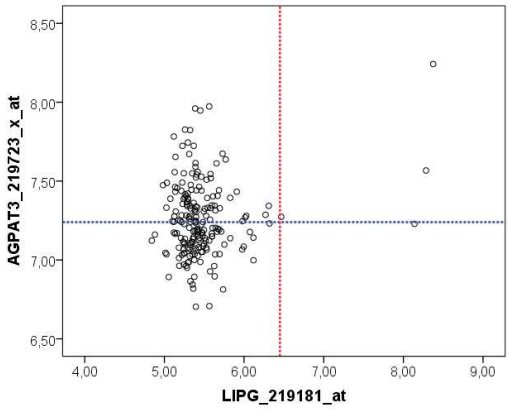

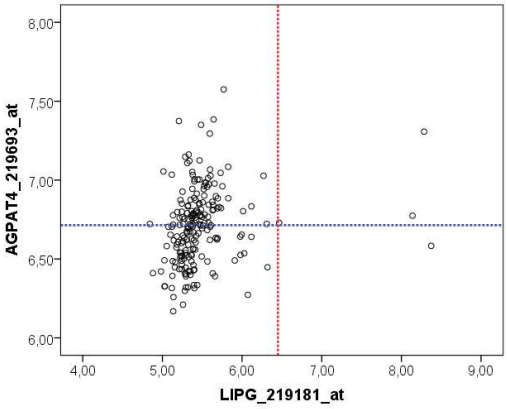

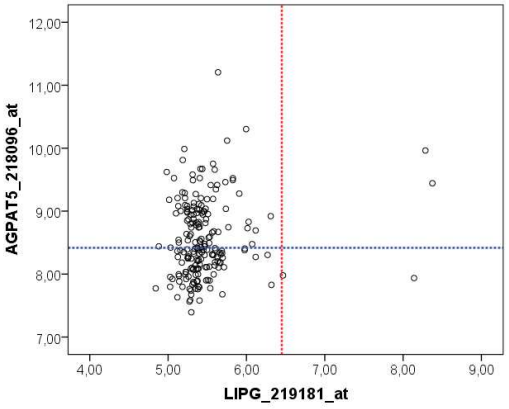

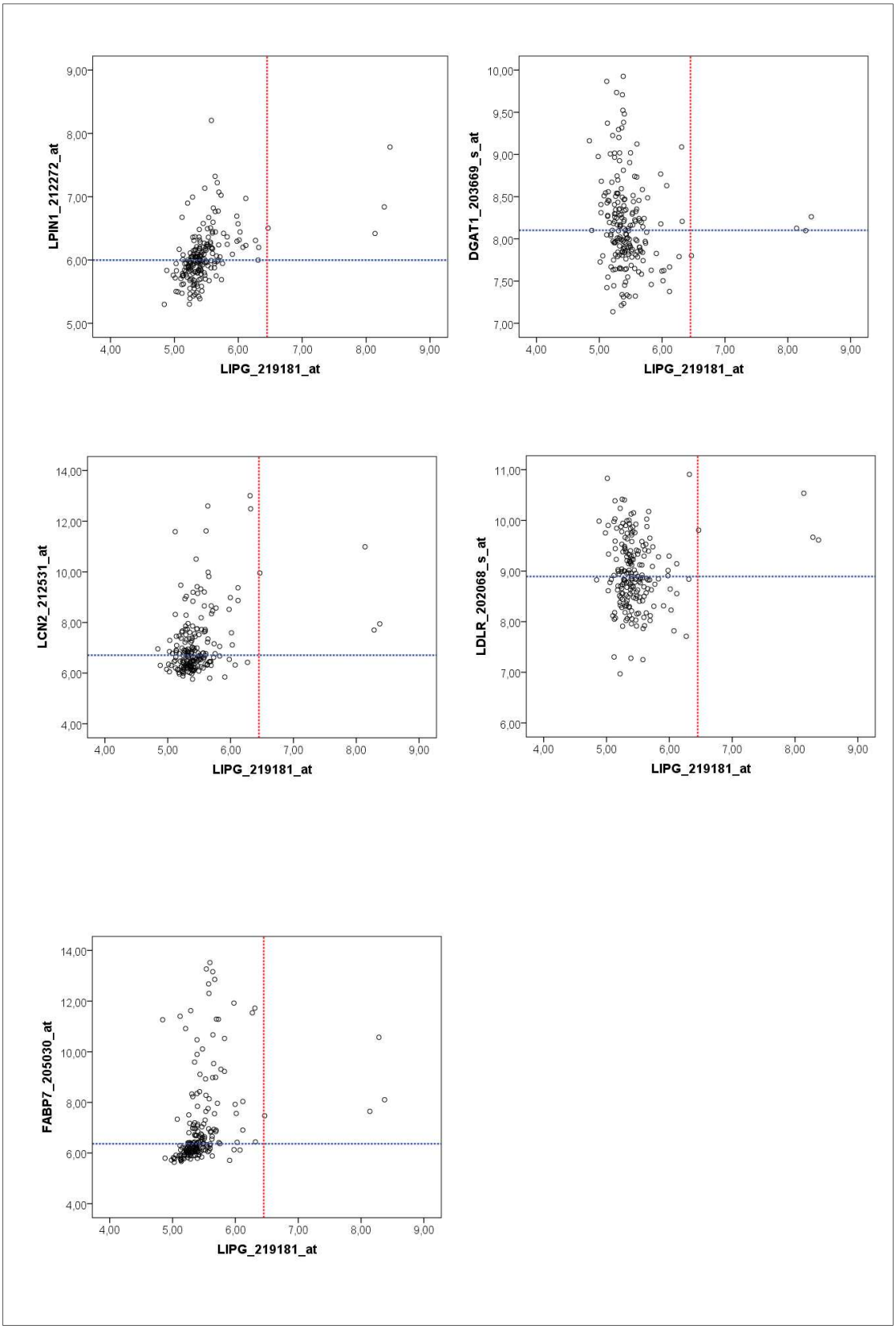
LPIN1_212272_at
LIPG_219181_at
DGAT1_203669_s_at
LIPG_219181_at
LCN2_212531_at
LIPG_219181_at
LDLR_202068_s_at
LIPG_219181_at
FABP7_205030_at
LIPG_219181_at

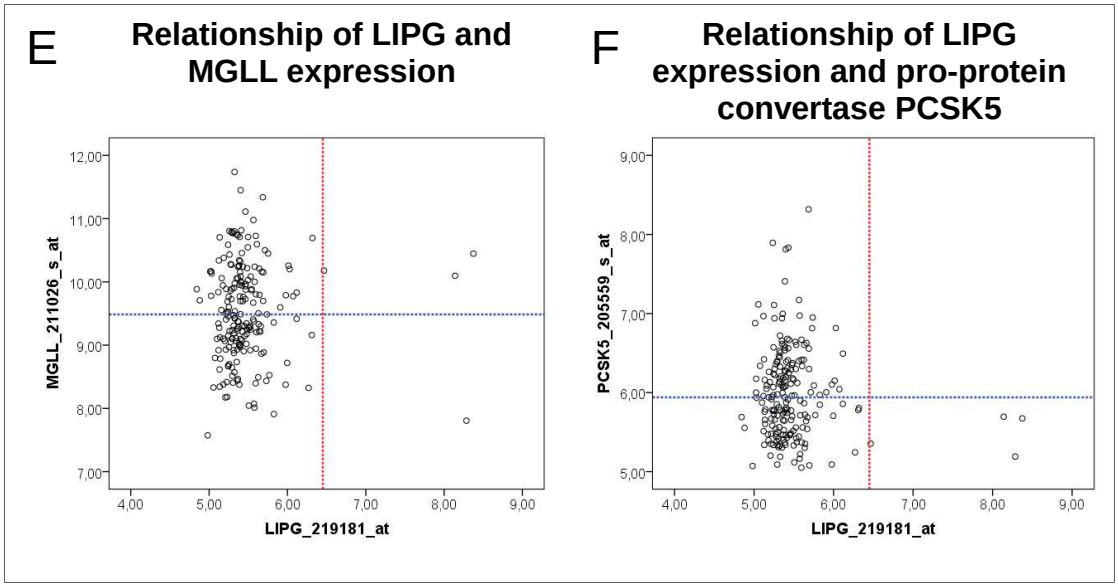

Fig. 3.46: Relationship of LIPG expression and genes involved in (A) *de novo* fatty acid synthesis, (B) involved in anti-oxidant response, (C) involved in hypoxic processes, (D) involved in TAG formation, (E) monoacylglycerol lipase (MAGL or MGLL) gene expression, (F) pro-protein convertase PCSK5 in Mainz patients. (A) Three out of four patients with LIPG >6.451 express higher level of fatty acid synthase (FASN) in two tested Affymetrix gene array probe sets. Similar results are observed with Acetyl-coenzyme A carboxylase (ACACA) in the two used probe sets. (B) LIPG-high tumors showed high levels of TXNRD1 and TXN but low levels of TXNIP. (C) All four LIPG >6.451 patients correlate with increased HIF-1α expression. Three out of four patients with increased LIPG expression show elevated PDK1 expression. All four patients with elevated LIPG expression represent increased VEGFa expression. (D) Most LIPG >6.451 patients also express increased AGPAT levels. All four patients with LIPG-high expression show enhanced Lipin1 amount. Three out of four with high LIPG exhibit also high DGAT expression. Increased LIPG expression correlates with enhanced LCN2-, LDLR- and FABP7 expression. (E) Three out of four LIPG >6.451 patients also show increased MGLL expression. (F) Patients with increased LIPG expression exhibit decreased PCSK5 expression in Mainz cohort. Red vertical line illustrates LIPG cut-point of 6.451; blue horizontal line marks the mean value of gene expression of tested metabolic genes

In summary, expression of LIPG in breast cancer *in vivo* is restricted to a very limited number of tumors. These are characterized by high grade and loss of ER expression, metastatic capacity and expression of oxidative stress and hypoxia markers, as well as high expression of genes involved in metabolism of triacylglycerides. Interestingly, oxidative stress was also observed in the *in vitro* models showing upregulation of LIPG. This strongly suggests that oxidative stress represents the biological context in which LIPG becomes induced to promote survival.

4. Discussion

The association of endothelial lipase LIPG and atherosclerosis is widely accepted (Hirata et al. 1999, Dalan et al. 2013), but there is only little known and published about LIPG in the context of human cancer. LIPG is a cell surface-associated protein that displays a strong phospholipase A1 and little triacylglycerol lipase activity towards high-density lipoproteins (HDL). This enzymatic function enables LIPG to cleave HDL into fatty acids and lysophosphatidylcholine (LPC), which can be followed by cellular fatty acid intake. An additional, non-enzymatic LIPG activity binds HDL and facilitates holoparticle or selective HDL-cholesterol ester uptake (Strauss et al 2002). Several diseases, including cancer, are accompanied by changes in lipid metabolism and in the lipid composition of cellular membranes. Santos and Schulze (2012) reported how lipids support several aspects of cancer development, including proliferation, resistance to oxidative stress and survival under energy stress. Furthermore, fatty acids are able to alter the immune cell behavior (Calder et al. 2011), which is bond to influence immunosurveillance. Therefore, our initial finding that LIPG is induced by oncogene overexpression in breast cancer cells (Cadenas et al. 2012) prompted us to explore the role of LIPG-mediated lipid supply in breast cancer and its possible contribution to tumor progression *in vivo*.

This work has revealed LIPG expression in breast cancer. However, LIPG-expression did not display a broad pattern but rather appeared in a very limited subset of dedifferentiated tumors *in vivo* and was induced only under particular circumstances *in vitro*. Interestingly, regardless of its limited expression, LIPG mRNA levels were significantly associated with poor outcome (short metastasis-free survival) and could discriminate a subset of particularly aggressive tumors within a group of grade III tumors, which is aggressive *per se*. Therefore, induction of LIPG in human breast cancer cells is a rare but relevant event during tumor progression.

Integrating our experimental data and our statistical analysis of LIPG-expressing tumors has enabled us to propose a hypothesis on how LIPG may contribute to tumor progression and in what biological context LIPG is required.

We hypothesize that LIPG becomes induced in cancer cells under conditions of high oxidative stress to enable uptake of fatty acids derived from HDL-lipoproteins, when the fatty acid requirement exceeds the cellular capacity to synthesize fatty acids *de novo*, or when it is repressed. A repression of fatty acid synthesis may take place under conditions of oxidative stress to avoid consumption of NADPH (Jeon et al. 2012), which should be instead redirected towards ROS detoxification and protein repair. LIPG-mediated lipid supply is NADPH-independent and therefore compensates the lack of lipid synthesis and helps maintain NADPH levels.

The following findings, reported in this thesis, support the aforementioned hypothesis and underline the importance of LIPG expression in cancer:

1) Only LIPG-expressing tumor cells can utilize serum HDL-lipoproteins as fatty acid sources to promote intracellular lipid accumulation. Therefore, LIPG induction confers a new ability to utilize additional exogenous lipid sources.
2) Intracellular lipid droplet accumulation confers a survival advantage upon nutrient shortage and - to a lesser extent - resistance to NK cell-mediated cytotoxicity. Moreover, LIPG-promoted lipid droplet accumulation is able to sustain mitochondrial integrity upon blockage of *de novo* fatty acid synthesis. Lipid droplet formation, triggered by addition of free fatty acids or by overexpression of LIPG in presence of its substrate, induced expression changes in genes known to support mitochondria, including PLIN2 and LCN2.
3) Oxidative stress appears to be the biological context in which LIPG expression is induced and may be required. This condition is shared by both cell culture models in which we observed LIPG induction and by the breast tumors displaying high levels of LIPG mRNA. In all three cases LIPG expression was accompanied by increased levels of the NADPH-consuming anti-oxidant enzyme thioredoxin reductase (TXNRD1). Under this condition fatty acid synthesis is often downregulated (Jeon et al. 2012, Bensaad et al. 2014).

These aspects are discussed in detail in what follows.

4.1 LIPG induction confers the ability to utilize HDL as alternative exogenous lipid sources

The *in vitro* experiments performed in MCF7 cells with oleic acid addition could show that breast cancer cells can take up extracellular fatty acids and incorporate them into lipid droplets, regardless of LIPG expression. However, only LIPG-expressing cells are capable of using HDL as an extracellular source of fatty acids. Circulating high-density lipoproteins are not reported so far to serve as lipid sources to cancer cells; thus, this represents a novelty. The function of HDL is to collect excess of cholesterol from peripheral tissues and to transport it to the liver. Thus, tumor-specific LIPG-mediated modification of HDL particles may impact cholesterol homeostasis as well. However, this remains unexplored.

4.2 LIPG-mediated intracellular lipid accumulation confers survival advantages

LIPG-overexpressing MCF7 breast cancer cells fed with PC-OA or HDL showed a strong intracellular lipid accumulation, that could be quantitatively confirmed by the triglyceride quantification assay, visualized by lipid droplets (LD) staining and verified by increased expression of the LD-coating protein PLIN2. These read outs could be mimicked by oleic acid incubation.

MCF7 breast cancer cells exposed to oleic acid (OA) showed survival advantages under harsh starvation conditions (no glucose and without serum) compared to control cells. This shows that upon nutrient shortage accumulated lipid droplets support cell metabolism and growth. Unfortunately, LIPG-overexpressing cells previously fed with PC-OA as a substrate failed to display this survival advantage under starvation. A plausible explanation could be a limited transfection efficiency or insufficient lipid accumulation, which is much lower than the triglyceride accumulation resulting from direct exposure to oleic acid. A further possible explanation is that the advantage of LIPG may only come up if the endogenous lipid synthesis is compromised. This is supported by the fact that LIPG-overexpressing MCF7 cell cultures displayed healthier mitochondria in presence of a fatty acid synthesis inhibitor.

How lipid droplet accumulation and turnover may support mitochondrial function? Aon et al. (2014) described a physical and metabolic interaction between lipid

droplets and mitochondria based on channeled lipid utilization. Perilipin 5 (PLIN5) regulates LD degradation by recruitment of mitochondria to LD surface and enables the flux of lipolysis-derived fatty acids to mitochondria for energy production. Mitochondrial fractions isolated from fasted rat hearts showed PLIN5 enriched mitochondria as well as PLIN5-coated LD (Aon et al. 2014, Wang et al. 2011). Beside increased PLIN2 expression LIPG-overexpressing cells fed with lipoprotein substrate also displayed increased LCN2 expression. Interestingly, Asimakopoulou et al. (2014) described LCN2 as a key modulator controlling intracellular LD formation via regulation of PLIN5 expression. Our findings showing increased lipid droplet formation and increased LCN2 levels upon LIPG overexpression argues for LIPG expression as a mechanism that promotes cell survival by preserving mitochondrial integrity under conditions of impaired fatty acid synthesis.

4.3 TAG-accumulation in K-562 cells facilitates survival advantage in killing assay

In our studies human leukemia K-562 cells incubated for 48h with oleic acid (OA) were less killed by natural killer (NK) cells compared to control cells, as measured by the ^{51}Chromium release assay (killing assay). NK cells are the major component of antitumor immune response. Their activity is inhibited by receptors that recognize MHC-I molecules which healthy cells carry on cell surface. Activated NK cells attack target cells by developing an immunological synapse (contact site between immune cells and target cells), creating pores in plasma membrane by released cytolytic proteins, including perforin and apoptosis-inducing proteases like granzymes (Mamessier et al. 2011). Several possible explanations exist why lipid-accumulated cells could be less killed: A) altered apoptosis pathways of target cells, B) less efficient uptake of perforin or granzymes by target cells.

NK cells ensure apoptosis of target cells by different means. Cytotoxic granula proteins like granzyme A, granzyme B, FAS-ligand (tumor necrosis factor superfamily) and TRAIL (tumor necrosis factor-related apoptosis-inducing ligand) have different targets (Rink et al. 2012, Spektrum Verlag). Granzyme A damages mitochondria whereas granzyme B cleaves and activates Caspase-3. Both appertain

to the intrinsic or mitochondrial apoptosis pathway. FAS-ligand, which binds to its FAS-receptor (CD95), and TRAIL, which recognizes the tumor-necrosis receptor (Murray et al. 2015), belong to the extrinsic pathway. Which of these pathways may be affected by lipid accumulation is not clear. On the other hand, it is known that the cellular membrane composition affects cell function. Phospholipids are the main building block of cellular membranes which can influence physiochemical characteristics of membranes and are essential for their proper functioning. The number of carbon atoms and saturation degree of membrane lipid acyl chains influence its fluidity, which decreases by less double bounds and longer carbon chain length (Cadenas et al. 2012). Also cholesterol accumulation in a higher ratio to phospholipids results in a fluidity decrease (Baritaki et al. 2007). We could speculate that lipid accumulation results in changes in membrane composition, which in turn affect membrane fluidity/rigidity. As a consequence receptor presentation and binding to ligands, or perforin binding on target cell could be compromised.

In order to elucidate the mechanism underlying the observed resistance to NK-mediated cytotoxicity in lipid-loaded cells further experiments should be performed. A loss of function of NK cells can for instance be investigated by FACS analysis. This technique enables the detection of lysosomal markers (LAMP-1 or CD107a) of active NK cells during granulation and development of immunological synapse (Claus and Watzl 2010).

4.4 Induction of LIPG expression upon oxidative stress may be a compensatory mechanism for reduced fatty acid synthesis

Induction of NeuT expression (oncogenic variant of HER2) leads to premature senescence in MCF7/NeuT breast cancer cells. LIPG mRNA became immediately induced upon NeuT overexpression and further increased as cells entered the senescence state (Cadenas et al. 2012). Upon NeuT overexpression in MCF7/NeuT cells upregulation of LIPG mRNA was reduced by the small molecule inhibitors of p38 MAPK (SB203580) and PI3K (LY294002). MEK1/2- (PD98059 inhibitor) and SAPK/JNK- (SP600125 inhibitor) pathway did not reveal any influence on LIPG expression. These results showed that p38 MAPK and PI3K are underlying signaling pathways involved in NeuT-triggered stimulation of LIPG expression. Both pathways

play a central role in the regulation of inflammatory processes and stress response (Cuenda and Rousseau 2007). Interestingly, these two pathways are known to lead to nuclear factor-kB (NF-kB) activation, which in turn is known to bind LIPG promotor (containing five functional NF-kB binding sites) to activate its transcription (Kempe et al. 2005, Kivelä et al. 2010).

In addition to NeuT, we studied LIPG expression upon overexpression of wildtype HER2 as well as of a HER2 mutant with YVMA insertion of four amino acids at codon 776 that results in enhanced tyrosine kinase activity (Greulich et al. 2012, Wang et al. 2006). Neither HER2-wildtype nor HER2 insYVMA-transfected cells exhibited altered LIPG expression levels (data not shown). Statistical analysis also failed to detect a correlation between LIPG expression and HER2-status in breast tumors. The ability to induce LIPG was therefore unique to the oncogenic variant NeuT and is not determined by HER2 overexpression/amplification. Since only NeuT overexpression in MCF7 cells results in oncogene-induced senescence (OIS), whereas HER2 wildtype and HER2 insYVMA-transfected cells still proliferate, this may indicate that LIPG induction by NeuT may be part of a senescence-associated metabolic reprogramming.

Previous work at IfADo has shown that NeuT-mediated senescence in MCF7 cells is accompanied by a strong increase in levels of reactive oxygen species (ROS) and induction of oxidative stress markers, including TXNRD1 (Cadenas et al. 2010). Importantly ROS generation is known to be a critical mediator of oncogene-induced senescence (Weyemi et al. 2012). This prompted us to investigate whether LIPG can be induced by other stimuli that generate high levels of ROS. We explored LIPG induction upon exposure to different concentrations of $CoCl_2$ and found parallel induction of LIPG and activation of the TXNRD1-TRX system, in a similar way as found in oncogene-induced senescence. Also the breast tumors displaying high levels of LIPG are characterized by expressing high levels of TXNRD1 and TXN and lower levels of TXNIP mRNA. Importantly, combined upregulation of TXNRD1 and downregulation of TXNIP help maintain levels of reduced thioredoxin that are necessary to combat oxidative stress.

Recently, a role of lipid droplets in protection against ROS has been reported (Bensaad et al. 2014). Moreover, it could be shown that lipid droplet formation under hypoxia-induced oxidative stress was due to fatty acid uptake while *de novo* lipid synthesis is repressed (Bensaad et al. 2014). Interestingly, Ras oncogene-induced senescent cells have also been reported to show reduced *de novo* synthesis of fatty acids (Quijano et al. 2012). This has prompted us to speculate that LIPG induction may compensate the reduced *de novo* synthesis of fatty acids occurring under oxidative stress.

Regularly, fatty acid synthesis consumes nicotinamide adenine dinucleotide phosphate (NADPH), which becomes oxidized to $NADP^+$. In addition to fatty acid synthesis, consumption of NADPH takes place for maintenance of proteins in their reduced native state via the thioredoxin system and for detoxification of H_2O_2 via peroxiredoxin, thioredoxin and glutathione peroxidase. Because redox homeostasis is critical for cell survival we speculated that under oxidative stress a reduction of the *de novo* synthesis of fatty acids takes place to allow the availability of NADPH for protection against the toxicity of ROS (Jeon et al. 2012). Under these conditions fatty acid supply may be overtaken by LIPG.

Induction of the NADPH-dependent TXNRD1 in both senescent MCF7/NeuT and $CoCl_2$-treated cells provided evidence for an increased demand of NADPH in our two cell models. Whether the *de novo* fatty acid synthesis is inhibited, is currently under investigation. An inhibition of the acetyl-CoA carboxylases ACC1 and ACC2 (the first step in fatty acid synthesis) by AMPK has been reported to maintain NADPH levels by decreasing NADPH consumption in fatty acid synthesis under metabolic stress conditions (Jeon et al. 2013). Therefore, to strengthen our hypothesis phosphorylation of ACC by AMPK in our cell models should be verified.

4.5 LIPG versus other extracellular lipases

In addition to LIPG, other phospholipases have been shown to promote intracellular lipid accumulation in breast cancer. Pucer et al. (2013) reported that the human group X secreted phospholipase A2 (hGX PLA2) induces lipid droplet formation by

releasing fatty acids from the cell membrane and from lipoproteins in invasive breast cancer cells to stimulate proliferation and survival in periods of serum starvation. In addition, hGX PLA2 mediates upregulation of PLIN2 and fatty acid oxidation enzymes, and activation of protein kinase B/ Akt and AMPK in MDA-MB-231 breast cancer cells. These phospholipase A2-based effects are also mimicked by oleic acid.

Kuemmerle et al. (2011) reported widespread expression of lipoprotein lipase (LPL) in solid breast tumors, which enables cells to acquire exogenous fatty acids from the circulation via lipolysis of lipoproteins. LPL has higher triglyceride lipase and less phospholipase activity than LIPG and preferentially hydrolyzes very low density lipoproteins (VLDL). Moreover, expression of LPL in breast tumors was independent of their HER2/ER status. LPL-mediated fatty acid uptake led to prevention of cytotoxic effect of FA synthesis inhibition by therapeutic drugs in cancer cells. This shows that fatty acid uptake derived from lipolysis of extracellular lipoproteins seems to occur frequently in breast cancer. However, there are important differences in the type of lipase that operates, its distribution, its association with clinico-pathological parameters, its substrate preference and specificity. According to our results, high expression of LIPG in breast tumors is very rare and it is remarkable that the majority of these tumors display low LPL expression. This fits to the finding that LIPG expression in cardiac tissue was markedly elevated in the early phase of cardiac hypertrophy in mice, whereas lipoprotein lipase expression was significantly reduced (Nakajima et al. 2013). A possible explanation is that upregulation of LIPG only takes place in a context of insufficient LPL action upon tissue injury (Nakajima et al. 2013).

Nomura et al. (2010) described the function of intracellular increased monoacylglycerol lipase- (MAGL/ MGLL) expression in aggressive human cancer cells. MGLL converts monacylglycerols into free fatty acids and glycerol and promotes tumorigenic malignancy by supporting tumor cells with fatty acids.

Thus, in addition to LIPG other lipases have been reported to contribute to tumor-specific lipid metabolism; however their expression patterns may differ temporarily or may be context-dependent.

4.6 Implication of lipid metabolism in breast cancer treatment

Cancer cells require high amounts of lipids based on the high proliferation rate whereby lipids support various aspects in development of cancer (Santos and Schulze 2012). Therapeutic targeting of lipid metabolism for cancer treatment was shown by several research groups *in vitro* and *in vivo* xenograft animal models. Several cancer types, including breast cancer, express high levels of fatty acid synthase (FAS) and display an elevated fatty acid synthesis capacity. This is associated with clinically aggressive tumor behavior and offers a target for therapeutic treatment as a strategy for early intervention (Kuhajda 2000, Milgraum et al. 1997). Pharmacological inhibition of FAS with cerulenin or of ACACA with TOFA in MCF7 breast cancer cells and human breast cancer xenografts induced apoptosis in cancer cells. This anti-tumor effect was accompanied by lack of toxicity to proliferating normal tissues (Thupari et al. 2001). Combined application of TOFA (inhibitor of ACACA in fatty acid synthesis) and etomoxir (inhibitor of fatty acid oxidation) was cytotoxic for MCF7 cells (Pizer et al. 2000, Thupari et al. 2001). Despite these promising results fatty acid synthesis has not been used as target of anticancer therapies in human breast cancer patient trials *in vivo* so far. In this thesis we could show that LIPG is induced (approximately three-fold) when the *de novo* fatty acid synthesis is blocked by pharmacological inhibition of ACACA by TOFA. Moreover, LIPG overexpression in presence of TOFA promoted cell survival by preserving mitochondrial integrity. Our results suggest that tumors treated with TOFA may be able to avoid cytotoxic effects of fatty acid inhibition by upregulation of alternative mechanisms of lipid supply (such as LIPG) that promote cell survival. It is also tempting to speculate that upregulation of LIPG may causes resistance towards therapies aimed to block endogenous lipogenesis.

In this context it is important to note that in contrast to TOFA- (an ACACA inhibitor), cerulenin- (a FAS inhibitor) treated MCF7 cells did not result in LIPG induction (data not shown). An important difference is that these inhibitors lead to accumulation of different intermediates (acetyl-CoA/malonyl-CoA). Thus, LIPG may not be induced by simply blocking *de novo* fatty acid synthesis but accumulation or shortage of key metabolites may play an important role as well. This deserves additional research.

5. Summary

The endothelial lipase LIPG is a cell surface-associated member of the triglyceride lipase family, discovered in 1999 in endothelial cells. LIPG displays phospholipase A1 activity towards high-density lipoproteins (HDL) as main substrate and releases fatty acids and lysophosphatidylcholine which can be taken up by cells. Besides its role in HDL metabolism, a function of LIPG in the development of atherosclerosis has been reported. However, a role for LIPG in cancer remains unexplored up to date.

The aim of the study was to investigate the expression and importance of LIPG in human breast cancer. For this purpose we studied 1) the consequences and possible advantages of LIPG overexpression in tumor cells *in vitro*, 2) the context in which LIPG becomes induced and 3) its expression and association with adverse outcome in a large collection of node-negative, untreated breast cancer tumors.

Overexpression of LIPG in MCF7 cells in presence of HDL or phosphatidylcholine (PC) leads to intracellular accumulation of lipid droplets and was accompanied by induction of perilipin 2 (PLIN2) and lipocalin 2 (LCN2). Remarkably, LIPG-mediated lipid supply was shown to support mitochondrial functionality after blocking *de novo* fatty acid synthesis by TOFA (an inhibitor of ACACA). We observed that LIPG expression becomes induced under cellular stress conditions including oncogene-induced senescence (OIS), and chemical hypoxia (cobalt chloride), both characterized by excessive accumulation of reactive oxygen species. LIPG induction could also be observed by pharmacological inhibition of the *de novo* fatty acid synthesis by TOFA, contributing to the assumption that LIPG becomes induced to compensate the reduced capacity to synthesize fatty acids upon metabolic stress.

Affymetrix gene array data analysis of breast tumors revealed that LIPG is only expressed in a very limited number of tumor samples and thus represents a rare event in breast cancer. In these samples LIPG correlates with grade III, negative estrogen receptor status and a shorter metastasis-free survival. Moreover, LIPG-expressing tumors were characterized by high expression of oxidative stress and angiogenesis markers.

In summary, based on the results presented in this thesis, LIPG supports tumor cells with fatty acids derived from exogenous lipid sources, and thus helps maintain mitochondrial functionality. This represents a survival advantage when *de novo* fatty acid synthesis capacity is compromised, a condition that arises under oxidative stress. The limited LIPG expression in 1) breast cancer *in vivo* - only confined to a few highly dedifferentiated aggressive tumors - and 2) under particular circumstances *in vitro* - OIS and high concentrations of the hypoxia mimicking agent cobalt chloride - explains the lack of data concerning LIPG in the context of breast cancer. It can be concluded that LIPG-mediated lipid supply occurs only under very adverse conditions and contributes to tumor progression by enabling survival of tumor cells.

6. Zusammenfassung

Die 1999 erstmalig beschriebene endotheliale Lipase LIPG gehört zu der Familie der Zelloberflächen-assoziierten Proteine. LIPG hydrolysiert, bedingt durch dessen Phospholipase A1 Aktivität, als Hauptsubstrat Lipoproteine mit hoher Dichte (HDL). HDL wird in Lysophosphatidylcholin und Fettsäuren gespalten, welche wiederum von Zellen aufgenommen werden können. Neben der Rolle im HDL-Metabolismus, ist LIPG mit Arteriosklerose assoziiert. Bis heute ist eine mögliche Funktion von LIPG in Krebs unklar.

Ziel dieser Arbeit war die Expression und Beteiligung von LIPG im humanen Brustkrebs zu erforschen. Zu diesem Zweck haben wir 1) die Konsequenz und möglichen Vorteile einer LIPG Überexpression in Tumorzellen *in vitro*, 2) den Kontext in welchem LIPG induziert wird und 3) die Expression und Assoziation mit dem ungünstigen Krankheitsverlauf in einer großen Kohorte von unbehandelten Brustkrebspatientinnen ohne Lymphknotenbefall untersucht.

Die LIPG Überexpression in MCF7 Zellen führt in der Präsenz von HDL oder Phosphatidylcholin (PC) zu einer intrazellulären Akkumulation von Lipidtröpfchen, begleitet von der Induktion von Perilipin2 (PLIN2) und Lipocalin2 (LCN2). Bemerkenswerterweise zeigte die LIPG-vermittelte Versorgung eine Aufrechterhaltung der mitochondrialen Funktionalität, sobald die *de novo* Fettsäuresynthese durch TOFA (Inhibitor von ACACA) blockiert wurde. Wir konnten feststellen, dass die LIPG Expression durch zelluläre Stressbedingungen wie Onkogen-induzierte Seneszenz (OIS) und chemische Hypoxie (Kobalt(II)-chlorid), beides charakterisiert durch exzessive Akkumulation von reaktiven Sauerstoffspezies, induziert wird. Eine erhöhte LIPG Expression durch die pharmakologische Blockade der *de novo* Fettsäuresynthese durch TOFA, trägt zu der Annahme bei, dass LIPG induziert wird, um die reduzierte Kapazität Fettsäuren zu synthetisieren unter metabolischem Stress zu kompensieren.

Affymetrix *gene array* Datenanalysen von Brusttumoren zeigen, dass LIPG lediglich in einer geringen Anzahl von Tumorproben exprimiert wird und daher ein seltenes

Ereignis im Brustkrebs darstellt. In den entsprechenden Proben korreliert das gesteigerte LIPG-Level mit Krebsstadium III, negativen Östrogenrezeptorstatus und einer kürzeren Metastasen-freien Überlebenszeit. Darüber hinaus konnte in LIPG-exprimierenden Tumoren eine erhöhte Expression von oxidativem Stress- und Angiogenese-Markern gemessen werden.

Basierend auf den in dieser Dissertation vorliegenden Ergebnissen, kann zusammengefasst werden, dass LIPG Tumorzellen mit Fettsäuren aus exogenen Lipidquellen versorgt und damit die mitochondriale Funktionalität aufrecht hält. Dies repräsentiert einen Überlebensvorteil sobald die *de novo* Fettsäuresynthese-Kapazität gefährdet ist, wie es unter oxidativem Stress der Fall ist. Die limitierte LIPG Expression in 1) Brustkrebs *in vivo* - begrenzt in wenigen stark-dedifferenzierten aggressiven Tumoren - und 2) unter bestimmten Umständen *in vitro* - Onkogen-induzierte Seneszenz und hohe Konzentrationen der Hypoxie-imitierenden Substanz Kobalt(II)-chlorid - erklären das fehlende Wissen über die Verbindung von LIPG und Brustkrebs. Zusammenfassend konnte gezeigt werden, dass die LIPG-vermittelte Versorgung mit Fettsäuren nur unter zellschädigenden Umständen stattfindet, dadurch ein Überleben von Tumorzellen ermöglicht und letztlich zu einer Tumorprogression beiträgt.

7. References

Aon, M. A., N. Bhatt, and S. C. Cortassa. 2014. Mitochondrial and cellular mechanisms for managing lipid excess. Front Physiol 5:282.

Asimakopoulou, Anastasia, Erawan Borkham-Kamphorst, Marc Henning, Eray Yagmur, Nikolaus Gassler, Christian Liedtke, Thorsten Berger, Tak W. Mak, and Ralf Weiskirchen. 2014. Lipocalin-2 (LCN2) regulates PLIN5 expression and intracellular lipid droplet formation in the liver. Biochimica et Biophysica Acta (BBA) - Molecular and Cell Biology of Lipids 1841 (10):1513-1524.

Azumi, Hiroshi, Ken-ichi Hirata, Tatsuro Ishida, Yoko Kojima, Yoshiyuki Rikitake, Shigeto Takeuchi, Nobutaka Inoue, Seinosuke Kawashima, Yoshitake Hayashi, Hiroshi Itoh, Thomas Quertermous, and Mitsuhiro Yokoyama. 2003. Immunohistochemical localization of endothelial cell-derived lipase in atherosclerotic human coronary arteries.

Badellino, Karen, Weijun Jin, and Daniel J. Rader. 2005. Endothelial Lipase: A Novel Drug Target for HDL and Atherosclerosis?, Lipases and Phospholipases in Drug Development: Wiley-VCH Verlag GmbH & Co. KGaA.

Badellino, Karen O., Megan L. Wolfe, Muredach P. Reilly, and Daniel J. Rader. 2008. Endothelial Lipase Is Increased In Vivo by Inflammation in Humans.

Bargmann, Cornelia I., Mien-Chie Hung, and Robert A. Weinberg. 1986. Multiple independent activations of the neu oncogene by a point mutation altering the transmembrane domain of p185. Cell 45 (5):649-657.

Baritaki, Stavroula, Stavros Apostolakis, Peggy Kanellou, MarieTherese Dimanche Boitrel, Demetrios A. Spandidos, and Benjamin Bonavida. 2007. Reversal of Tumor Resistance to Apoptotic Stimuli by Alteration of Membrane Fluidity: Therapeutic Implications. In Advances in Cancer Research: Academic Press.

Baumann, Jan, Christopher Sevinsky, and Douglas S. Conklin. 2013. Lipid biology of breast cancer. Biochimica et biophysica acta 1831 (10):1509-1517.

Bensaad, K., E. Favaro, C. A. Lewis, B. Peck, S. Lord, J. M. Collins, K. E. Pinnick, S. Wigfield, F. M. Buffa, J. L. Li, Q. Zhang, M. J. Wakelam, F. Karpe, A. Schulze, and A. L. Harris. 2014. Fatty acid uptake and lipid storage induced by HIF-1alpha contribute to cell growth and survival after hypoxia-reoxygenation. Cell Rep 9 (1):349-65.

Bezwoda, W. R., D. Derman, N. G. De Moor, M. Lange, and J. Levin. 1982. Treatment of metastatic breast cancer in estrogen receptor positive patients a randomized trial comparing tamoxifen alone versus tamoxifen plus CMF. Cancer 50 (12):2747-2750.

Cadenas, Cristina, Dennis Franckenstein, Marcus Schmidt, Mathias Gehrmann, Matthias Hermes, Bettina Geppert, Wiebke Schormann, Lindsey J. Maccoux, Markus Schug, Anika Schumann, Christian Wilhelm, Evgenia Freis, Katja Ickstadt, Jörg Rahnenführer, Jörg I. Baumbach, Albert Sickmann, and Jan G. Hengstler. 2010. Role of thioredoxin reductase 1 and thioredoxin interacting

protein in prognosis of breast cancer. Breast Cancer Research : BCR 12 (3):R44-R44.

Cadenas, Cristina, Sonja Vosbeck, Eva-Maria Hein, Birte Hellwig, Alice Langer, Heiko Hayen, Dennis Franckenstein, Bettina Büttner, Seddik Hammad, Rosemarie Marchan, Matthias Hermes, Silvia Selinski, Jörg Rahnenführer, Begüm Peksel, Zsolt Török, László Vígh, and Jan G. Hengstler. 2012. Glycerophospholipid profile in oncogene-induced senescence. Biochimica et Biophysica Acta (BBA) - Molecular and Cell Biology of Lipids 1821 (9):1256-1268.

Calder, P. C. 2011. Fatty acids and inflammation: the cutting edge between food and pharma. Eur J Pharmacol 668 Suppl 1:S50-8.

Campisi, Judith, and Fabrizio d'Adda di Fagagna. 2007. Cellular senescence: when bad things happen to good cells. Nat Rev Mol Cell Biol 8 (9):729-740.

Casalini, Patrizia, Marilena V. Iorio, Enrico Galmozzi, and Sylvie Ménard. 2004. Role of HER receptors family in development and differentiation. Journal of Cellular Physiology 200 (3):343-350.

Choi, Sungshin Y., Ken-ichi Hirata, Tatsuro Ishida, Thomas Quertermous, and Allen D. Cooper. 2002. Endothelial lipase: a new lipase on the block. Journal of Lipid Research 43 (11):1763-1769.

Claus, Maren, and Carsten Watzl. 2001. Evaluation of Human Natural Killer Cell Activities in Whole Blood. In Current Protocols in Immunology: John Wiley & Sons, Inc.

Cuenda, Ana, and Simon Rousseau. 2007. p38 MAP-Kinases pathway regulation, function and role in human diseases. Biochimica et Biophysica Acta (BBA) - Molecular Cell Research 1773 (8):1358-1375.

Cui, Meizi, Haofan Jin, Xiumin Shi, Ge Qu, Lidi Liu, Xiaobo Ding, Yanbo Wang, and Chao Niu. 2014. Lipase member H is a novel secreted protein associated with a poor prognosis for breast cancer patients. Tumor Biology 35 (11):11461-11465.

Dalan, Altay Burak, Bahar Toptas, Zehra Bugra, Nihat Polat, Hülya Yilmaz-Aydogan, Arif Cimen, and Turgay Isbir. 2013. The effects of endothelial lipase gene (LIPG) variants on inflammation marker levels and atherosclerosis development. Molecular Biology Reports:1-7.

Dong, Xueyan, Guoqing Wang, Guoqing Zhang, Zhaohui Ni, Jian Suo, Juan Cui, Ai Cui, Qing Yang, Ying Xu, and Fan Li. 2013. The endothelial lipase protein is promising urinary biomarker for diagnosis of gastric cancer. Diagnostic Pathology 8:45-45.

Drexler, Hans G. 2000. Malignant hematopoietic cell lines: in vitro models for the study of myelodysplastic syndromes. Leukemia Research 24 (2):109-115.

Enns, Linda, and Warren Ladiges. 2012. Mitochondrial redox signaling and cancer invasiveness. Journal of bioenergetics and biomembranes 44 (6):635-638.

Eren, Esin, Necat Yilmaz, and Ozgur Aydin. 2012. High Density Lipoprotein and it's Dysfunction. The Open Biochemistry Journal 6:78-93.

Fahy, Eoin, Shankar Subramaniam, H. Alex Brown, Christopher K. Glass, Alfred H. Merrill, Robert C. Murphy, Christian R. H. Raetz, David W. Russell, Yousuke Seyama, Walter Shaw, Takao Shimizu, Friedrich Spener, Gerrit van Meer, Michael S. VanNieuwenhze, Stephen H. White, Joseph L. Witztum, and Edward A. Dennis. 2005. A comprehensive classification system for lipids. Journal of Lipid Research 46 (5):839-862.

Fahy, Eoin, Shankar Subramaniam, Robert C. Murphy, Masahiro Nishijima, Christian R. H. Raetz, Takao Shimizu, Friedrich Spener, Gerrit van Meer, Michael J. O. Wakelam, and Edward A. Dennis. 2009. Update of the LIPID MAPS comprehensive classification system for lipids. Journal of Lipid Research 50 (Supplement):S9-S14.

Fire, Andrew, SiQun Xu, Mary K. Montgomery, Steven A. Kostas, Samuel E. Driver, and Craig C. Mello. 1998. Potent and specific genetic interference by double-stranded RNA in Caenorhabditis elegans. Nature 391 (6669):806-811.

Fuki, Ilia V., Nadine Blanchard, Weijun Jin, Dawn H. L. Marchadier, John S. Millar, Jane M. Glick, and Daniel J. Rader. 2003. Endogenously Produced Endothelial Lipase Enhances Binding and Cellular Processing of Plasma Lipoproteins via Heparan Sulfate Proteoglycan-mediated Pathway.

Fűri, István, Alexandra Kalmár, Barnabás Wichmann, Sándor Spisák, Andrea Schöller, Barbara Barták, Zsolt Tulassay, and Béla Molnár. 2015. Cell Free DNA of Tumor Origin Induces a 'Metastatic' Expression Profile in HT-29 Cancer Cell Line. PLoS ONE 10 (7):e0131699.

Gauster, Martin, Andelko Hrzenjak, Katja Schick, and Sasa Frank. 2005. Endothelial lipase is inactivated upon cleavage by the members of the proprotein convertase family.

Glatz, J. F., J. J. Luiken, and A. Bonen. 2010. Membrane fatty acid transporters as regulators of lipid metabolism: implications for metabolic disease. Physiol Rev 90 (1):367-417.

Gomez-Cambronero, Julian. 2010. New concepts in PLD signaling in inflammation and cancer. TheScientificWorldJournal 10:1356-1369.

Gottfried, Eva, Marina Kreutz, and Andreas Mackensen. 2012. Tumor metabolism as modulator of immune response and tumor progression. Seminars in Cancer Biology 22 (4):335-341.

Greulich, Heidi, Bethany Kaplan, Philipp Mertins, Tzu-Hsiu Chen, Kumiko E. Tanaka, Cai-Hong Yun, Xiaohong Zhang, Se-Hoon Lee, Jeonghee Cho, Lauren Ambrogio, Rachel Liao, Marcin Imielinski, Shantanu Banerji, Alice H. Berger, Michael S. Lawrence, Jinghui Zhang, Nam H. Pho, Sarah R. Walker, Wendy Winckler, Gad Getz, David Frank, William C. Hahn, Michael J. Eck, D. R. Mani, Jacob D. Jaffe, Steven A. Carr, Kwok-Kin Wong, and Matthew Meyerson. 2012. Functional analysis of receptor tyrosine kinase mutations in lung cancer identifies oncogenic extracellular domain mutations of ERBB2. Proceedings of the National Academy of Sciences of the United States of America 109 (36):14476-14481.

Grzyb, Joanna, Dariusz Latowski, and Kazimierz Strzałka. 2006. Lipocalins – a family portrait. Journal of Plant Physiology 163 (9):895-915.

Hajri, T., and N. A. Abumrad. 2002. Fatty acid transport across membranes: relevance to nutrition and metabolic pathology. Annu Rev Nutr 22:383-415.

Hanahan, Douglas, and Robert A. Weinberg. 2000. The Hallmarks of Cancer. Cell 100 (1):57-70.

Hanahan, Douglas, and Robert A Weinberg. 2011. Hallmarks of Cancer: The Next Generation. Cell 144 (5):646-674.

Hart, Christopher D., Ilenia Migliaccio, Luca Malorni, Cristina Guarducci, Laura Biganzoli, and Angelo Di Leo. 2015. Challenges in the management of advanced, ER-positive, HER2-negative breast cancer. Nat Rev Clin Oncol advance online publication.

Henneberry, Annette L., Graeme Wistow, and Christopher R. McMaster. 2000. Cloning, Genomic Organization, and Characterization of a Human Cholinephosphotransferase. Journal of Biological Chemistry 275 (38):29808-29815.

Herber, D. L., W. Cao, Y. Nefedova, S. V. Novitskiy, S. Nagaraj, V. A. Tyurin, A. Corzo, H. I. Cho, E. Celis, B. Lennox, S. C. Knight, T. Padhya, T. V. McCaffrey, J. C. McCaffrey, S. Antonia, M. Fishman, R. L. Ferris, V. E. Kagan, and D. I. Gabrilovich. 2010. Lipid accumulation and dendritic cell dysfunction in cancer. Nat Med 16 (8):880-6.

Hirata, Ken-ichi, Helen L. Dichek, Joseph A. Cioffi, Sungshin Y. Choi, Nicholas J. Leeper, Leah Quintana, Gregory S. Kronmal, Allen D. Cooper, and Thomas Quertermous. 1999. Cloning of a Unique Lipase from Endothelial Cells Extends the Lipase Gene Family.

Hochachka, P. W., J. L. Rupert, L. Goldenberg, M. Gleave, and P. Kozlowski. 2002. Going malignant: the hypoxia-cancer connection in the prostate. Bioessays 24 (8):749-57.

Holbro, Thomas, Gianluca Civenni, and Nancy E. Hynes. 2003. The ErbB receptors and their role in cancer progression. Experimental Cell Research 284 (1):99-110.

Holliday, Deborah L., and Valerie Speirs. 2011. Choosing the right cell line for breast cancer research. Breast Cancer Research : BCR 13 (4):215-215.

Hulbert, A. J. 2006. The links between membrane composition, metabolic rate and lifespan. Comparative Biochemistry and Physiology Part A: Molecular & Integrative Physiology 150 (2):196-203.

Ishida, Tatsuro, Zhi Zheng, Helén L. Dichek, Huijian Wang, Ismael Moreno, Eugene Yang, Ramendra K. Kundu, Said Talbi, Ken-ichi Hirata, Lawrence L. Leung, and Thomas Quertermous. 2004. Molecular cloning of nonsecreted endothelial cell-derived lipase isoforms. Genomics 83 (1):24-33.

Jaye, Michael, Kevin J. Lynch, John Krawiec, Dawn Marchadier, Cyrille Maugeais, Kim Doan, Victoria South, Dilip Amin, Mark Perrone, and Daniel J. Rader. 1999. A novel endothelial-derived lipase that modulates HDL metabolism. Nat Genet 21 (4):424-428.

Jemal, Ahmedin, Rebecca Siegel, Elizabeth Ward, Yongping Hao, Jiaquan Xu, and Michael J. Thun. 2009. Cancer Statistics, 2009. CA: A Cancer Journal for Clinicians 59 (4):225-249.

Jeon, Hyesung, and Stephen C. Blacklow. 2005. Structure and physiologic function of the low-density lipoprotein receptor. Annual Review of Biochemistry 74 (1):535-562.

Jeon, Sang-Min, Navdeep S. Chandel, and Nissim Hay. 2012. AMPK regulates NADPH homeostasis to promote tumour cell survival during energy stress. Nature 485 (7400):661-665.

Jha, Mithilesh Kumar, Sangmin Jeon, Myungwon Jin, Jiyeon Ock, Jong-Heon Kim, Won-Ha Lee, and Kyoungho Suk. 2014. The pivotal role played by lipocalin-2 in chronic inflammatory pain. Experimental Neurology 254:41-53.

Jiang, Weihua, Jing Zhu, Xun Zhuang, Xiping Zhang, Tao Luo, Karyn A. Esser, and Hongmei Ren. 2015. Lipin1 Regulates Skeletal Muscle Differentiation through Extracellular Signal-regulated Kinase (ERK) Activation and Cyclin D Complex-regulated Cell Cycle Withdrawal. Journal of Biological Chemistry 290 (39):23646-23655.

Jin, Weijun, Gwo-Shing Sun, Dawn Marchadier, Edelyn Octtaviani, Jane M. Glick, and Daniel J. Rader. 2003. Endothelial Cells Secrete Triglyceride Lipase and Phospholipase Activities in Response to Cytokines as a Result of Endothelial Lipase.

Jin, Yixin, Bassam B Damaj, and Azzam A Maghazachi. 2005. Human resting CD16–,CD16+ and IL-2-, IL-12-, IL-15- or IFN-α-activated natural killer cells differentially respond to sphingosylphosphorylcholine, lysophosphatidylcholine and platelet-activating factor. European Journal of Immunology 35 (9):2699-2708.

Kempe, Sybille, Hans Kestler, Andrea Lasar, and Thomas Wirth. 2005. NF-κB controls the global pro-inflammatory response in endothelial cells: evidence for the regulation of a pro-atherogenic program. Nucleic Acids Research 33 (16):5308-5319.

Kersten, Sander. 2014. Physiological regulation of lipoprotein lipase. Biochimica et Biophysica Acta (BBA) - Molecular and Cell Biology of Lipids 1841 (7):919-933.

Kivelä, Annukka M., Petri I. Mäkinen, Henna-Kaisa Jyrkkänen, Eero Mella-Aho, Yifeng Xia, Emilia Kansanen, Hanna Leinonen, Inder M. Verma, Seppo Ylä-Herttuala, and Anna-Liisa Levonen. Sulforaphane inhibits endothelial lipase expression through NF-kB in endothelial cells. Atherosclerosis 213 (1):122-128.

Klaunig, James E., and Lisa M. Kamendulis. 2004. The role of oxidative stress in carcinogenesis. Annual Review of Pharmacology and Toxicology 44 (1):239-267.

Kojma, Yoko, Ken-ichi Hirata, Tatsuro Ishida, Yasushi Shimokawa, Nobutaka Inoue, Seinosuke Kawashima, Thomas Quertermous, and Mitsuhiro Yokoyama.

2004. Endothelial Lipase Modulates Monocyte Adhesion to the Vessel Wall. Journal of Biological Chemistry 279 (52):54032-54038.

Kuemmerle, Nancy B., Evelien Rysman, Portia S. Lombardo, Alison J. Flanagan, Brea C. Lipe, Wendy A. Wells, Jason R. Pettus, Heather M. Froehlich, Vincent A. Memoli, Peter M. Morganelli, Johannes V. Swinnen, Luika A. Timmerman, Leila Chaychi, Catherine J. Fricano, Burton L. Eisenberg, William B. Coleman, and William B. Kinlaw. Lipoprotein Lipase Links Dietary Fat to Solid Tumor Cell Proliferation.

Kuhajda, Francis P. 2000. Fatty-acid synthase and human cancer: new perspectives on its role in tumor biology. Nutrition 16 (3):202-208.

Lagadari, Mariana, Krisztina Truta-Feles, Katja Lehmann, Luciana Berod, Mirjana Ziemer, Marco Idzko, Dagmar Barz, Thomas Kamradt, Azzam A. Maghazachi, and Johannes Norgauer. 2009. Lysophosphatidic acid inhibits the cytotoxic activity of NK cells: involvement of Gs protein-mediated signaling.

LeGrand TS, Aw TY. 1996. Chronic hypoxia and glutathione-dependent detoxication in rat small intestine. Am J Physiol. 270(4 Pt 1):G725-9.

Liu, Qin, Rodrigo M. P. Siloto, Richard Lehner, Scot J. Stone, and Randall J. Weselake. 2012. Acyl-CoA:diacylglycerol acyltransferase: Molecular biology, biochemistry and biotechnology. Progress in Lipid Research 51 (4):350-377.

Lodish, Berk, Kaiser, Krieger, Bretscher, Ploegh, Amon, Scott. 2012. Molecular cell biology. 7th edition.

Lottspeich Friedrich, Engels Joachim W.. 2012. Bioanalytik. Spektrum Akademischer Verlag ISBN 978-3-8274-2942-1

Mamessier, E., A. Sylvain, M. L. Thibult, G. Houvenaeghel, J. Jacquemier, R. Castellano, A. Goncalves, P. Andre, F. Romagne, G. Thibault, P. Viens, D. Birnbaum, F. Bertucci, A. Moretta, and D. Olive. 2011. Human breast cancer cells enhance self tolerance by promoting evasion from NK cell antitumor immunity. J Clin Invest 121 (9):3609-22.

Mashek, Douglas G, and Rosalind A Coleman. 2006. Cellular fatty acid uptake: the contribution of metabolism. Current Opinion in Lipidology 17 (3):274-278.

McCoy, Mary G., Gwo-Shing Sun, Dawn Marchadier, Cyrille Maugeais, Jane M. Glick, and Daniel J. Rader. 2002. Characterization of the lipolytic activity of endothelial lipase.

Ménard, S., P. Casalini, M. Campiglio, S. M. Pupa, and E. Tagliabue. 2004. Oncogenic protein tyrosine kinases. Cellular and Molecular Life Sciences CMLS 61 (23):2965-2978.

Ménard, S., S. Fortis, F. Castiglioni, R. Agresti, and A. Balsari. 2001. HER2 as a Prognostic Factor in Breast Cancer. Oncology 61(suppl 2) (Suppl. 2):67-72.

Milgraum, L Z, L A Witters, G R Pasternack, and F P Kuhajda. 1997. Enzymes of the fatty acid synthesis pathway are highly expressed in in situ breast carcinoma. Clinical Cancer Research 3 (11):2115-2120.

Miller, Gwen C., Christopher J. Long, Ekaterina D. Bojilova, Dawn Marchadier, Karen O. Badellino, Nadine Blanchard, Ilia V. Fuki, Jane M. Glick, and Daniel J.

Rader. 2004. Role of N-linked glycosylation in the secretion and activity of endothelial lipase.

Moiseeva, Olga, Véronique Bourdeau, Antoine Roux, Xavier Deschênes-Simard, and Gerardo Ferbeyre. 2009. Mitochondrial Dysfunction Contributes to Oncogene-Induced Senescence. Molecular and Cellular Biology 29 (16):4495-4507.

Mudvari, P., K. Ohshiro, V. Nair, A. Horvath, and R. Kumar. 2013. Genomic insights into triple-negative and HER2-positive breast cancers using isogenic model systems. PLoS One 8 (9):e74993.

Mullen, Genevieve E., and Larry Yet. 2015. Progress in the development of fatty acid synthase inhibitors as anticancer targets. Bioorganic & Medicinal Chemistry Letters 25 (20):4363-4369.

Muñoz-Pinedo, C., N. El Mjiyad, and J. E. Ricci. 2012. Cancer metabolism: current perspectives and future directions. Cell Death & Disease 3 (1):e248.

Munro, S., and H. R. Pelham. 1984. Use of peptide tagging to detect proteins expressed from cloned genes: deletion mapping functional domains of Drosophila hsp 70. The EMBO Journal 3 (13):3087-3093.

Murray, Michael, Adam Hraiki, Mary Bebawy, Curtis Pazderka, and Tristan Rawling. 2015. Anti-tumor activities of lipids and lipid analogues and their development as potential anticancer drugs. Pharmacology & Therapeutics 150:109-128.

Nakajima, Hideto, Tatsuro Ishida, Seimi Satomi-Kobayashi, Kenta Mori, Tetsuya Hara, Naoto Sasaki, Tomoyuki Yasuda, Ryuji Toh, Hidekazu Tanaka, Hiroya Kawai, and Ken-ichi Hirata. 2013. Endothelial Lipase Modulates Pressure Overload-Induced Heart Failure Through Alternative Pathway for Fatty Acid Uptake.

Neve, RM, Sutterlüty H, Pullen N, Lane HA, Daly JM, Krek W, Hynes NE. 2000. Effects of oncogenic ErbB2 on G1 cell cycle regulators in breast tumour cells. Oncogene. 2000 Mar 23;19(13):1647-56.

Nielsen, J. E., M. L. Lindegaard, L. Friis-Hansen, K. Almstrup, H. Leffers, L. B. Nielsen, and E. Rajpert-De Meyts. 2010. Lipoprotein lipase and endothelial lipase in human testis and in germ cell neoplasms. International Journal of Andrology 33 (1):e207-e215.

Nomura, Daniel K., Jonathan Z. Long, Sherry Niessen, Heather S. Hoover, Shu-Wing Ng, and Benjamin F. Cravatt. 2010. Monoacylglycerol lipase regulates a fatty acid network that promotes cancer pathogenesis. Cell 140 (1):49-61.

Oh, Se Won, Yun-Mi Lee, Sejoong Kim, Ho Jun Chin, Dong-Wan Chae, and Ki Young Na. 2014. Cobalt Chloride Attenuates Oxidative Stress and Inflammation through NF-κB Inhibition in Human Renal Proximal Tubular Epithelial Cells. Journal of Korean Medical Science 29 (Suppl 2):S139-S145.

Ohtani, N., D. J. Mann, and E. Hara. 2009. Cellular senescence: its role in tumor suppression and aging. Cancer Sci 100 (5):792-7.

Okada, Hitoshi, and Tak W. Mak. 2004. Pathways of apoptotic and non-apoptotic death in tumour cells. Nat Rev Cancer 4 (8):592-603.

Ory, Daniel S. 2004. The Niemann-Pick Disease Genes: Regulators of Cellular Cholesterol Homeostasis. Trends in Cardiovascular Medicine 14 (2):66-72.

Paradis, Marie-Eve, Karen O. Badellino, Daniel J. Rader, Yves Deshaies, Patrick Couture, Wiedad R. Archer, Nathalie Bergeron, and BenoÃ®t Lamarche. 2006. Endothelial lipase is associated with inflammation in humans.

Perou, Charles M., Therese Sorlie, Michael B. Eisen, Matt van de Rijn, Stefanie S. Jeffrey, Christian A. Rees, Jonathan R. Pollack, Douglas T. Ross, Hilde Johnsen, Lars A. Akslen, Oystein Fluge, Alexander Pergamenschikov, Cheryl Williams, Shirley X. Zhu, Per E. Lonning, Anne-Lise Borresen-Dale, Patrick O. Brown, and David Botstein. 2000. Molecular portraits of human breast tumours. Nature 406 (6797):747-752.

Pizer, Ellen S., Thupari Jagan, Han Wan Fang, Pinn Michael L., Chrest Francis J., Frehywot Gojeb L., Townsend Craig A., Kuhajda Francis P. 2000. Malonyl-Coenzyme-A Is a Potential Mediator of Cytotoxicity Induced by Fatty-Acid Synthase Inhibition in Human Breast Cancer Cells and Xenografts. CANCER RESEARCH 60, 213–218.

Potter, D Sorrentino, and P D Berk. 1989. Mechanisms of Cellular Uptake of Free Fatty Acids. Annual Review of Nutrition 9 (1):253-270.

Prat, Aleix, and Charles M. Perou. 2011. Deconstructing the molecular portraits of breast cancer. Molecular Oncology 5 (1):5-23.

Pucer, Anja, Vesna Brglez, Christine Payré, Jože Pungerčar, Gérard Lambeau, and Toni Petan. 2013. Group X secreted phospholipase A(2) induces lipid droplet formation and prolongs breast cancer cell survival. Molecular Cancer 12:111-111.

Qiu, Guosong, Alexander C. Ho, Willie Yu, and John S. Hill. 2007. Suppression of endothelial or lipoprotein lipase in THP-1 macrophages attenuates proinflammatory cytokine secretion.

Quijano, Celia, Liu Cao, Maria M. Fergusson, Hector Romero, Jie Liu, Sarah Gutkind, Ilsa I. Rovira, Robert P. Mohney, Edward D. Karoly, and Toren Finkel. 2012. Oncogene-induced senescence results in marked metabolic and bioenergetic alterations. Cell Cycle 11 (7):1383-1392.

Razzaghi, H., A. Tempczyk-Russell, K. Haubold, S. A. Santorico, T. Shokati, U. Christians, and M. E. Churchill. 2013. Genetic and structure-function studies of missense mutations in human endothelial lipase. PLoS One 8 (3):e55716.

Riederer, Monika, Harald Köfeler, Margarete Lechleitner, Michaela Tritscher, and Saša Frank. 2012. Impact of endothelial lipase on cellular lipid composition. Biochimica et Biophysica Acta 1821 (7):1003-1011.

Rink, Lothar, Kruse, Andrea, Haase, Hajo. 2012. Immunologie für Einsteiger. Springer Spektrum Verlag. ISBN 978-3-8274-2440-2

Robert-Koch Institut. Gesellschaft der epidemiologischen Krebsregister in Deutschland e.V. 2009/2010. Krebs in Deutschland 2009/2010. ISBN 978-3-89606-221-5

Rodier, Francis, and Judith Campisi. 2011. Four faces of cellular senescence. The Journal of Cell Biology 192 (4):547-556.

Rodvold, Jeffrey J., Navin R. Mahadevan, and Maurizio Zanetti. 2012. Lipocalin 2 in cancer: When good immunity goes bad. Cancer Letters 316 (2):132-138.

Ross, Jeffrey S., and Jonathan A. Fletcher. 1999. The HER-2/neu oncogene: prognostic factor, predictive factor and target for therapy. Seminars in Cancer Biology 9 (2):125-138.

Roudkenar, Mehryar Habibi, Yoshikazu Kuwahara, Taisuke Baba, Amaneh Mohammadi Roushandeh, Shigeko Ebishima, Shinya Abe, Yasuhito Ohkubo, and Manabu Fukumoto. 2007. Oxidative Stress Induced Lipocalin 2 Gene Expression: Addressing its Expression under the Harmful Conditions. Journal of Radiation Research 48 (1):39-44.

Rysman, Evelien, Koen Brusselmans, Katryn Scheys, Leen Timmermans, Rita Derua, Sebastian Munck, Paul P. Van Veldhoven, David Waltregny, Veerle W. Daniëls, Jelle Machiels, Frank Vanderhoydonc, Karine Smans, Etienne Waelkens, Guido Verhoeven, and Johannes V. Swinnen. 2010. De novo Lipogenesis Protects Cancer Cells from Free Radicals and Chemotherapeutics by Promoting Membrane Lipid Saturation. Cancer Research 70 (20):8117-8126.

Santos, Claudio R., and Almut Schulze. 2012. Lipid metabolism in cancer. FEBS Journal 279 (15):2610-2623.

Schneider, Paul M., Mien-Chie Hung, Susanna M. Chiocca, John Manning, Xiaoyan Zhao, Kang Fang, and Jack A. Roth. 1989. Differential Expression of the c-erbB-2 Gene in Human Small Cell and Non-Small Cell Lung Cancer. Cancer Research 49 (18):4968-4971.

Sewing, A., B. Wiseman, A. C. Lloyd, and H. Land. 1997. High-intensity Raf signal causes cell cycle arrest mediated by p21Cip1. Molecular and Cellular Biology 17 (9):5588-5597.

Simon, Michael A. 2000. Receptor Tyrosine Kinases: Specific Outcomes from General Signals. Cell 103 (1):13-15.

Skropeta, Danielle, Chatri Settasatian, Monica R. McMahon, Kate Shearston, Daniela Caiazza, Kristine C. McGrath, Weijun Jin, Daniel J. Rader, Philip J. Barter, and Kerry-Anne Rye. 2007. N-Glycosylation regulates endothelial lipase-mediated phospholipid hydrolysis in apoE- and apoA-I-containing high density lipoproteins. Journal of Lipid Research 48 (9):2047-2057.

Slamon, Dennis J. 1987. Proto-Oncogenes and Human Cancers. New England Journal of Medicine 317 (15):955-957.

Smith, P. K., R. I. Krohn, G. T. Hermanson, A. K. Mallia, F. H. Gartner, M. D. Provenzano, E. K. Fujimoto, N. M. Goeke, B. J. Olson, and D. C. Klenk. 1985. Measurement of protein using bicinchoninic acid. Analytical Biochemistry 150 (1):76-85.

Sørlie, Therese, Charles M. Perou, Robert Tibshirani, Turid Aas, Stephanie Geisler, Hilde Johnsen, Trevor Hastie, Michael B. Eisen, Matt van de Rijn, Stefanie S. Jeffrey, Thor Thorsen, Hanne Quist, John C. Matese, Patrick O. Brown, David Botstein, Per Eystein Lønning, and Anne-Lise Børresen-Dale. 2001. Gene expression patterns of breast carcinomas distinguish tumor subclasses with clinical implications. Proceedings of the National Academy of Sciences of the United States of America 98 (19):10869-10874.

Soupene, Eric, and Frans A. Kuypers. 2008. Mammalian Long-Chain Acyl-CoA Synthetases. Experimental Biology and Medicine (Maywood, N.j.) 233 (5):507-521.

Spangenberg, Christian, Ekkehart U. Lausch, Tatjana M. Trost, Dirk Prawitt, Andreas May, Romy Keppler, Stephan A. Fees, Dirk Reutzel, Carolin Bell, Steffen Schmitt, Ilka B. Schiffer, Achim Weber, Walburgis Brenner, Matthias Hermes, Ugur Sahin, Özlem Türeci, Heinz Koelbl, Jan G. Hengstler, and Bernhard U. Zabel. 2006. ERBB2-Mediated Transcriptional Up-regulation of the α5β1 Integrin Fibronectin Receptor Promotes Tumor Cell Survival Under Adverse Conditions. Cancer Research 66 (7):3715-3725.

Stäge, Martin S., Hesse Manuela and Max Daniela. 2010. Lipases and Related Molecules in Cancer Cancer Growth and Metastasis 2010:3 11–20

Strauss, Juliane G., Marianne Hayn, Rudolt Zechner, Sanja Levak-Frank, and Sasa Frank. 2003. Fatty acids liberated from high-density lipoprotein phospholipids by endothelial-derived lipase are incorporated into lipids in HepG2 cells. Biochemical Journal 371 (Pt 3):981-988.

Strauss, Juliane G., Robert Zimmermann, Andelko Hrzenjak, Yonggang Zhou, Dagmar Kratky, Sanja Levak-Frank, Gert M. Kostner, Rudolf Zechner, and Sasa Frank. 2002. Endothelial cell-derived lipase mediates uptake and binding of high-density lipoprotein (HDL) particles and the selective uptake of HDL-associated cholesterol esters independent of its enzymic activity. Biochemical Journal 368 (Pt 1):69-79.

Stulnig, TM, Markus Berger, Michael Roden, Harald Stingl, Daniel Raederstorff, and Werner Waldhäusl. 2000. Elevated serum free fatty acid concentrations inhibit T lymphocyte signaling. The FASEB Journal 14 (7):939-947.

The Cancer Genome Atlas Network. 2012. Comprehensive molecular portraits of human breast tumors. Nature. 490(7418): 61–70. doi:10.1038/nature11412.

Thupari, J. N., M. L. Pinn, and F. P. Kuhajda. 2001. Fatty acid synthase inhibition in human breast cancer cells leads to malonyl-CoA-induced inhibition of fatty acid oxidation and cytotoxicity. Biochem Biophys Res Commun 285 (2):217-23.

Trost, Tatjana M., Ekkehart U. Lausch, Stephan A. Fees, Steffen Schmitt, Thorsten Enklaar, Dirk Reutzel, Lili R. Brixel, Peter Schmidtke, Marko Maringer, Ilka B. Schiffer, Carolin K. Heimerdinger, Jan G. Hengstler, Gerhard Fritz, Ernst O. Bockamp, Dirk Prawitt, Bernhard U. Zabel, and Christian Spangenberg. 2005. Premature Senescence Is a Primary Fail-safe Mechanism of ERBB2-Driven Tumorigenesis in Breast Carcinoma Cells. Cancer Research 65 (3):840-849.

Trost, TM. 2005. Konditionale Modellsysteme zur Untersuchung der ErbB2-induzierten Tumorgenese. Fachbereich Biologie. Universität Mainz. Dissertation

Vogel, Charles L., Melody A. Cobleigh, Debu Tripathy, John C. Gutheil, Lyndsay N. Harris, Louis Fehrenbacher, Dennis J. Slamon, Maureen Murphy, William F. Novotny, Michael Burchmore, Steven Shak, Stanford J. Stewart, and Michael Press. 2002. Efficacy and Safety of Trastuzumab as a Single Agent in First-

Line Treatment of HER2-Overexpressing Metastatic Breast Cancer. Journal of Clinical Oncology 20 (3):719-726.

Wang, Hong, Urmilla Sreenivasan, Hong Hu, Andrew Saladino, Brian M. Polster, Linda M. Lund, Da-wei Gong, William C. Stanley, and Carole Sztalryd. 2011. Perilipin 5, a lipid droplet-associated protein, provides physical and metabolic linkage to mitochondria. Journal of Lipid Research 52 (12):2159-2168.

Wang, Shizhen Emily, Archana Narasanna, Marianela Perez-Torres, Bin Xiang, Frederick Y. Wu, Seungchan Yang, Graham Carpenter, Adi F. Gazdar, Senthil K. Muthuswamy, and Carlos L. Arteaga. 2006. HER2 kinase domain mutation results in constitutive phosphorylation and activation of HER2 and EGFR and resistance to EGFR tyrosine kinase inhibitors. Cancer Cell 10 (1):25-38.

Wang, Ziyun, Shen Li, Lidan Sun, Jianglin Fan, and Zhenming Liu. 2013. Comparative Analyses of Lipoprotein Lipase, Hepatic Lipase, and Endothelial Lipase, and Their Binding Properties with Known Inhibitors. PLoS ONE 8 (8):e72146.

Watt, M. J., and L. L. Spriet. 2004. Regulation and role of hormone-sensitive lipase activity in human skeletal muscle. Proc Nutr Soc 63 (2):315-22.

Weyemi, U., O. Lagente-Chevallier, M. Boufraqech, F. Prenois, F. Courtin, B. Caillou, M. Talbot, M. Dardalhon, A. Al Ghuzlan, J. M. Bidart, M. Schlumberger, and C. Dupuy. 2012. ROS-generating NADPH oxidase NOX4 is a critical mediator in oncogenic H-Ras-induced DNA damage and subsequent senescence. Oncogene 31 (9):1117-1129.

Wu, Xiaoqian, Heqing Huang, Futian Tang, Kang Le, Suowen Xu, and Peiqing Liu. Regulated expression of endothelial lipase in atherosclerosis. Molecular and Cellular Endocrinology 315 (1-2):233-238.

Yamashita, Atsushi, Yasuhiro Hayashi, Naoki Matsumoto, Yoko Nemoto-Sasaki, Saori Oka, Takashi Tanikawa, and Takayuki Sugiura. 2014. Glycerophosphate/Acylglycerophosphate Acyltransferases. Biology 3 (4):801-830.

Yang, Bo, Pengcheng Fan, Aimin Xu, Karen S. L. Lam, Thorsten Berger, Tak W. Mak, Hung-Fat Tse, Jessie W. S. Yue, Erfei Song, Paul M. Vanhoutte, Gary Sweeney, and Yu Wang. 2012. Improved functional recovery to I/R injury in hearts from lipocalin-2 deficiency mice: restoration of mitochondrial function and phospholipids remodeling. American Journal of Translational Research 4 (1):60-71.

Yarden, Y. 2001. The EGFR family and its ligands in human cancer: signalling mechanisms and therapeutic opportunities. European Journal of Cancer 37, Supplement 4:3-8.

Yarden, Yosef, and Mark X. Sliwkowski. 2001. Untangling the ErbB signalling network. Nat Rev Mol Cell Biol 2 (2):127-137.

Yasuda, Tomoyuki, Ken-ichi Hirata, Tatsuro Ishida, Yoko Kojima, Hanayo Tanaka, Takeaki Okada, Thomas Quertermous, and Mitsuhiro Yokoyama. 2007. Endothelial Lipase is Increased by Inflammation and Promotes LDL Uptake in Macrophages. Journal of Atherosclerosis and Thrombosis 14 (4):192-201.

Yu, Dihua, and Mien-Chie Hung. 2000. Role of erbB2 in breast cancer chemosensitivity. BioEssays 22 (7):673-680.

Zaidi, Nousheen, Leslie Lupien, Nancy B. Kuemmerle, William B. Kinlaw, Johannes V. Swinnen, and Karine Smans. 2013. Lipogenesis and lipolysis: the pathways exploited by the cancer cells to acquire fatty acids. Progress in lipid research 52 (4):585-589.

http://www.lifetechnologies.com 08/2015

http://www.proteinatlas.org 11/2015

http://www.sinobiological.com 08/2015

8. Supplement

8.1 Abbreviation

ACACA	acetyl-coenzyme A carboxylase
ACSL3	acyl-CoA synthase long chain
AMPK	adenosine monophosphate activated protein kinase
ATP	adenosine triphosphate
BMI	body mass index
BSA	bovine serum albumin
cDNA	complementary deoxyribonucleic acid
CDP	cytidine diphosphate
CHPT1	choline phosphotransferase 1
CMP	cytidine monophosphate
CMV	cytomegalovirus promoter
CP	cut-point
CPT-1	carnitine palmitoyltransferase-1
Cr	chromium
DAG	diacylglycerol
DGAT	diacylglycerol acyltransferase
DMSO	dimethyl sulfoxide
DNA	deoxyribonucleic acid
dox	doxycyclin
DTT	dithiothreitol
EDTA	ethylendiamintetraessigsäure
e:t	effector to target ratio
eGFP	enhanced green fluorescent protein
EGFR	epidermal growth factor receptor
EMT	epithelial-to-mesenchymal transition
ER	estrogen receptor
EV	empty vector
FABP7	fatty acid binding protein 7
FASN /FAS	fatty acid synthase
FFA	free fatty acids
Fig.	figure
FM	full media
h	hours
HDL	high density lipoproteins
HDL-PC	high density lipoproteins phosphatidylcholine
HER2	human epidermal growth factor receptor 2
hGX PLA2	human group X secreted phospholipase A2
HIF-1α	hypoxia-inducible factor-1 alpha
HL/ LIPC	hepatic lipase
HR	hazard ratio
HSPG	heparan sulfate proteoglycans
IDL	intermediate-density lipoprotein
IL-1β	interleukin 1 beta
IL-6	interleukin-6
IL-8	interleukin-8
ILCNC	International Lipid Classification and Nomenclature Committee

kd	knock down
kDa	kilo dalton
kg/ g/ mg	kilogram/ gram/ milligram
L/ mL/ µL	litre/ milliliter/ microlitre
LCN2	lipocalin2
LD	lipid droplets
LDL	low density lipoproteins
LDLR	low-density lipoprotein receptor
LDHA	lactate dehydrogenase A
LIPG/ EL/ EDL	lipoprotein lipase G; endothelial lipase
LPC	lyso-phosphatidylcholine
LPE	lysophosphatidylethanolamine
LPIN1	lipin1
LPL/ LIPD	lipoprotein lipase
LPS	lipopolysaccharide
lyso-PC	lysophosphatidylcholine
M/ mM/ µM/ nM	mole/ millimole/ micromole/ nanomole
mA	milliampere
MAG	monoacylglycerol
MAGL/ MGLL	monoacylglycerol lipase
MCP-1	monocyte chemoattractant protein-1
MFS	metastatic free survival
MHC-I	major histocompatibility complex-I
min	minute
NADPH	nicotinamide adenine dinucleotide phosphate
NC	negative control
NF-kB	Nuclear factor-kB
NK cells	natural killer cells
NPC1	niemann-Pick C1
OA	oleic acid
OE	overexpression
OIS	oncogene-induced senescence
PA	phosphatidic acid
PC	phosphocholine
PC-OA/ DOPC	1,2-dioleoyl-sn-glycero-3-phosphocholine
PC-PA/ DPPC	1,2-dipalmitoyl-sn-glycero-3-phosphocholine
PC-SA/ DSPC	1,2-distearoyl-sn-glycero-3-phosphocholine
PDK1	3-Phosphoinositide dependent protein kinase-1
PLD1	phospholipase D1
PLIN2	perilipin2
PLIN5	perilipin 5
PMSF	phenylmethylsulfonylfluorid
pPC	proprotein convertases
PR	progesterone receptor
qRT-PCR	quantitative realtime polymerase chain reaction
RNA	ribonucleic acid
ROS	reactive oxygen species
siRNA	small interfering RNA
SDS	sodium dodecyl sulfate polyacrylamide gel electrophoresis
Tab.	table
TAG	triacylglycerol
TBARS	thiobarbituric acid reactive substances
TEMED	N,N,N',N'-Tetramethylethylendiamin
TLR4	toll-like receptor4

TMRE	tetramethylrhodamine ethyl ester perchlorate
TNF-α	tumor necrosis factor alpha
TOFA	5-(tetradecyloxy)-2- furoic acid
TRAIL	tumor necrosis factor- related apoptosis-inducing ligand
Tris	Tris(hydroxymethyl)-aminomethan
TXN	thioredoxin
TXNIP	thioredoxin-interacting protein
TXNRD	thioredoxin reductase
UBC	ubiquitin C
VEGF	vascular endothelial growth factor
VLDL	very low density lipoproteins

8.2 List of figures

8.3 Acknowledgements

First of all I would like to thank my supervisor Prof. Dr. J.G. Hengstler for giving me the possibility to work in his labs. He was always interested in also small progresses and supported this thesis with fruitful discussions.

I would like to express my gratitude to Prof. Dr. F. Wehner for being the referee of my work.

My warm-hearted thanks go to my co-supervisor Dr. Cristina Cadenas. We had hard LIPG times filled with frustrations. Nevertheless have you encouraged and supported me thousand times weekdays but also on the weekends. We laughed and complained together but now ,,we brought LIPG into the world finally''.

My gratitude goes to all members of my research group. Especially Dr. Rosie Marchan, Kathrin Gianmoena and Bettina Büttner thank you for listening and giving advices as well as chocolate several times. I would like to thank Silke Hankinson and Beate Graf for the occupational and especially private encouragements. I had a great time with all of you.

8.4 Eigenständigkeitserklärung

Hiermit versichere ich Sonja Vosbeck, dass ich die vorliegende Dissertation mit dem Titel ‚The functional role of the endothelial lipase LIPG in breast cancer' selbstständig und ohne unzulässige fremde Hilfe angefertigt habe. Ich habe keine anderen als die angegebenen Quellen und Hilfsmittel benutzt, sowie wörtliche und sinngemäße Zitate kenntlich gemacht. Die Arbeit hat in gegenwärtiger oder ähnlicher Form weder an der technischen Universität Dortmund noch an einer anderen Universität vorgelegen.

Ort, Datum

Unterschrift